Effects of gases on E-glass fibers

by

Shin Moo Oh

A Dissertation Submitted to the

Graduate Faculty in Partial Fulfillment of

The Requirements for the Degree of

DOCTOR OF PHILOSOPHY

Department: Materials Science and Engineering

Major: Ceramic Engineering

Approved:

Signature was redacted for privacy.

In Charge of Major Work

Signature was redacted for privacy.

For the Major Department

Signature was redacted for privacy.

For the Graduate College

Iowa State University
Ames, Iowa

1975

TABLE OF CONTENTS

NOMENCLATURE

a = absorption of coefficient (cm^{-1})

a_i = activity

A = surface area (cm^2) or constant

c = crack depth (cm) or constant

c_p = specific heat (cal/gm)

C = concentration

d = fiber diameter (cm)

D = diffusion coefficient (cm^2/sec) or inside diameter of nozzle (cm)

D_o = pre-exponential term of diffusion coefficient (cm^2/sec)

e = exponent

E = elastic (Young's) modulus (psi)

E_i = energy or work or experimental error

E_λ = emissivity

E_{eff} = effective emissivity

F = force

ΔF = free energy change (cal/mole)

g = gravity acceleration

h = gravity head (cm) or coefficient of heat transfer ($cal/sec \cdot cm^2 \cdot °C$)

ΔH = heat of adsorption (cal/mole)

k_o = number of active site

k_i = reaction rate constant

K = constant or thermal conductivity ($cal/sec \cdot cm \cdot °C$)

L = length of nozzle (cm) or breaking load (gm)

M = molecular weight (gm) and mean value

n = number of molecules/cm^2/sec

n_D = index of refraction

N = number of molecules/sec of number of specimens

$(Nu)_D$ = Nusselt number, hD/K

p = pressure (atm)

p_o = saturation vapor pressure (atm)

p_x = vapor pressure in the gas phase (atm)

P = permeability (cm^3/stp $cm^3 \cdot$atm)

P.E. = probable error (%)

q = mass adsorbed (gm)

q_m = mass adsorbed by monomolecular layer

q_o = mass adsorbed at p_o

Q = activation energy for viscous flow (cal/mole)

Q_D = activation energy of the diffusion (cal/mole)

Q_p = activation energy of the permeability (cal/mole)

r = radius of jet (cm)

r_f = final radius of glass fiber (cm)

r_o = radius of jet at $z = 0$ (cm)

R = gas constant or reflection factor

Re = Reynolds number, $U_\infty D\rho/\eta$

R_o = inside radius of nozzle, $D/2$

R.H. = relative humidity (%)

S = strength (psi) or solubility

t = time (sec)

T = temperature (°C) or transmission factor

$\dot{T}$ = cooling (or heating) rate (°C/sec)

T_o = nozzle temperature (at z = 0) or drawing temperature (°C)

T_∞ = ambient temperature (°C)

U_∞ = velocity of the air far from the cylinder (cm/sec)

v = specific volume (cm^3) or velocity (cm/sec)

V = volume (cm^3) or specific reaction rate

w = mass flow rate (gm/sec)

W = weight (gm)

x = thickness (cm)

z = axial distance from the nozzle exit (cm)

α = variation coefficient (%)

β = constant

γ = surface tension (dyne/cm)

Γ_i = surface excess

ϵ = strain

η = viscosity (poise)

η_o = pre-exponential constant of viscosity (poise)

θ = angle (°) or fraction of surface covered

λ = wavelength (cm)

μ_i = chemical potential

ρ = density (gm/cm^3)

σ = standard deviation or stress (psi)

τ = mean time (sec) or parameter

ABSTRACT

The effects of selected gases such as water vapor and CF_4 on E-glass fibers at high and low temperature were investigated. Fine E-glass fibers (3.5-5.8 μm diameter) drawn in these atmospheres were aged in a controlled humidity atmosphere (36% R.H.) for certain periods of time from one-half day up to 30 days and the tensile strengths were measured. Losses of strengths of fibers drawn in both high humidity and CF_4 atmosphere were observed. The initial strength of E-glass fibers fluorinated by CF_4 in the drawing atmosphere was lower than that for fibers drawn in humidity atmospheres. However, the fibers drawn in the CF_4 atmosphere showed greater resistance to attack by water during aging in a humid atmosphere.

INTRODUCTION

Freshly produced fine glass fibers manufactured and tested under controlled conditions will have high breaking strengths approaching a theoretical strength of one to four million psi. Unfortunately, these values are in general greatly reduced when the glass surface is damaged either by physical or chemical attack. For instance, weathering by exposure to atmospheric moisture results in rapid degradation of strength at a rate depending on environmental conditions.

Modern glass technology has recognized the importance of surface reaction phenomena from the standpoint of its influence on glass workability and devitrification. The most dramatic examples of the importance of glass-atmosphere reaction are to be found in the behavior of glass fibers since surface corrosion problems are magnified in filaments due to their huge relative amount of hydrophilic surface area. Many attempts have been made to study surface-atmospheric gas reaction phenomena including adsorption, diffusion and ion exchange. These phenomena are still generally poorly understood due to a complex combination of physical and chemical reaction processes when glass fiber surfaces are subjected to variable environmental conditions. The rate of gas reaction on a surface is governed by many variables such as temperature, concentration, time, surface area, molecular weight of gas, bonding energy of surface materials and so forth.

One method for taking advantage of the high strength of commercial glass fibers is to use coupling agents for fiber glass reinforced plastics as means of stress transfer between the hydrophobic polymer and the

hydrophilic glass surface. Even though many chromic and silane coupling agents have been developed to improve the fiber-matrix bond, the fiber composite may lose strength by water penetration at the glass-resin interface. The strength reduction by water penetration at the resin-fiber interface is probably affected by compression at the glass-resin interface and the thermodynamics of water adsorption at the interface.

The object of this investigation was to study the interaction of various gases with the surface of glass at both high and low temperatures. Glass fibers were used in order to obtain as much surface area as possible. Gas reactions on glass fibers during forming may contribute to changes in surface composition and microstructure as well as properties such as surface tension and viscosity which in turn may affect the drawing conditions; final fiber diameter, cooling rate, jet shape, drawing force and other parameters. These drawing conditions are also factors affecting the mechanical strength of glass fibers.

The procedures for this investigation were based on theories and techniques obtained in the literature and from industry. It consisted essentially of drawing glass fibers under controlled atmospheric conditions (i.e., high and low humidity and Freon-14 gas atmospheres) and evaluating the resistance of the fiber to corrosion by atmospheric water vapor. The effects of drawing gas atmospheres on the physical and chemical properties of glass fiber surfaces were determined by analyzing the results of drawing conditions and the tensile strength after exposure to corrosive environments.

LITERATURE SURVEY

Glass Fiber Drawing

Glass fiber drawing is by no means a recent discovery; it is older than the technique of glass blowing because many Egyptian vessels were made by winding coarse glass fibers. In the 13th century the Venetian glassmakers employed the technique of glass fiber drawing by drawing heat-softened glass into fine fibers and they decorated glassware with bundles of glass fibers (1). Because of high flexibility and high strength of fine glass fibers, interest in using glass fibers for textile applications developed in France. In the early 19th century fine glass fibers were used in textile industries, for example, woven with silk brocades. In Germany, during World War I, fiber glass was developed for use as thermal insulation because of a shortage of asbestos. As new applications developed in other fields, demand led to rapidly increasing production.

There are many methods of commercial glass fiber production, which can be categorized into two principal methods. One is the continuous-filament process in which molten glass flows from a number of orifices and is drawn into fibers by mechanical means, such as winding on a rapidly rotating drum. The other is the wool and staple process in which jets of high-velocity gas impinge on streams of molten glass, and fibers are formed by the frictional drag of the glass stream. Recently Loewenstein (2) reviewed the manufacturing technology of continuous glass fibers and discussed the general technical problems in the fiber glass industry. In the continuous-filament process, steady conditions prevail and the configuration of the glass stream as it is drawn into a fiber can be

studied by static methods. However, in the wool processes the pattern of movement of the glass changes continuously and the motion is too rapid to be followed by the eye or an ordinary camera. de Dani and Jellyman (3) established the mechanism by which fiberization of glass takes place in the Owens-Corning wool process by use of a high speed camera.

The overall physical process during the drawing of a glass fiber is extremely complex, because a huge surface area is created under conditions of mechanical stress, viscous flow and rapidly varying temperature. The interactions of glass fibers with the drawing atmosphere will depend on this complex physical process and will include such variables as cooling rate (time), drawing temperature, drawing speed, mass flow rate and drawing force.

Cooling rate and cooling time

In glass-forming processes, the cooling rates are often more important than the drawing temperature itself. Glass is defined as being in a supercooled liquid state so that different cooling rates, corresponding to different relaxation times in transition range, give rise to a different configuration of the glass structure. According to Bateson (4), high strength glass fibers result when cooling rates are so rapid that insufficient time is provided for relaxation of shearing stresses by viscous flow. The cooling time for a 5-μm diameter glass fiber, if defined as the time required for the glass to reach the final fiber diameter, could be as little as 10^{-3} sec as compared with about 1/2 sec for 2-mm diameter glass rod (4).

The calculation of cooling rate is not too difficult from the heat transfer point of view if certain simplifying assumptions are made including the applicability of Newtonian conditions, i.e. internal gradients of temperature are negligible. In general, heat transfer rates vary greatly with different geometrical shapes (5); thus, the cooling rate of the glass fiber during forming depends strongly on jet shapes.

Deeg and Dietzel (6), and Anderson (7) calculated that the time for cooling fibers from the drawing temperature to ambient temperature is of the order of 10^{-4} sec, which is approximately the Maxwell relaxation time. By observing jet shapes, Kutukov and Khodakovskii (8) determined the total cooling time to be $0.2 \sim 1.0$ sec, depending upon the volume of glass jet. Arridge and Prior (9) found that cooling time in a coarse silica fiber (4mm in diameter) was considerably longer than was predicted by Anderson's calculation (7). Subsequently, Manfre (10) calculated the cooling time from photographs of the upper jet and found it to disagree with Anderson (7), but to be in the same range as reported by Kutukov and Khodakovskii (8) and Arridge and Prior (9).

Glicksman (11) developed a cooling rate equation, which had the same form as Anderson's equation except that he used the conductivity of air instead of that of glass, an error in Anderson's work which was pointed out by Manfre (10). The equation for the cooling rate derived by Glicksman is

$$\frac{\partial T}{\partial t} = \dot{T} = -(T-T_\infty)\frac{K_{air}(Nu)_D}{\rho c_p r^2} \qquad (1)$$

He also computed the approximate cooling time for a constant diameter fiber by using Equation 1 with an average Nusselt number, i.e.,

$$t = - \frac{c_p r^2}{K_{air}} \frac{1}{(\overline{Nu})_D} \ln \frac{T-T_\infty}{T_o-T_\infty} . \qquad (2)$$

He found disagreement between his calculated values and those of other workers (7, 9) at very low temperatures. However, the cooling times for fibers predicted from Nusselt number in his calculation agreed closely with his experimental results and he concluded that actual cooling times are much longer than previous workers had predicted in the region where fiber is still attenuating (above about 870°C). Under the assumptions that heat losses by radiation are neglectable and that jet volume remains constant, he also showed that cooling equation as a function of axial distance (2) can be derived from the first law of thermodynamics and is given by

$$\frac{dT}{dz} = - \frac{\pi K_{air} Nu}{wc_p} (T-T_\infty) = -\beta(\overline{T}-\overline{T}_\infty) \qquad (3a)$$

or

$$\frac{T-T_\infty}{T_o-T_\infty} = e^{-\beta z} . \qquad (3b)$$

He also found that increasing flow rate or decreasing the drawing force results in faster cooling of the fiber (i.e., $r>r_f$ at higher temperatures).

By using the experimental glass flow rate and measured upper jet shape, Burgman and Hunia (12) used the following relationship to calculate the total fiber cooling time.

$$t = \frac{\pi\rho}{w} \int_o^z r^2(z)dz \qquad (4)$$

They found the time to vary from 0.2 sec to as much as 1.0 sec, depending upon the drawing conditions. They also showed experimentally that cooling time has no effect on fiber breaking strength.

Drawing force

In the spinning process for continuous filament production hot molten glass flows through a capillary nozzle into air to form a free liquid glass jet at the nozzle exit. The glass fiber is made by rapid attenuation from the jet by contacting a rotating drum which maintains tension on the jet due to the dynamic balance between the forces due to surface tension and traction. The analysis of the mechanisms of a similar attenuation case can be found in the studies of polymer spinning phenomena (13,14). However, many assumptions used for the solutions of the rheology of polymers are unrealistic for the glass fiber formation.

In a model of pulling of thread from viscous liquid, Bateson (4) expressed the drawing force (F_x) acting on the surface as a balance between surface tension and traction, i.e.,

$$F_x = 2\pi r\gamma \sin\theta \qquad (5)$$

where θ is a contact angle. He added that this equation can be applied in the drawing of a glass fiber only if gravity and the weight of glass outside the orifice are neglected. According to his hypothesis, i.e., vanishing shearing stress on a fine fiber drawn with sufficiently high speed so that no radial temperature gradient exists, the tension in the fiber as it is drawn is believed to influence the final strength of the fiber due to the effect of thermal history on surface flaw formation.

Glicksman (15) calculated the magnitude of the net tensile force (F_o) acting normal to the glass cross-section at the nozzle exit. He found that it consists of two components; a viscous force and a surface tension force. Glicksman's force equation was derived from the momentum equation for steady-state flow under assumptions of one-dimensional temperature and velocity distribution.

$$F_o = - \frac{6\eta w}{\rho r} \frac{dr}{dz} + \pi r\gamma \cos \theta \qquad (6)$$

where $\tan \theta = - \frac{dr}{dz}$. He also showed experimentally that the tension in the jet is approximately constant throughout the upper jet and affects cooling times at high temperature (above 870°C), i.e., low tension showed faster cooling of the fiber.

Manfre's work (16) on the main forces acting in the continuous drawing of glass fibers described the external net force (F) as being equal to the sum of four forces; the tensile force (drawing force; F_d), the surface tension force (F_s), the gravitational force (F_g) and the aerodynamic force (F_a). These forces are balanced as follows.

$$F = F_d + F_s + F_g + F_a \qquad (7)$$

He calculated the gravitational force and the aerodynamic force and found that they are negligible compared to the surface tension force. The drawing force, therefore, was shown to be balanced mainly by the surface tension force at the nozzle and was determined experimentally by a device which measured the torque on the winding machine during spinning. He computed numerical values of F_s by using the following equation derived from the balance between the surface tension component in the z-direction

and the forces due to both hydrostatic pressure and weight of the hanging thread, i.e.,

$$F_s = \left\{ \frac{[1+(\frac{dr}{dz})^2]^2 - r\frac{d^2r}{dz^2}}{[1+(\frac{dr}{dz})]^{3/2}} \right\} \pi\gamma r \qquad (8)$$

The surface tension and other data in his computation were obtained from the literature and from measurements of the jet shape. He concluded that the surface tension plays an important role in the magnitude of F_s, which is the only important external force component acting in opposition to pulling force. The greatest influence of F_c is in the first part of jet ($z \leq 0.3$ cm).

Later Burgman (17) reviewed Glicksman's momentum equation for steady state flow and discussed the relationship between the forces acting on the element of the glass jet and the jet shape. According to his analysis of jet shape, in the upper part of a concave jet (See Fig. 2), the viscous force at the nozzle exit is the dominant force. The viscous force increases while surface tension decreases in order to maintain constant normal force along the axis of the upper jet. He concluded that, from the practical point of view, the strong dependence between glass viscosity and temperature is the key to drawing glass into fine glass fibers.

Krishman and Glicksman (18) attempted to calculate the drawing force more accurately by using a two-dimensional analysis of heated upper jet solution. However, inclusion of two-dimensional fluid dynamic effects did not significantly improve the accuracy of the solution. Glicksman's recent paper (19) showed that the viscous force term in Equation 6 should be:

$$F_o = -\left[4 + \frac{2}{1+\left(\frac{dr_o}{dz}\right)^2}\right] \frac{\eta w}{\rho r_o}\left(\frac{dr_o}{dz}\right) + \pi r_o \gamma_T \cos\theta \qquad (9)$$

This equation demonstrated closer agreement with the experimental tension data.

More recently Oh and Martin (20) derived the approximate drawing force equation from Glicksman's one-dimensional flow differential equation (15) with the assumption of the viscous force predominating, and noted that the drawing force is independent of flow rate and depends most strongly on viscous flow terms,

$$F_o = -\frac{6\pi KNuQ\eta_o e^{-Q/RT_o}}{c_p \rho R(T-T_\infty)} \ln \frac{r_f}{r_o} \qquad (10)$$

Jet shape

As mentioned in the previous sections, numerous authors drew attention to jet shape analysis to make possible the prediction of the cooling rates and the forces acting on a glass fiber during drawing. The analysis of the dynamics of liquid glass jets is possible in principle, but numerical techniques must be employed for practical solutions. A further difficulty is that jet shapes are governed by fluid flow at the nozzle exit and will be influenced by the strong dependence of glass viscosity on the glass temperature.

Glicksman (15) analyzed the behavior of variable viscosity jets and predicted the jet shapes by simultaneously solving the momentum equation for steady flow, the continuity equation and the energy equation. To perform his analysis he divided the glass jet into three regions depending

on the magnitude of slope (dr/dz); the upper jet region (dr/dz > 0.1), the central jet region (dr/dz $\leq$ 0.1) and the constant radius jet region (dr/dz = 0). Figure 1 shows schematically Glicksman's three jet regions in glass fiber drawing.

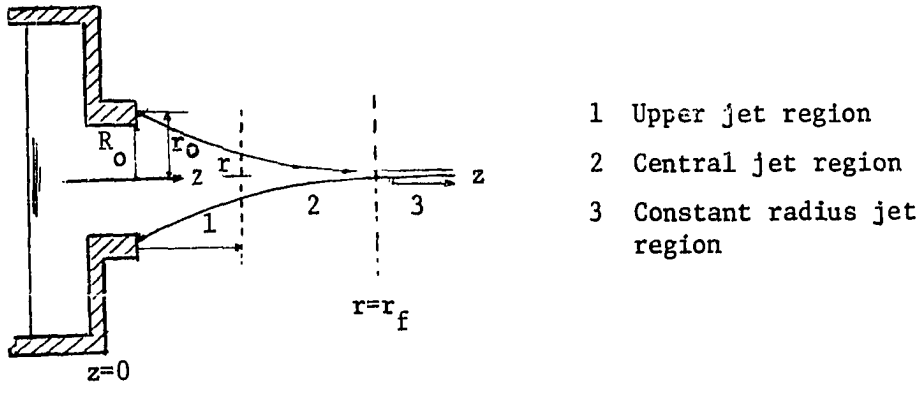

Figure 1. Three jet regions of Glicksman's jet analysis.

He concluded that the assumption of one dimensional flow conditions in the upper jet region, even though not physically justified, yields results that are qualitatively correct. He suggested that improved results in the upper jet region may be obtained by taking into account the radial variation in the temperature due to radiant heat transfer.

Subsequently, Manfre (21) investigated jet shape by observing photographs of the glass jet, and developed a non-linear heat transfer equation for determining the temperature distribution in the glass jet. It was also reported that Kutukov and Khodakovskii (8) analyzed jet shapes by means of high speed photographs and found high speed oscillations of the glass jet which did not affect the fiber drawing process. However, Manfre (22) found earlier that low speed oscillations which interrupt the fiber process can be related to the gravity head of the glass in bushing.

Burgman (17) observed three basically different jet shapes; concave which is normally reported in the literature, convex, and a combination of concave and convex. He related these shapes to the Reynolds number (Re) for flow through the drawing nozzle. He actually divided the jet types into four categories as shown in Figure 2 and stated that the jet shapes were independent of the nozzle geometry or fiber drawing speed for surface tension ranging from 300 to 330 dyne/cm.

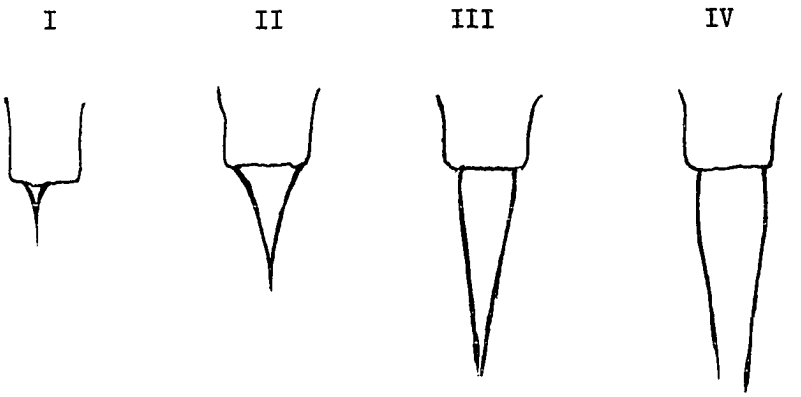

Figure 2. Four categories of glass jet shape by Burgman. (17)

He also stated that there is jet instability at low viscosity and high Reynolds number, but at high viscosity (> 500 poise) the upper jet in categories III and IV is stable, i.e., no noticeable change in jet shape occurs with time.

In order to emphasize the important parameters of the drawing process, Oh and Martin (20) used the assumptions of Glicksman (15) and approximate integration techniques to develop closed-form solutions to the fiber drawing equations. The drawing equations can be expressed in terms of temperature or in terms of axial distance, and can be written;

$$\ell n\ r/r_f = \ell n\ r_o/r_f \left[\frac{\exp(-Q/RT)(T-T_\infty)}{\exp(-Q/RT_o)(T_o-T_\infty)} \right] \qquad (11a)$$

or $$\ell n\ r/r_f = \ell n\ r_o/r_f \exp\left[e^{-(Q/RT - Q/RT_o)}\ e^{-\beta z} \right] . \qquad (11b)$$

Equation 11a indicates that the shape of the jet in temperature coordinates depends only on the temperature and activation energy for viscous flow with the logarithmic drawing ratio appearing as a scaling parameter. The equation 11b can be approximated as follows and shows good agreement between experimental and predicted jet shapes close to the drawing nozzle, i.e., at small value of z,

$$\ell n\ \ell n\ r/r_f = \ell n\ \ell n\ r_o/r_f - \left[\frac{Q}{RT_o}\left(1 - \frac{T_\infty}{T_o}\right) + 1\right] \frac{KNu}{c_p r^2 v\rho}\ z \qquad (11c)$$

Flow rate

The rate of glass fiber production from a given bushing is entirely a function of the flow rate of glass through nozzle. In dealing with transport processes in viscous liquids, the flow rate (w) is an important parameter. According to Poiseuille's equation, the flow rate of glass through the nozzle is proportional to the fourth power of nozzle diameter (D) and is independent of the rate of attenuation, i.e., of the diameter of the fiber made (2). The flow rate is given approximately by the following equation;

$$w = \frac{\pi \Delta p D^4}{2\eta L} = \frac{K'}{\eta} \qquad (12)$$

Δp is equal to $(p_h - p_o)$ when p_h and p_o are the gravity head pressure of glass above the nozzle and at the nozzle exit, respectively. Tiede (23)

measured glass viscosity by determining the relationship between temperature and flow rate of glass fibers drawn through a single hole bushing. He pointed out that it is not possible to exactly predict the flow rate from Poiseuille's equation due to the complicated situation in the orifice, i.e., the increase of viscosity of glass during its passage through the nozzle because of temperature drop.

Manfre (22) observed three different regimes in the outflow of molten glass from a capillary which he referred to as drop formation, stationary spinning, and oscillatory spinning. He was partially successful in establishing a relationship between the flow rates in these regimes to interpret the oscillation phenomena. He introduced an extrusion law which is of the same form as Poiseuille's equation written as a function of the gravity head (h),

$$w = dV/dt = Ah \tag{13}$$

where $A = \frac{\pi D^4 \rho g}{8(L+nD)\eta}$ and n is the Couette correction. He found that in the spinning process, the flow rate is constant and that the value of the flow rate for the onset of oscillation depends on the ratio between viscosity and surface tension. He could not explain physically this fact, and he suggested that it is necessary to study viscoelastic theory in order to explain his results.

The radius of a glass fiber can be calculated from flow rate through the continuity equation;

$$w = \rho \pi r^2 v \tag{14a}$$

If the cross-section velocity distribution is not constant, Equation 12 should be modified as follows;

$$w = 2\pi\rho\int_{o}^{r_f} rv(r)dr \qquad (14b)$$

If velocity is constant, i.e., the fiber is cold, the final radius can be predicted from the mass flow rate and drawing speed by combining Equation 12 and 14a ;

$$d = 2r_f = \left\{\frac{K'}{\eta(T)v}\right\}^{1/2} = 2\left\{\frac{w}{\pi\rho v}\right\}^{1/2} \qquad (15)$$

where K' is a drawing constant which can be determined experimentally.

Thomas (24) showed experimentally that fiber diameter varies as function of bushing temperature and drawing speed. For a fixed head of glass and a fixed pulling speed the relationship between fiber diameter and bushing temperature is linear. It might be expected to show exponential dependence on temperature due to the viscosity parameter. He also found that the slope of the diameter vs. bushing temperature curves increases with a decrease in drawing speed, and that the fiber diameter decreases parabolically with increase in drawing speed.

Many investigators (17,24) have shown experimentally that the flow rate from the nozzle is almost independent of drawing speed. Thomas (24) found that, for a given nozzle diameter, temperature and drawing speed, the flow rate varies linearly with the glass head. The dependence of flow rate on head was found to increase with increase in temperature. Otto (25) obtained different fiber diameters for a strength study by controlling the drawing speed. He suggested that the fiber diameter could also be controlled by varying the flow rate of glass through the drawing nozzle by changing the glass head while holding the temperature and drawing speed constant.

Glass Surface Reactions with Gases

Glass is widely employed in contact with gases. Certain gases such as water vapor, hydrogen and oxygen, which dissolve molecularly in glass, can react with the glass network and consequently modify the composition and microstructure as well as physical properties such as surface tension and viscosity. Useful reviews of reactions of glass with gases will be found in the treatises by Holland (26), Doremus (27) and Stanworth (28).

When a solid surface is in contact with a gas, an interaction may occur which causes a concentration of gas close to the surface due to attractive forces resulting from a different thermodynamic properties of the surface and bulk phases. This spontaneous behavior is a dynamic process (29). In other words, the adsorbed molecules may return to the gas (desorption), or they may either migrate to other sites on the solid surface (surface diffusion) or dissolve into the bulk (bulk diffusion). Deitz (30) described the general reaction at a gas/solid interface in terms of an adsorption complex, i.e.,

$$X_{Solid} + A_{gas} \longrightarrow X_{Solid}\text{---}A_{complex} \qquad (16)$$

The surface mobility of this adsorption complex is governed by many variables such as temperature, concentration and molecular weight of the gas.

The structure of glass is regarded as an open network of relatively strong-bonded oxygen ions and glass forming ions, containing within its holes relatively loose-bonded glass modifying cations. The exchange of these modifying ions with other ions by adsorption or diffusion at the glass surface may also result in changes in surface properties of glass.

Gas reactions during the drawing of glass fibers are an extremely complex combination of these reaction processes. When analyzing gas adsorption on a glass fiber surface mass transport processes such as diffusion and ion exchange must be taken into account. Large changes in final properties and in drawing behavior may result from the influence of the gas reactions during the drawing of fibers.

Mechanisms of gas-glass reactions

Adsorption Adsorption phenomena can be classified into two categories depending on the magnitude of the attractive forces. Adsorption due to weak bonding forces of the van der Waals type is called physical adsorption (physisorption). In contrast, chemical adsorption (chemisorption) involves considerable binding energies associated with a significant modification in the electron charge distribution of the adsorbed molecules. In general, chemisorption leads to monolayer adsorption at relatively high temperature, whereas in physisorption, multilayer adsorption occurs at lower temperature and may occur on top of a chemisorbed layer (30).

Two important descriptions of adsorption are the Gibbs adsorption isotherm (31) and the Polanyi potential theory (32). In a broad sense both are chemical potential theories of adsorption. Gibbs' description is largely concerned with correlating changes in surface tension (γ) with quantities adsorbed as shown in the following equation;

$$(d\gamma)_T = -\Sigma\, \Gamma_i d\mu_i \qquad (17a)$$

or

$$\Gamma_i = \frac{-d\gamma}{RTd\ell na_i} \simeq \frac{-d\gamma}{RTd\ell nC_i} \qquad (17b)$$

where Σ is an operator signifying summation and Γ_i is the excess surface

concentration which can be determined experimentally. Using Equation 17a, a number of equations for free energy change (ΔF) accompanying the process of transferring saturated vapor onto a unit area of solid surface can be derived. The most convenient equation in terms of relative vapor pressure was derived by Demirel and Enüstün (33);

$$\Delta F = -RT\int_{o}^{p/p_o} q/q_o \; d\ell n\frac{p}{p_o} \qquad (18)$$

This equation implies that the adsorption process is terminated when the equilibrium pressure reaches p_o.

Polanyi's theory correlates heats of adsorption and changes in "film pressure" with the thickness adsorbed. According to his theory, the work done (E_i) by adsorption is given by the following equation;

$$E_i = \int_{\rho_x}^{\rho_i} V dp = \int_{p_x}^{p_o} \frac{RT}{p}\, dp = RT\; \ell n\, \frac{p_o}{p_x} \qquad (19)$$

where ρ_i and ρ_x are the densities in the adsorbed gas layer and in the gas phase respectively. Analysis of gas adsorption by using Polanyi's theory is particularly successful in predicting the temperature-dependence of adsorption.

Physical or chemical adsorption is affected by a large number of variables such as surface structure (roughness, capillarity), the nature of interaction between adsorbent and adsorbate, and most importantly by surface area. The most common method for the determination of the surface area by gas adsorption uses the BET theory, or one of its modifications. The following equation is one of the modified BET equations expressed in terms of mass of gas adsorbed (34);

$$\frac{p}{q(p_o-p)} = \frac{1}{q_m c} + \frac{c-1}{q_m c}\frac{p}{p_o} \qquad (20)$$

where q is the mass of vapor adsorbed at pressure p and q_m is the mass adsorbed at monolayer coverage of the adsorbent surface. The latter quantity can be calculated from experimental data of q and p/p_o. Using the known area occupied by a single molecule, the parameter q_m gives the surface area covered by a monomolecular layer of adsorbate.

Since the treatment of adsorption kinetics is similar to diffusion problems, corresponding to gas diffusion into a pore, a number of authors (35,36,37) have developed theories of adsorption rate based upon diffusion.

The experimental observed rate of adsorption can be calculated by considering the general form of equation (17);

$$X + A \text{ gas} \underset{k_2}{\overset{k_1}{\rightleftharpoons}} X \ldots\ldots A \text{ complex} \xrightarrow{k_3} \text{products} \qquad (17)$$

The total rate of gas adsorption is given by the following equation;

$$\frac{d\theta}{dt} = k_1(1-\theta) - k_2\theta - k_3\theta \qquad (21)$$

where θ is the fraction of the surface covered by the adsorbed gas at constant pressure, and k_1, k_2, and k_3 are rate constants (38). θ can be determined by integrating with boundary conditions; i.e., $\theta=0$ when $t=0$. Then the specific rate of gas adsorption (V) can be expressed

$$V = \frac{d\theta}{dt}\frac{1}{v} = k_o\theta k_3 \qquad (22)$$

where k_o is a number of active sites per unit area and v is the unit volume.

The equilibrium number (N) of molecules adsorbed per unit area can be calculated for low coverage from the simple numerical consequences of the Langmuir isotherm (37) and de Boer's work (39), i.e.,

$$N = n\tau \tag{23}$$

τ is the mean time of sojourn and n is the number of molecules sticking on each cm^2 per second given by;

$$n = \frac{3.52 \times 10^{22}}{(MT)^{1/2}} p(1-\theta) \tag{24}$$

Here p is the pressure in torr and M is the molecular weight of the gas.

Infrared spectra give direct information about adsorption phenomena by analyzing molecular vibrations on the adsorbed layer; changes in spectra show the effects of the surrounding on molecules, and band shifts and intensity changes indicate the chemical nature of the gases adsorbed onto surfaces. Gas adsorption phenomena on glass surfaces have been investigated using infrared analysis, and various investigators have found that surface hydroxyl groups are the most important sites for gas adsorption (27). There are several types of hydroxyl groups for silica glass; namely, isolated SiOH groups, hydrogen-bonded H_2O groups, internal OH groups and molecularly-adsorbed water. Hydroxyl groups such as AlOH, BOH and POH groups are likely to occur on the surface of complex glasses. Due to different surface free energy factors for the various components, it is probable that one glass former will appear preferentially at the surface. This will give a distribution of surface hydroxyl groups which differs from the bulk composition of the glass.

Band shifts after adsorption of a number of gases on or near hydroxyl groups have often been reported (40). Large band shifts for water indicate

strong hydrogen bonds on SiOH groups (40). Basilə (41) showed a relationship between the band shift and the ionization potential of adsorbed gas. Good correlation between the measured heats of adsorption and band shift for a number of organic molecules adsorbed on silica was found by Kiselev (42).

A number of adsorption isotherm equations as a function of pressure for silica and other silicate glass have been proposed, but none is entirely satisfactory. Many results show disagreement with Henry's law, which may result from heterogeneous adsorption sites in complex glasses; i.e., BOH, AlOH and POH rather than SiOH. These adsorption sites may also change with time and thermal history. Deitz (30) stated that the influence of pretreatment of the surface is probably the most important parameter in determining the adsorption sites on glass.

The formation of SiOH and other hydroxyl group adsorption sites occurs when a freshly formed glass surface is contacted with water vapor. The water chemisorbs rapidly at surface silicon atoms having unpaired electrons (dangling bonds) thereby producing SiOH groups (27). The density of dangling bonds depends on the thermal history of the glass, relative humidity of the atmosphere and surface treatment during melting and cooling.

The effects of surface pretreatment on gas adsorption have been reported by many investigators. Mikhail and Shebl (43) showed that a heating pretreatment of silica gel produced surfaces that were partly hydrophobic. Kawasaki et al. (44) observed that the number of adsorption sites on silica glass was decreased by heat treatment and that there were two states of water sorption, i.e., reversible and irreversible adsorption.

It is possible that heating the sample to higher temperatures progressively destroys the adsorption sites because of diffusion and reaction of atoms from the interior of the glass. Thus, a change in the adsorption capacity is often observed after a glass is heated (26).

Young (45) studied water vapor interaction with silica surfaces at higher temperatures (>400°C) and found that water vapor cannot be chemisorbed due to irreversible dehydroxylation of the glass following such treatments.

The mechanisms of water vapor adsorption on glass surfaces at room temperature have been extensively studied in the past. Folman and Yates (46) described that adsorbed water molecules are bonded to the hydrogen atom on an SiOH group. This hydrogen bonding is intermediate in energy between physisorption and chemisorption. Deitz (47) reported a study of the interactions of water vapor with E-glass fiber and that there is a strong, rapid chemisorption process accompanying or following physisorption of water on glass surfaces.

Recently Johnson (48) studied the effect of water vapor adsorption on specific surface of E-glass fibers and found that water vapor contact increases the specific surface area of E-glass by surface corrosion. It is believed that successive prolonged contact with water vapor increases the number of surface silanol groups with removal of calcium and sodium ions. Huang et al. (49) also studied the mechanisms of vapor sorption on E-glass fibers and observed capillary type of adsorption in the E-glass-water system. They also determined the various properties of adsorption in the water and benzene-E-glass systems.

An important observation about chemisorption occurring on silica surface is that surface hydroxyl groups can be replaced by halogen atoms, which change some surface properties substantially. Because of similarity in chemistry between fluoride and hydroxyl ions (i.e., approximate same size and valence) evidence for fluoride ion substitution for hydroxyl ion can be found not only in nature; e.g., in Topaz, $Al_2[F,OH]_2SiO_4$, but also in synthesized minerals (50).

There are also many evidences for substitution of fluoride ions for hydroxyl groups in glasses. Sprecht (51) showed that fluoride ions in aqueous solution are either adsorbed on the surface or bound on the lattice of borosilicate glass. In a study of wettability of soda-lime glass, Sonders et al. (52) found that a glass surface which contains ions of high polarizability, such as fluoride introduced by substitution for hydroxyl ions, becomes hydrophobic.

Elmer et al. (53) observed that in infrared spectra analysis the OH adsorption band at 2.7μm can be eliminated by the introduction of ammonium fluoride in porous glass. This fact indicates that fluoride ion substitutes for hydroxyl groups on the glass surface. They found that successively heating the fluorinated surface to 800°C causes complete removal of hydroxyl groups and the resultant surface is hydrophobic. Jorgensen and Jensen (54) also reported that the hydrogen ions of hydroxyl groups on partially-fluorinated glass and quartz surfaces are more easily ionized because of neighboring SiF groups and this consequently increases surface acidity.

The substitution of fluoride ions for hydroxyl groups will result in a stronger effect on the hydrophilic surface properties of glass if the

hydroxyl groups are removed completely. The corrosive effect of water on a hydrophilic glass surface may be reduced by fluorine compound treatment.

Ion exchange For complex glasses the modifying cations (R^+), such as the alkali ions, Na^+ or K^+, can be replaced by ionc of metals and other substances. For example, an ion exchange process with H_2O is,

$$H_2O + SiOR \longrightarrow SiOH + ROH \qquad (25)$$

in which H^+ ions diffuse into the glass to preserve the electrical neutrality as the R^+ ions diffuse out.

At higher temperature the silica network may also be disrupted by OH^- ions released in the water by dissolved R^+ ions. Charles (55) described this process occurring in the following steps.

Step 1.

$$[-\overset{|}{\underset{|}{Si}}-O-Na^+] + H_2O \longrightarrow -\overset{|}{\underset{|}{Si}}OH + Na^+ + OH^- \qquad (26a)$$

Step 2.

$$[-\overset{|}{\underset{|}{Si}}-O-\overset{|}{\underset{|}{Si}}-] + OH^- \longrightarrow -\overset{|}{\underset{|}{Si}}OH + -\overset{|}{\underset{|}{Si}}-O^- \qquad (26b)$$

Step 3.

$$[-\overset{|}{\underset{|}{Si}}-O^-] + H_2O \longrightarrow -\overset{|}{\underset{|}{Si}}OH + OH^- \qquad (26c)$$

Step 4.

$$[-\overset{|}{\underset{|}{Si}}-O-\overset{|}{\underset{|}{Si}}-] + H_2O \longrightarrow 2[-\overset{|}{\underset{|}{Si}}OH] \qquad (26d)$$

The Step 1 is evidently an ion-exchange process which breaks the very strong Si-O-Si bond. As the first three reactions are completed, excess hydroxyl ions are formed in an amount equivalent to each Na^+ ion that is no longer associated with silica. A reaction such as Step 1 gives rise to SiOH groups at the cation sites which leads to a tensile stress at the glass surface due to the marked differences in atomic volume of the Na^+ and H^+ ions.

The chemical durability of glass is a crucial property in determining the applicability of glass for uses in humid atmospheres. The rate of attack of glasses by water depends critically, and in some cases in complex ways, upon diffusion-controlled processes which are governed by parameters such as time, temperature and dissolution of the silica reaction product from the surface (27).

The attack of water on an alkali silicate glass involves ionic diffusion. Thus, reducing the rate of this diffusion should increase the chemical durability of glass. Many of the effects of glass composition on chemical durability can be understood from the changes in ion exchange mechanisms and diffusion coefficients of alkali and hydrogen ions in the glass (26).

On the other hand, when a large ion is exchanged for a smaller one at a temperature below the glass transition, a stress builds up in the exchange region, e.g., compressive stresses are set up on the surface of the glass when Na^+ ions are replaced by a large ion such as K^+ ion. Therefore, an ion exchange mechanism is one of the methods used to strengthen glass as well as rapid cooling and surface crystallization in order to produce compressive stress on the surface. The amount of strengthening by ion exchange depends on the glass composition, time, and temperature of exchange (56).

Diffusion Gas diffusion in glasses is characterized by high values for diffusion coefficient (D) and low values for the activation energy (Q_D) due to the open nature of the random structure, i.e., a low density, relatively large interstices, and the distance of individual diffusion jumps covering a range of values. The large holes, about 3 Å

diameter in the glass structure, allow the ready diffusion of small molecules such as helium and the halogens. Gas molecular diffusion is important in fining or removing bubbles from glass melts. The amount of gas dissolved in glass is proportional to the gas pressure at pressures far above that required for saturation of surface adsorption (27).

Many papers have dealt with the steady-state permeability (P) of gases through glass. The permeability of a gas in glass is equal to the diffusion coefficient times the solubility (S).

$$P = A_P \exp\left(\frac{-Q_P}{RT}\right) = DS \qquad (27)$$

where Q_P is the activation energy of permeability. The solubility of gases in glass shows a small temperature dependence and a similarity between different gases (57).

The well-known Arrhenius equation for temperature dependence of diffusion, $D=D_o\exp(-Q_D/RT)$, does not adequately describe the temperature dependence of gas diffusion in glass since the values obtained for D_o and Q_D are functions of the temperature. It has been suggested that the pre-exponential term is temperature dependent while Q_D is temperature independent and that the correct expression for the temperature dependence of diffusivity is given by the following equation.

$$D = D_o T^N \exp(-Q_D/RT) \qquad (28)$$

where N is either 1/2 or 1 (58).

Diffusion of some gases in silica are complicated by reactions of gases with the silica lattice. For instance, water vapor reacts with silica glass to form -OH groups and a proton jumps from SiOH groups to a neighboring Si-O-Si bridge followed by a jump of -OH groups. Because of

this two step process a high activation energy is required. Therefore, it was emphasized that from a strictly statistical viewpoint more than one model can satisfactorily describe the deviation from Arrhenius behavior observed for gas diffusion in glass due to the effects of a distribution of activation energies.

There are a variety of diffusion data in the literature which vary with the glass composition and the experimental method. Moulson and Roberts (59), Stephenson and Jack (60) and Hetherington and Jack (61) calculated the same order of magnitude for the diffusion coefficient of water in silica at 1000°C, i.e. 10^{-10} cm^2/sec, while Doremus (62) gave the molecular diffusion coefficient of water in fused silica at 1000°C as 3.0×10^{-9} cm^2/sec. The activation energy at 1000°C for water diffusion varies from 15 Kcal/mole to 19 Kcal/mole. Huang (63) calculated a water vapor diffusivity into E-glass of 10^{-17} cm^2/sec at room temperature from studies of adsorption rates.

In addition to temperature, the rate of diffusion depends on the interface between gas and glass including the geometrical shape of the medium, the concentration of alkali and alkaline earth ions and the character of diffusing gas and ions which occupy holes in the glass structure.

Oh and Martin (20) solved the equation for the diffusion which occurs at the surface of a glass fiber during drawing. They assumed that the diffusion coefficient was independent of concentration and was related to temperature through Arrhenious equation. The basic nonsteady diffusion equation was formulated in terms of a reduced parameter, τ, given by

$$\tau = \int_0^t \frac{D}{r^2}\,dt = \frac{\rho C_p R}{NuKQ_D}(T_o - T_\infty)D_o \exp(-Q_D/RT_o) \qquad (29)$$

Near the fiber surface the diffusion profile could be expressed by

$$\frac{C-C_\infty}{C_o-C_\infty} = \frac{1-\xi}{2\sqrt{\tau}} \qquad (30)$$

where $\xi = \frac{r_i}{r_o}$, the relative distance from the fiber axis. Equations 29 and 30 imply that the extent of diffusion at glass fiber surfaces during drawing is independent of the detailed conditions under which the fiber is manufactured. The extent of diffusion which occurs at a glass fiber surface is proportional to the fiber radius.

Effects of gas reactions on glass surface properties

The chemical composition of the surface of the glass is markedly different from that of the interior because of the following processes in complex glasses;

1. In an attempt to maintain minimum surface energy species which reduce the surface tension of the glass are concentrated in the surface layer.
2. Some constituents of glass are markedly more volatile than others, so they are lost from the surface during the forming process.
3. There may be selective solution or gas adsorption at a surface in contact with fluids or vapors. An obvious example is water which may form hydroxyl groups by ion exchange, direct reaction, or diffusion.

Considering process 1 the surface composition of a known bulk composition can be estimated from the relationship between the excess surface concentration in Equation 17a and the surface tension factors for the oxides proposed by Babcock (64) on a mole % basis and Dietzel (65), Lyon (66) and Pavlish and Mockrin (67) on wt % basis. Rubenstein (68) estimated values for surface tension factors for the oxides at 1200°C from a correlation between measured hardness and factors proposed by Lyon.

Evidence for process 2 can be found in the recent results of Auger electron spectroscopy study of E-glass fibers by Rynd and Rastogi (69). They found that E-glass fiber surfaces are low in Mg, B and Ca, but high in F, Si and Al. These results were explained by high volatility of the constituents. Process 3 should be very important in gas reactions with glass and may not be limited to complex glasses. Consideration of surface composition changes by the above processes are important in analyzing adsorption and its effect on the surface properties such as surface tension and surface viscosity.

The influence of surface tension on certain aspects of the glass making processes is of considerable importance, i.e., in refining, in the wetting of, and heat transfer between glass and mold materials. As shown by Equation 6 surface tension is one of the major parameters determining the drawing force for glass fibers. Another important effect of surface tension can be seen in the fracture strength (S) of glass in accordance with Griffith's equation (70);

$$S = [2E\gamma/c]^{1/2} \tag{31}$$

where E is the modulus of elasticity, γ is surface energy (which is equivalent to surface tension in glass) and c is the crack depth.

Unfortunately very few attempts have been made to provide a theory of surface tension of glass and its dependence on chemical composition despite its technological importance. The measurement of the surface tension of glass presents some difficulty even though a large number of methods have been applied to glass at high temperatures.

Parikh (71) investigated the effects of various atmospheres on surface tension of soda-lime glass in the temperature range 500-700°C by using a simple method, fiber elongation, and showed that water vapor exhibited the most pronounced effect, causing a lowering of the surface tension from 315 to 205 dyne/cm for a water vapor pressure of 16 mmHg.

The addition of other oxides to silica invariably lowers its viscosity. Oxides such as water in the form of -OH groups and alkali oxides are particularly effective in lowering viscosity. It is believed that the infinite network with its strong silicon-oxygen bonds is broken down by addition of impurity oxides which results in the glass becoming more fluid (72). The viscosities of different glasses vary enormously with composition and are strong functions of temperature. Present theories are quite inadequate for theoretical calculations of glass viscosity. The problems arising in measuring the viscosity of glasses involve the variation of viscosity with time and with the applied force. The exact structural nature of viscous flow is also uncertain (73).

Strength of Glass Fibers

Glass in the form of fibers is known to have physical properties that differ substantially from those of more massive specimens of glass. It is characteristic of fiber glass to yield very high strength approaching the

theoretical strength of glass. There have been many discussions of the reasons for this, but there is still controversy in this area. In general, the following distinct phenomena in glass fibers occur.

1. The surface and axial temperatures have reached the same value (room temperature) by high cooling rate, therefore, no thermally induced stress gradients will be introduced.
2. The glass structure has retained a high temperature configuration due to the rapid cooling. Consequently, the high strength of fine fibers may be due to a stress free structure or the fact that the glass maintains a high temperature configuration.

Various investigators (24,25) succeeded in producing high strength glass fibers. According to their data, the strength of flawless glass fibers is between 400 and 700 ksi. The variation can probably be explained by differences in the composition and in the structure of original glasses. However, the strength of glass fibers is affected by many factors determined by manufacturing conditions (drawing conditions) and testing conditions including drawing temperature, drawing atmosphere, thermal history, cooling rate, testing temperature, loading rate, strain rate, heating, aging, sample size, etc.

Sample size

According to Griffith's microcrack theory, glass will display a very marked dependence of strength on sample dimensions such as diameter and length due to a statistical distribution of flaws. It was a general belief that the strength of glass fibers increased significantly as their diameter decreased in accordance with Griffith's work in 1920 (70). Thomas (24)

and Otto (25) found that glass fiber strength can be independent of diameter in the range 5 to 20 μm. In contrast with their work, Aslanova and Khazanov (74) reported that strength fell rapidly with increasing diameter between 5 and 25 μm, and they concluded that glass fiber strength is related to the rate of cooling in the glass fiber drawing through its connection with the diameter of glass fibers. The diameter of fiber glass is strongly dependent on drawing speed and viscosity (temperature), i.e., on the drawing conditions as shown in the previous review of the drawing glass fibers.

Since few authors in the literature give data on the length of the fiber samples, it is difficult to analyze the strength data from different sources. Thomas (75) investigated the factors affecting the strength of glass strands and found that the average value of strength depends of the length of strand tested, i.e., a 20% reduction with an increase in gauge length from 1 inch to 16 inches.

Temperature

The effect of temperature on glass fiber strength can be discussed from different points of view; namely, the temperatures used in the manufacturing process and in the post-manufacturing process (i.e., heating and testing at temperature and heat treatment followed by testing at room temperature).

The effects of drawing temperature on strength is equivalent to the influence of diameter on strength. In other words, drawing ratio and cooling rate are governed by the drawing temperature. McKinnis and Sutton (76) showed that E-glass preheated above the drawing temperature

of 1200°C produces stronger fibers than fiber produced directly from a 1200°C melt. Otto (25) also found that increasing the drawing temperature of E-glass fiber from 1200°C to 1371°C increased the mean strength of the fibers from 250 to 480 ksi. Thomas (24) showed that the amount of scatter in tensile strength of glass fibers was reduced to less than 1% of variation by a slight increase of bushing temperature to 1340°C. Cameron (77) heated the E-glass melt above the drawing temperature (to about 1400°C) to condition the glass and produced fibers of uniform strength (mean strength of 545 ksi with a 1% coefficient of variation). He also pointed out that the high scatter in strength values with lower strength fibers resulted from the spontaneous creation of defects in the glass from stagnating with nozzle of the fiber-forming apparatus during a pause in the drawing operation.

The effects of elevated temperatures on glass fiber strength is not at all clearly understood and few results reported are consistent. Jurkov (78) in 1935 showed an increase in strength of borosilicate glass fiber from room temperature upward to 400°C, a decline in strength at still higher temperatures and no dependence of strength on diameter at 650°C. Bartenev (79) reviewed the results of several Russian workers on the temperature dependence of the strength of various glass fibers and stated that the maximum strength at certain temperatures depends on the composition.

Cameron (80) investigated the strength of glass fibers in nitrogen gas atmosphere at various temperatures below room temperature and found that the strength increased rapidly with decreasing temperature, i.e., a 50% higher strength than the normal air strength at -190°C. This

indicates that the moisture adsorbed on the glass has a very important effect on strength.

Thomas (24), Cameron (81), Otto (82) and others reported that heating in a certain range of temperature before testing caused a strength decrease. However, if mechanically damaged glass is heated to a sufficiently high temperature below the vitrification range and then annealed, the room temperature strength will increase with heating temperature even though stress corrosion during testing may increase with temperature (81). The effect of heating is associated not only with temperature and time, but also with surface conditions.

Time

The time is a very important parameter in determining the strength of any solid material either with or without stress. Its effect on strength of glass include the effects of loading time (i.e., fatigue effect), strain rate and aging.

It is known that the strength of glass increases with increasing strain rate. Slow strain rates enable a greater degree of water induced flaw growth during stressing. Thus, the variety of reported strength data should take into account the strain rates used in the tests.

Thomas (24) tested the strength of virgin fibers within a fairly narrow strain rate range and obtained strength values with very low data scatter. Recently, Thomas (75) found that the average value of strength of glass fiber strand increases linearly with increasing logarithm strain rate. More recently, the effect of strain rate on E-glass fiber strength was studied by Cameron (83) and he found that the mean strength increases

as the strain rate increases in the range 0.01 to 0.7 in/in/min and remains constant up to 1.0 in/in/min; further increases in strain rate above this value causes a strength decrease.

The dependence of the fracture stress of silicate glasses on the time of loading, e.g., fatigue effect, results from a stress-dependent chemical reaction between H_2O vapor and the surface of the glass which causes a pre-existing flaw to grow to critical dimensions for spontaneous crack propagation. In studies of the dependence of strength on the surrounding atmosphere in relation to the surface energy of glass, Orowan (84) pointed out that the fatigue effect is caused by a slow extension of Griffith cracks, this extension being dependent upon the diffusion of adsorbed moisture along the crack. Metcalfe and Schmitz (85) reported that the mechanism of static fatigue in E-glass fibers is ion exchange between alkali metal ions in the glass and hydrogen ions from either adsorbed moisture or aqueous solution that generates tension in the surface layer and noted the similarity of the static fatigue curves of fused silica due to trace amounts of Na in E-glass. Thus, many investigators (86,87) have maintained that the fatigue of glass is dependent upon environmental moisture and glass composition.

The effect of exposure to water vapor prior to stressing on strength is called aging. The aging effect is dependent on time and environmental moisture content. Thomas (24) and Cameron (81) observed that the strength of E-glass fibers stored stress free in moist atmospheres (even very low relative humidity in Thomas' work) decreased rapidly in the first few days of storage and then gradually reduced. They found little variation in the strength of E-glass fibers stored under vacuum conditions. They concluded

that any damage to the surface of fiber by moisture attack would cause a large reduction in the strength. The depth of the corrosion layer as a function of time can be estimated as indicated by Charles (55) from water in normal laboratory atmospheres diffusing into the glass. According to his corrosion rate calculations based on diffusion, a rate of 2-5 Å per hour was predicted. Recently, Bartenev (88) showed from experimental results that the depth of corrosion layer is less than the thickness of the strong surface layer and probably does not exceed 0.01 μm (100 Å).

However, opposite effects of water on the strength of damaged specimens were reported by a number of authors (87,89). They believed that high pressure steam decreases the severity of the surface flaws by a rounding out process. Proctor et al. (90) found no deterioration for pristine silica specimens after storage for 12 months in a normal laboratory atmosphere.

Recently, Burgman and Hunia (12) found a significant effect of water vapor in the fiber forming and testing environments on the strength of the fibers, i.e., a decrease in strength with an increase in moisture in the forming environment, but the data did not show the time dependence of fiber strength.

Summary of Review

It can be seen from the review of literature that gas reactions with glass fibers are of both technical and scientific importance even though there are some qualitative disagreements on certain aspects of the experimental work conducted under different drawing and testing conditions.

Glass surface reactions in the drawing atmosphere are extremely complex, involving both chemical and physical reaction processes. The mechanisms of gas-glass reaction include not only adsorption but also diffusion processes. However, the following comments may be made;

a. The final diameter of a fiber drawn from a constant diameter of nozzle is the most important parameter controlling the history of glass fiber. The cooling rate which determines the transformation temperature in the forming process is a strong function of final diameter and the mechanical strength measured in terms of tensile strength may also depend on final diameter. Therefore, accuracy in measuring the final diameter by using the best methods of electron microscope was essential in this work. However, the final diameter can be controlled by the strong dependence of temperature on viscous flow. Since the cooling rate is also a function of heat transfer properties such as Nusselt number and thermal conductivity of the drawing atmosphere, the influence of various gas atmospheres on drawing glass fiber may be seen in the observed jet shapes and by the measured strength of glass fibers. Thus, jet shape analysis in various gas atmospheres is necessary.

b. Due to large range of reaction temperature, the mechanisms of initial gas-glass reaction in the drawing atmosphere may be a combination of chemical and physical adsorption. The nature of both chemical and physical adsorption is dependent on the surface structure such as surface hydroxyl groups which are formed rapidly from dangling bonds of freshly formed silicate surface. Thermal

history and pretreatment of glass fiber surfaces play a most important role in the study of gas adsorption behavior. Thus, adsorption isotherm and infrared adsorption analysis are very helpful in analyzing the gas-glass reactions.

c. The process following gas adsorption is a gas diffusion process which will depend strongly on the concentration differences between the glass fiber and the gas atmosphere in the drawing and testing environments, i.e., the gases may either diffuse into or diffuse out of the glass. Thus, the diffusion data for selected gases and physical and chemical surface properties of glass fibers should be determined.

d. Surface corrosion by the attack of water vapor depends on surface hydroxyl groups formed by ion-exchange process, which leads to a tensile stress on the glass surface. However, these hydroxyl groups can be replaced completely by fluoride ions at high temperature making the surface hydrophobic. This fact indicates that the surface corrosion can be either prevented or reduced by fluoride treatment.

e. There are many controllable factors affecting the strength of fine glass fibers. However, in order to determine the effect of gases on glass fibers variables of the manufacturing and post-manufacturing conditions should be minimized, i.e., constant drawing temperature, drawing speed, strain rate and moisture content for aging and testing. By this means significant discrepancies in the measured strengths for different gas treatments will be

reduced. The resistance to corrosion as a function of time, i.e., aging effect, will be influenced by the gas reactions.

MATERIALS

E-glass Marbles

E-glass is a common type of glass used in glass fiber production. "E" stands for electrical, as the composition has high electrical resistance due to the nearly alkali-free composition. It is known that the strength of E-glass fibers is almost independent of diameter under certain conditions (2).

E-glass in marble form of 2.5 cm diameter was provided by the Owens-Corning Research Center at Granville, Ohio. Its chemical composition and selected physical properties are shown in Table 1. The volume of an E-glass marble is about 9 cm^3.

Table 1. Chemical composition and selected physical properties of E-glass (91)

1)	Composition	wt%		Composition		wt%		
	SiO_2	54.5		Na_2O		0.5		
	Al_2O_3	14.5		K_2O				
	CaO	17.5		TiO_2		0.5		
	MgO	4.5		Fe_2O_3		0.3		
	B_2O_3	8.5		F_2		0.3		
2)	Annealed bulk density: 2.60 gm/cc							
3)	Surface tension: 303 dyne/cm at 1200°C 313 dyne/cm at 1430°C							
4)	Viscosity (poise)	3310	1260	563	282	159	93	56
	Temp. (°C)	1149	1204	1259	1315	1371	1427	1483

A chemical analysis of the E-glass marbles used in this work was also conducted by the Analytical Services Laboratory, Engineering Research Institute, Iowa State University. The results of the chemical analysis are shown in Table 2.

Table 2. Chemical composition of E-glass marble

Composition	wt%	Limits %
SiO_2	53.98	± 0.15
Al_2O_3	13.90	± 0.20
CaO	18.10	± 0.60
MgO	3.80	± 0.08
Na_2O	0.63	± 0.02
B_2O_3	5.50	± 0.30
F_2	0.42	± 0.02

Distilled Water

The distilled water used for the water vapor drawing atmosphere was obtained from a laboratory distillation apparatus, F. J. Stokes Machine Co., Philadelphia, Penn. This distilled water was also used for making a constant solution of NaOH in the humidity-controlled aging chamber.

Freon-14 Gas (carbon tetrafluoride)

Freon-14 (CF_4) gas was selected as a fluorine compound due to its simple chemical formula. Freon-14 gas was obtained from Matheson Gas Products Co., Milwaukee, Wisconsin. Freon-14 is extremely stable, reacting slightly even at the temperature of a carbon arc and is generally

resistant to oxidizing and reducing agents except under very drastic conditions. Freon-14 reacts with alkali metals at about 400°C giving the metal fluoride and carbon and reacts with carbon dioxide at temperatures above 1000°C giving carbonylfluoride. Other chemical and physical properties are available from the manufacturer (92).

The spontaneous reaction of Freon-14 gas with silica glass at higher temperature (i.e. 1000°K) can be predicted from the free energy of formation for each of the participating compounds in the following equation (93).

$$SiO_2 \text{ (glass)} + CF_4 \xrightarrow[\Delta F^o = -137 \text{ Kcal/mole}]{1000^\circ K} SiF_4\uparrow + CO_2\uparrow \quad (32)$$

Sodium Hydroxide

Since one effect of dissolving a salt in water is to depress the vapor pressure of the water, sealed chambers containing constant solutions of certain salts are often used as a simple method providing atmosphere of known humidities. A pure sodium hydroxide salt, reagent grade, obtained from General Chemical Division, New York, was used for this purpose and the vapor pressure of water over various solutions was available in the literature (94).

METHODS OF INVESTIGATION

Preliminary Work

Properties of E-glass

Thermal Analyses To investigate the thermal properties of the marbles used for fiber drawing, TGA and DTA were conducted using a Rigaku thermal analyzer, Rigaku Denki Co. Ltd, Tokyo, Japan. In addition to TGA and DTA a differential-thermogravimetric analysis (DTGA) curve was obtained by plotting the loss in weight per degree rise in temperature against temperature, which is essentially a plot of the slope of the corresponding thermogravimetric analysis curve.

A piece of an E-glass marble, ground in a mortar to about 100 mesh, was weighed in a platinum crucible. The weight of the E-glass marble powder was 51.3 mg. It was heated in an air atmosphere at a rate of 40°C/min but cooled at a lower rate since it was difficult to cool at a constant rate greater than 28°C/min. The temperature was monitored by a platinel thermocouple.

Density The bulk density (ρ_b) of E-glass marble was measured by employing the following water immersion method, which is based on the bulk volume (V_b) (95)

$$\rho_b = W_d/V_b = W_d\ \rho_\ell/(W_s - W_{ss}) \tag{33}$$

where W_d = Unsaturated (dry) weight of sample

W_s = Saturated weight of the sample

W_{ss} = Weight of the saturated sample when it is submerged in the liquid with a density ρ_ℓ.

The density of fiber glass was also measured accurately by the pycnometric method (96). A weighed amount of fiber (W_s) was introduced into a pycnometer of known volume (V_p = 25 cc but it was calibrated at a different testing temperature) and distilled water of known density (ρ_ℓ) was added to the reference mark. Weighing of the empty (W_p) and filled pycnometer with liquid (W_T) and fiber are used to compute the density as follows:

$$\rho_s = \frac{\rho_\ell W_s}{V_p \rho_\ell + W_p + W_s - W_T} \tag{34}$$

Viscosity and activation energy The activation energy of E-glass for viscous flow was computed from the manufacturer's data (91). The activation energy of E-glass can be calculated from the flow rate of E-glass fibers drawn under known drawing conditions as shown in reference (23).

The viscosity calculated from this method is the approximate viscosity at the nozzle due to the complicated situation in the orifice because of nonuniform temperature distribution. The activation energy was calculated from the flow rate by measuring the final diameter at different drawing temperatures.

Glass Fiber Drawing

E-glass marbles cleaned by acetone were melted and fibers were drawn from a special device known as a single hole platinum bushing. This platinum drawing crucible was designed in consultation with personnel of the Owens-Corning Research Center and technical personnel at Mathy-Bishop Inc., Malvern, Pa.--the manufacturer of the crucible. The drawing crucible

or bushing (shown in Figure 3) which has a capacity of about 50 cc and a nozzle of 0.132 cm internal diameter and 0.40 cm in length is heated by resistance and is maintained at constant drawing temperature by an automatic controller monitored by means of thermocouples welded near the nozzle. Since the thermocouples do not measure the actual glass temperature, the actual drawing glass temperature at the tip of the nozzle was calibrated by optical pyrometer (radiation type) as a function of thermocouple temperature. The results of this calibration are shown in the Appendix.

As the glass flows from the cylindrical nozzle within a temperature range of 1100°C to 1300°C, it is attenuated into a solid filament and wound on a rotating mandrel driven either by a variable or a single speed motor. A hand held fused-quartz rod was used to catch a small blob of molten glass at the nozzle and draw it downwards. It was then connected to the double-stick taped drum which was already rotating beneath the bushing.

In order to draw filaments in a controlled atmosphere, the drawing crucible and mandrel were completely enclosed in a hermetically sealed plexiglass chamber with suitable air locks and dry box gloves to permit operation of the equipment. A total of eight feed-throughs for gases and eight electrical feed-thoughs were incorporated into the chamber. The total chamber volume was about 13 ft^3, but the actual gas-occupied volume of the inside of the chamber was measured as described in the Appendix.

The fiber glass drawing apparatus and its schematic diagram are shown in Figures 4 and 5.

Figure 3. Platinum drawing crucible

Figure 4. Experimental apparatus for glass fiber drawing

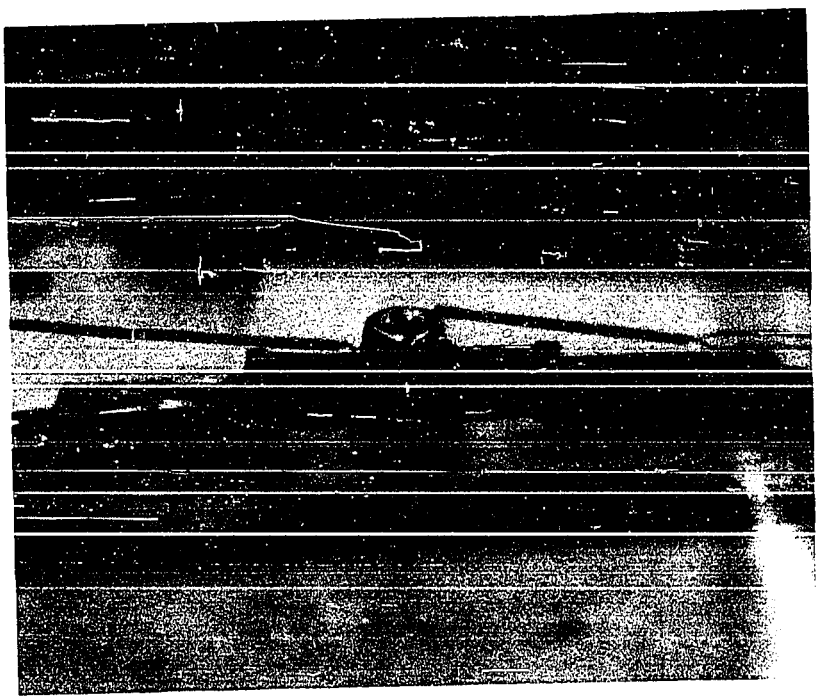

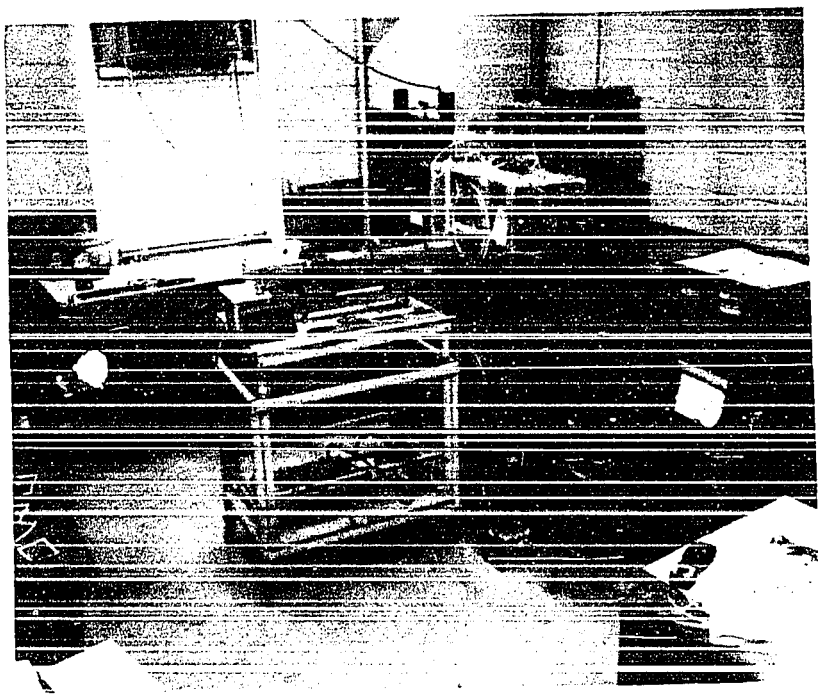

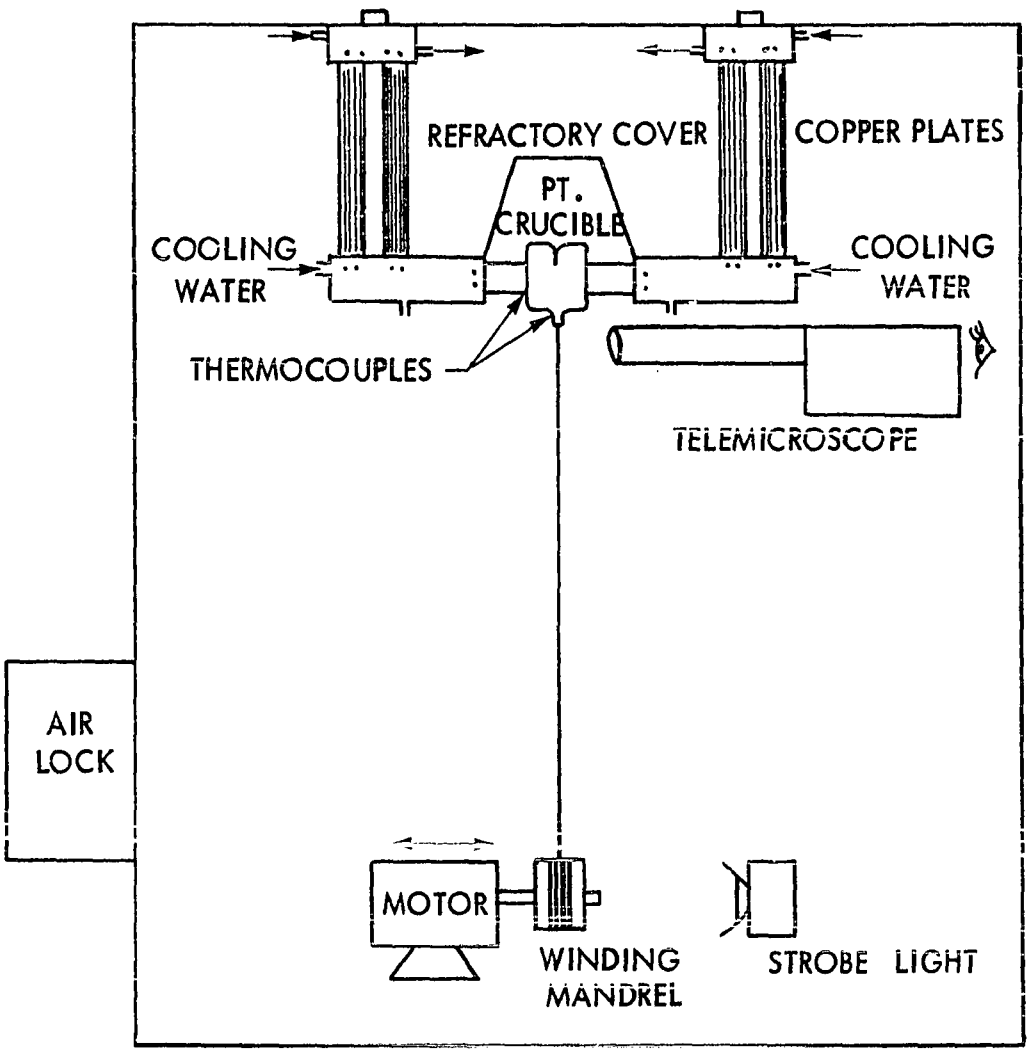

Figure 5. Schematic drawing of the experimental apparatus.

Drawing Gas Atmospheres

Water vapor atmosphere

High humidity High humidity atmospheres were created by means of exposure of distilled water to air in the completely sealed drawing chamber. One hundred percent relative humidity was obtained from distilled water stored in the chamber overnight. To control the partial pressure of the atmosphere during heating, the distilled water was held in insulated containers with lids and all cooling water pipelines in the chamber were wrapped by insulating materials. The psychrometer was calibrated by measuring wet and dry bulb temperatures as described in the Appendix.

Low humidity For the low humidity tests the glass fiber was drawn in room air at a relative humidity ranging from 25 to 35 percent.

Freon-14 gas atmosphere

The chamber was typically dried for Freon-14 gas treatment by means of $CaSO_4$ desiccant driers, Drierite, the W. A. Hammond Drierite Co., Xenia, Ohio, which had been baked up to 200°C. Very low relative humidity was obtained and Freon-14 gas was introduced into the drawing chamber. The desired concentration of Freon-14 gas in the drawing chamber was computed as described in the Appendix and was maintained at a constant concentration during drawing of glass fibers. Figure 6 is a schematic diagram of the Freon-14 gas supply into the drawing chamber.

Since no information is available about the toxicity of Freon-14 gas at higher temperatures (even though it is known to have a low order of

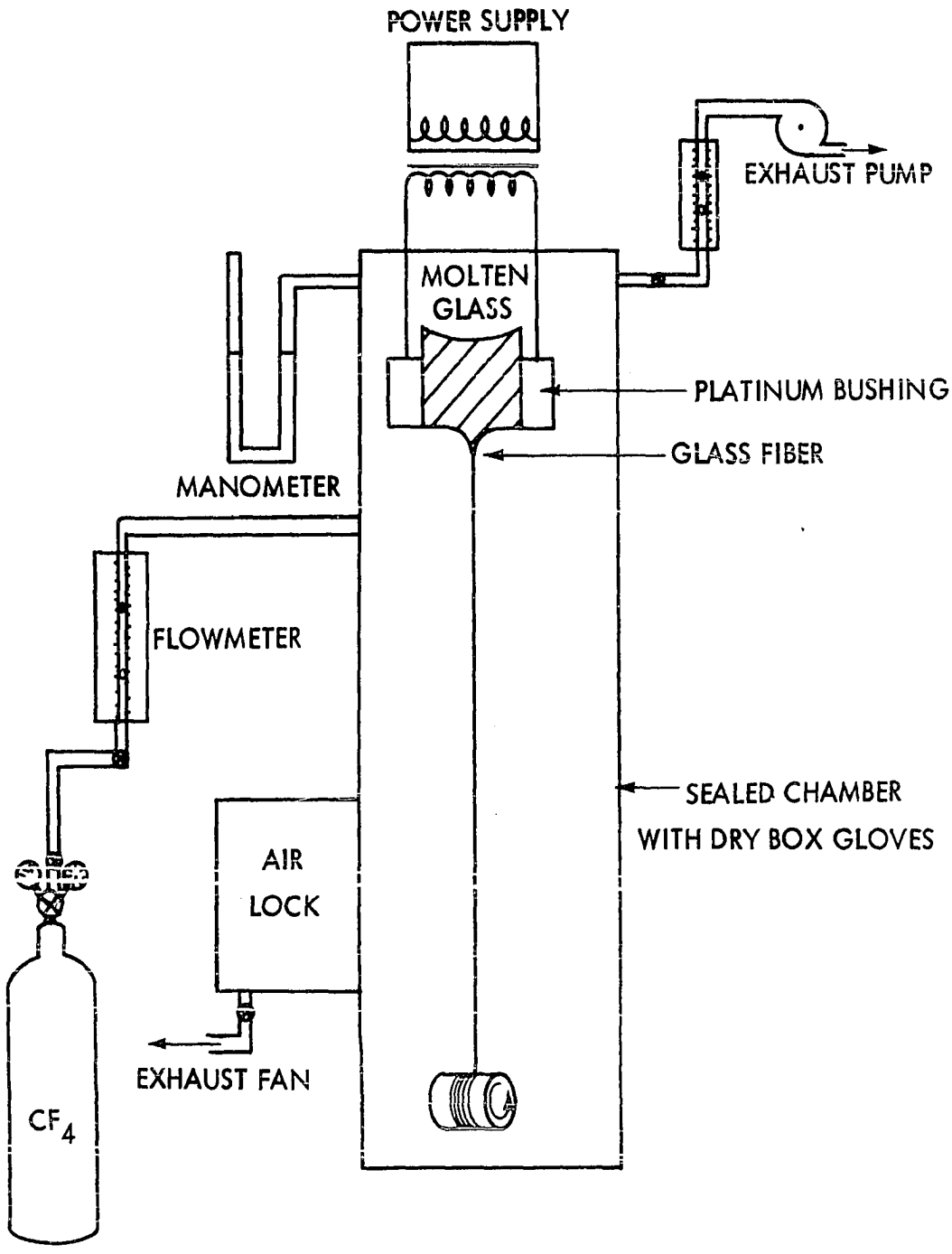

Figure 6. Freon-14 gas supply.

toxicity at room temperature), a gas mask was worn during this gas treatment for safety. Prior to the work white mice were introduced around the Freon-14 gas atmosphere chamber to insure safety.

Specimen Preparation and Measurement of Tensile Strength

In order to determine the effect of selected drawing atmospheres on the strength of glass fibers, glass fibers in different atmospheres were drawn under basically constant drawing conditions, i.e. drawing temperature, drawing speed, head of glass and the diameter of nozzle. If not held constant, these parameters may affect the mechanical strength of the glass fiber due to different cooling rates. However, one uncontrolled variable was the environmental temperature in the drawing chamber, which varied with the heating time of platinum crucible, i.e. environmental temperature varied from 25 °C to 35 °C in the case of closed chamber atmosphere, but this should have a small effect on cooling rate.

The drawing temperature was decided by the relationship between temperature and the desired fiber diameter from Equation 15. The temperature controller, West Instrument Co., Schiller Park, Ill., was set at 1200 °C which corresponded to 1265 °C actual glass drawing temperature from the calibration of temperature as shown in the Appendix. The crucible was heated by manually controlling the current passing through the bushing. The temperature was raised at a rate of approximately 200 °C every 5 minutes until the desired drawing temperature had been reached.

To maintain constant drawing speed a voltage regulator, Stableline, The Superior Electric Co., Bristol, Conn., was used for the variable speed motor, but there was still a 5 percent variation in speed when measured

with a strobe light. The fibers for tensile strength tests were drawn by using a single speed motor, Bodine Electric Co., Chicago, Ill., which had a constant speed of 1850 rpm. A constant drawing speed of 1046 cm/s was obtained by winding on a 10.8 cm-diameter drum.

By measuring the depth of the crucible from the top edge to the glass surface the head of glass above the base of the bushing was determined and was maintained at a constant level by adding an amount of E-glass powder computed from the glass mass flow rate.

An undamaged single filament was collected by an I-shaped collecting wood frame with two small arms faced with a strip of double stick Scotch tape. The frame was brought through the gap between the bushing tip and the drum. A fine single filament was visible under the lamp located in the front of the drawing chamber. The fine fiber filament collected by hitting with the collecting frame from a constant position was placed carefully with the collecting frame on the top of a slotted black paper strip so that the filament was centrally positioned along the length of the paper. Then the filament was glued to the paper strip for the tensile strength test specimens as shown in the following figure.

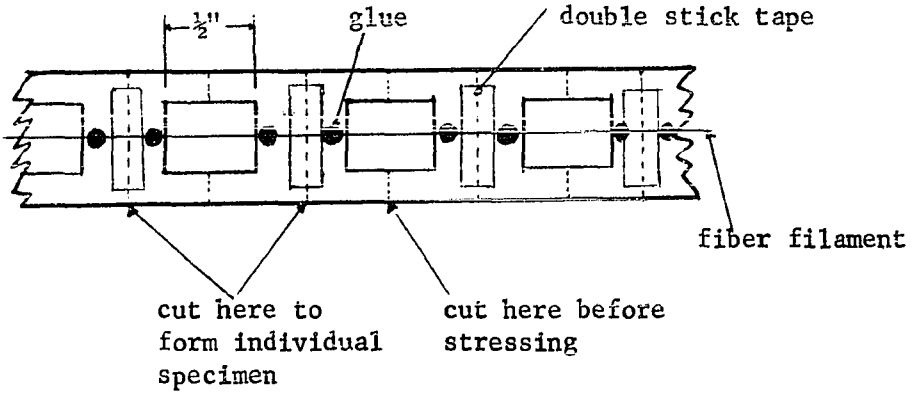

Figure 7. Details of specimen paper mount

Super Strength Adhesive "Scotch," 3M Co., St. Paul, Minn., was used for zero-day aging specimen which was actually aged in the room atmosphere for at least 1.5 hours due to the minimum setting time of the glue. However, it was not used for longer-time aging specimens due to the high vapor pressure of the allyl isothiocyanate contained in the glue. Epoxy glue from the same source was used for long-time aging specimens and the strip was stored in a chamber maintained at 36% R.H. by means of a constant NaOH solution for the desired aging periods (see Appendix).

After aging for the desired time the mounted fiber strip was cut into 10 individual specimens and the tensile strength was measured for each of the fibers drawn in different drawing atmospheres and aged for certain periods. To eliminate moisture attack on glass fiber from breath during specimen preparation a mask covering the mouth and nose was used. The sample specimen preparation desk was equipped with a fluorescent lamp with a magnifying lens so that heat from an ordinary lamp was eliminated.

The measurement of tensile strength of glass fiber was conducted in the temperature-humidty controlled testing room with a floor model Instron Universal Testing Machine, Canton, Mass. The room was maintained at 21°C and 35% R.H. as described in the Appendix. The strain rate was set at 0.2 cm/min and a type CM load cell which has a tension load range of 0-100 gm full scale was used. The load calibration was checked before each test. An individual specimen with paper strip frame was inserted into the screw action grips, type 1B, and tightened. Before cutting the holder part of the paper frame with scissors the cross head was raised to avoid the introduction of tension on the fiber prior to stressing.

Microscopic Observation

The accurate measurement of fiber diameter is very important in determining the final properties of glass fiber such as cooling rate and strength of fibers. A Zeiss Microscope was used for this purpose with both transmitting and reflecting polarized images at magnification of 1000X, but it was hard to focus on the edge of the glass fiber due to the limited depth of field even though a drop of immersion oil (which has a refractive index just slightly different from E-glass) was placed on the fiber in order to reduce edge effects.

A scanning electron microscope (SEM), Model JSM-U3, Japan Electron Optic Co., Japan, calibrated with a standard grid, was used to determine the final fiber diameter with an accuracy of $\pm$ 0.15 μm at a magnification of 3000X. Carbon-gold evaporation in an Edwards Vacuum Evaporator, was necessary to make the glass fiber conductive for SEM observation. The thickness of coated carbon and gold was estimated to be 500 Å.

The glass jet was observed through a telemicroscope, American Optical Co., which has a long focal length with an eye piece containing a 7X lens. The image was enlarged an additional 5 times, giving a total magnification of 35X. The jet was photographed using a polaroid camera and the radius of the jet was determined in this experiment by enlarging the negative from 5 to 10X.

PRESENTATION OF RESULTS

Preliminary Work

Properties of E-glass

Thermal analyses Thermal analyses, including TGA, DTA, and DTGA were carried out in order to investigate the thermal behavior of E-glass. The results of the thermal analyses are shown in Figure 8. The heating rate of 40 °C/min was the same as the heating rate of platinum drawing crucible. The cooling rate was set at 40 °C/min but it was found that it was impossible to keep a constant high cooling rate by means of convective heat loss. Because of slow cooling rate, the tests were terminated after cooling to 500 °C. The time-temperature curve indicates the cooling rate was 28 °C/min in the region of the glass transition. The transformation temperature at a heating rate of 40 °C/min was estimated to be 730 °C but at a cooling rate of 28 °C/min the transformation temperature was found to be 700 °C.

The weight loss, as measured by an analytical balance after first heating to 1000 °C, was 1.56%; however, the TGA curve showed a weight gain of 0.35% after heating to 1000 °C and cooling to 500 °C.

Density The results of bulk density of E-glass marbles as measured by water immersion method are shown in Table 3. In order to obtain a high degree of accuracy, the weighed test pieces were boiled in distilled water for two hours for complete saturation. The average value of density is 2.558 gm/cm^3 with a variation of 0.82%. Also in Table 3 the bulk density of E-glass marbles is compared with the density of E-glass fibers measured by the pycnometric method.

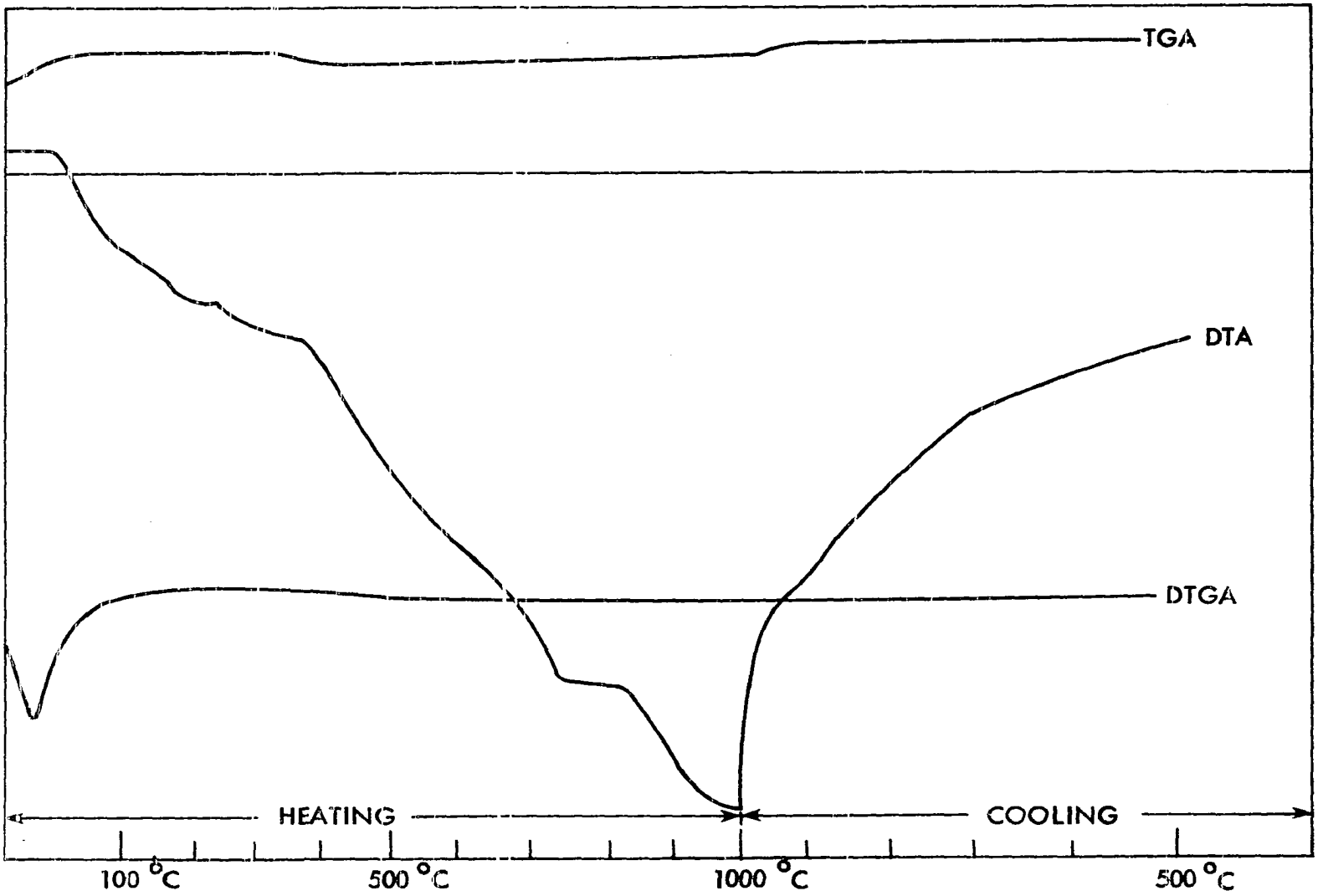

Figure 8. Thermal analysis of E-glass.

Table 3. Densities of E-glass bulk and fiber (in gm/cc)

	1	2	3	4	5	Avg.	σ	α(%)
Bulk	2.537	2.597	2.547	2.542	2.568	2.558	0.021	0.82
Fiber	2.4493	2.5042	2.5120	2.4945	2.5026	2.5025	0.006	0.24

Viscosity and activation energy The activation energy for viscous flow of E-glass is 59,900 cal/mole with variation of about 10% determined by plotting the manufacturer's data in Table 1 against the reciprocal temperatures as shown in Figure 9. The viscosity equation for the E-glass used in this experiment as computed by least squares method from the manufacturer's data (91) was:

$$\eta \text{ (in poise)} = 1.798 \times 10^{6} \exp(30,134.75/T\ ^{\circ}K). \tag{34}$$

The approximate activation energy for viscous flow in fiber drawing can be determined from Equation 15, i.e.

$$r_f^2 = \left(\frac{K'}{\eta v}\right) = \frac{K'}{v} \frac{1}{\eta_o e^{Q/RT}} = A \exp(-Q/RT) \tag{35a}$$

or

$$- \log r_f^2 = - \log A + \frac{Q}{2.303R} \frac{1}{T\ ^{\circ}K} \quad . \tag{35b}$$

By plotting the measured final diameters versus the reciprocal drawing temperatures in Figure 10, the activation energy was found to be 58,400 cal/mole.

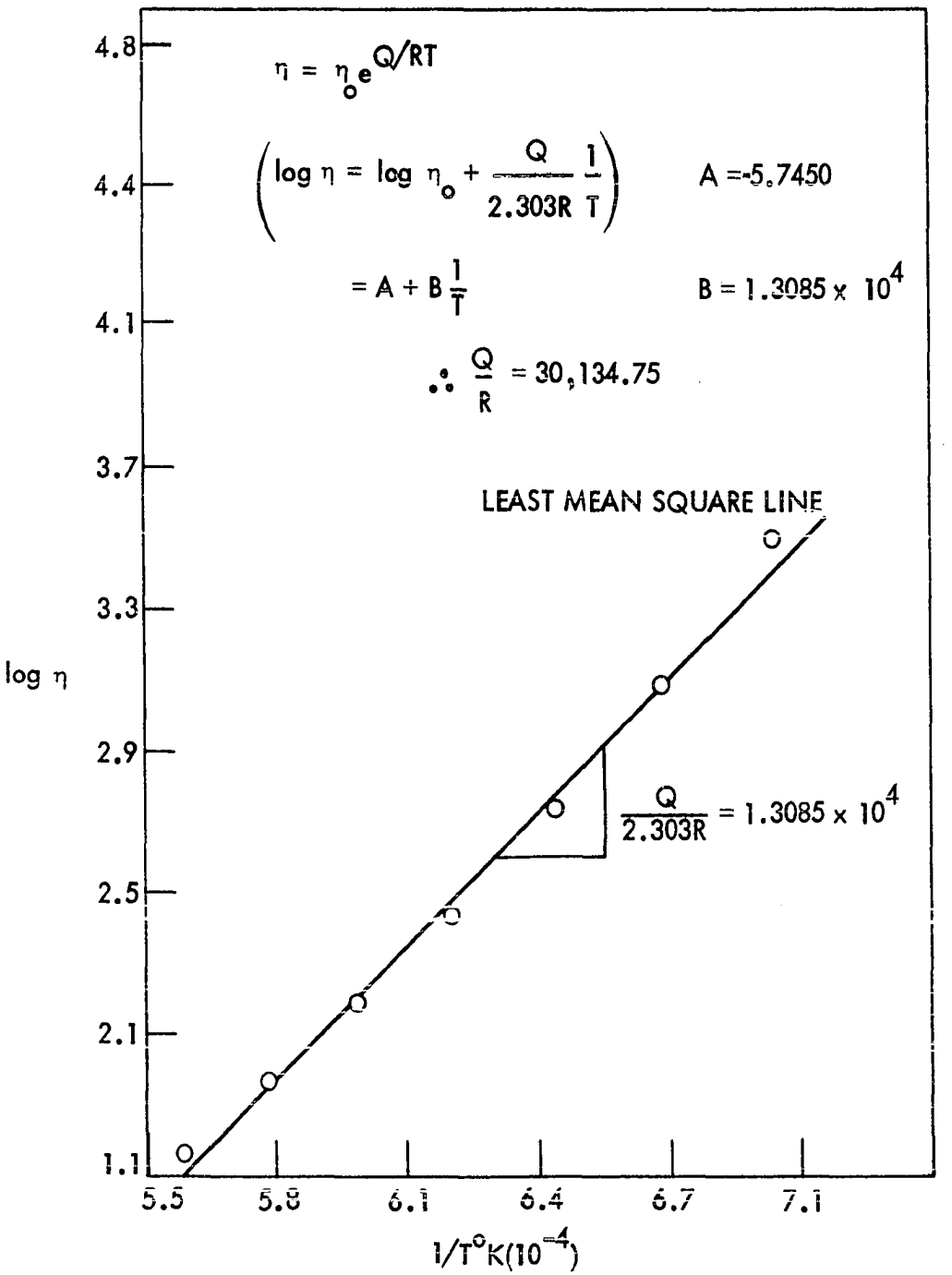

Figure 9. Viscosity of E-glass as a function of temperature (Manufacturer's data).

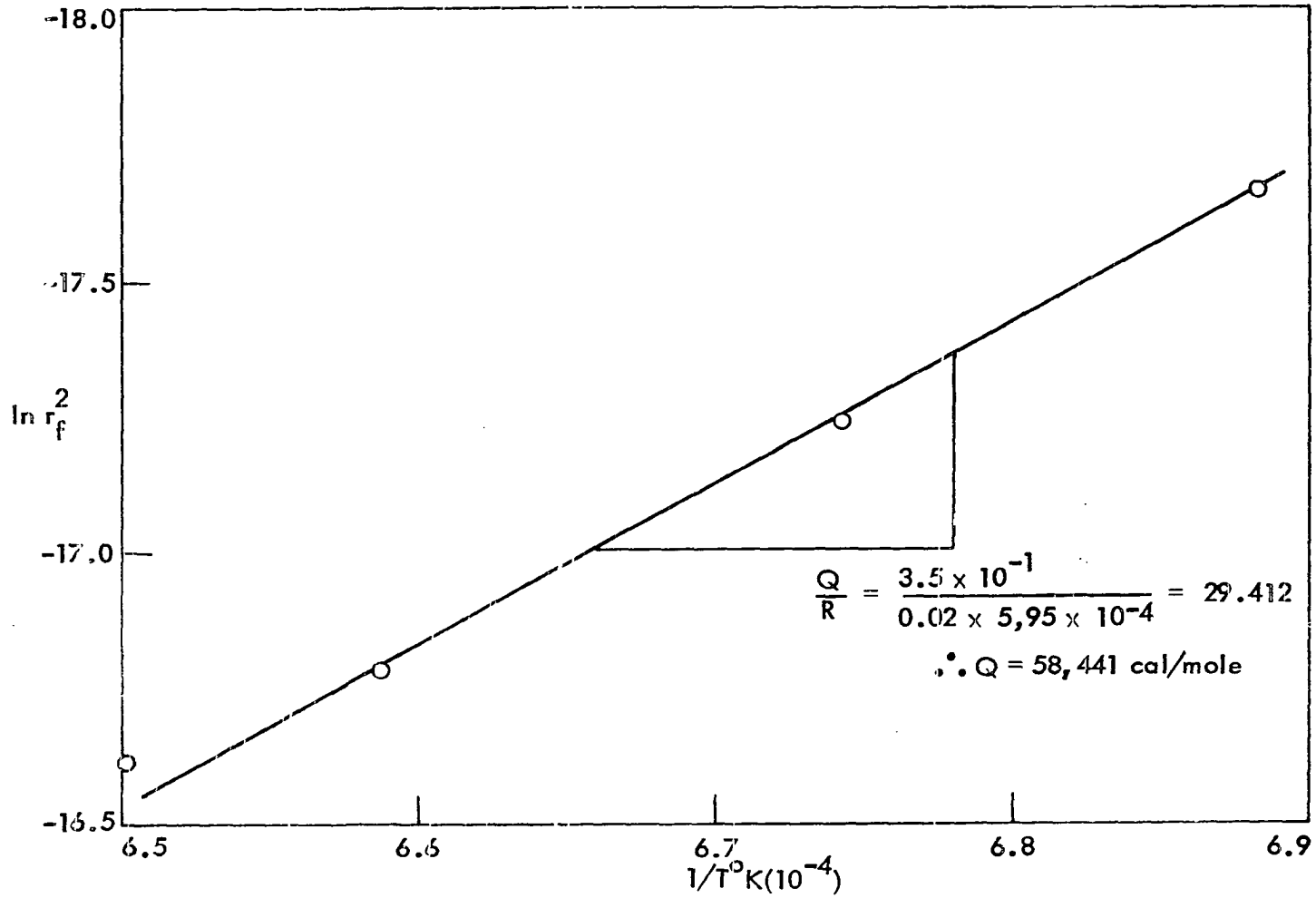

Figure 10. Data for activation energy calculation from the measured diameter.

Drawing Conditions

Diameter of glass fiber The drawing constant K' in Equation 12 was calculated from the measured flow rate under certain drawing conditions. K' was 6.648×10^{-3} gm. cm^2/sec^2 when the head of glass was 1.70 cm. Table 4 and Figure 11 show the final fiber diameters as functions of drawing temperature and drawing speed. For example, a 5μm diameter fiber could be produced at drawing temperature of 1265°C with a drawing speed of 1045 cm/sec (obtained by using 33.8 cm circumference drum with 1855 rpm motor).

Table 4. Calculated diameters of fiber as function of drawing temperature and drawing speed at a glass head of 1.70 cm (in μm)

Speed (cm/sec)	1207°C	1218°C	1253°C	1278°C	1325°C
1045	3.34	4.00	4.62	5.40	7.13
946	3.51	4.20	4.86	5.68	7.49
844	3.72	4.45	5.14	6.01	7.93
742	3.97	4.74	5.48	6.41	8.46

The final diameters of glass fibers were measured by a Zeiss microscope and a Jeol JSM-U3 Scanning Electron Microscope. Figure 12 shows typical micrographs of glass fibers used for measurement of diameter. The results of measured diameters as a function of drawing temperature and drawing speed are given in Tables 5 and 6 and are also compared with calculated values.

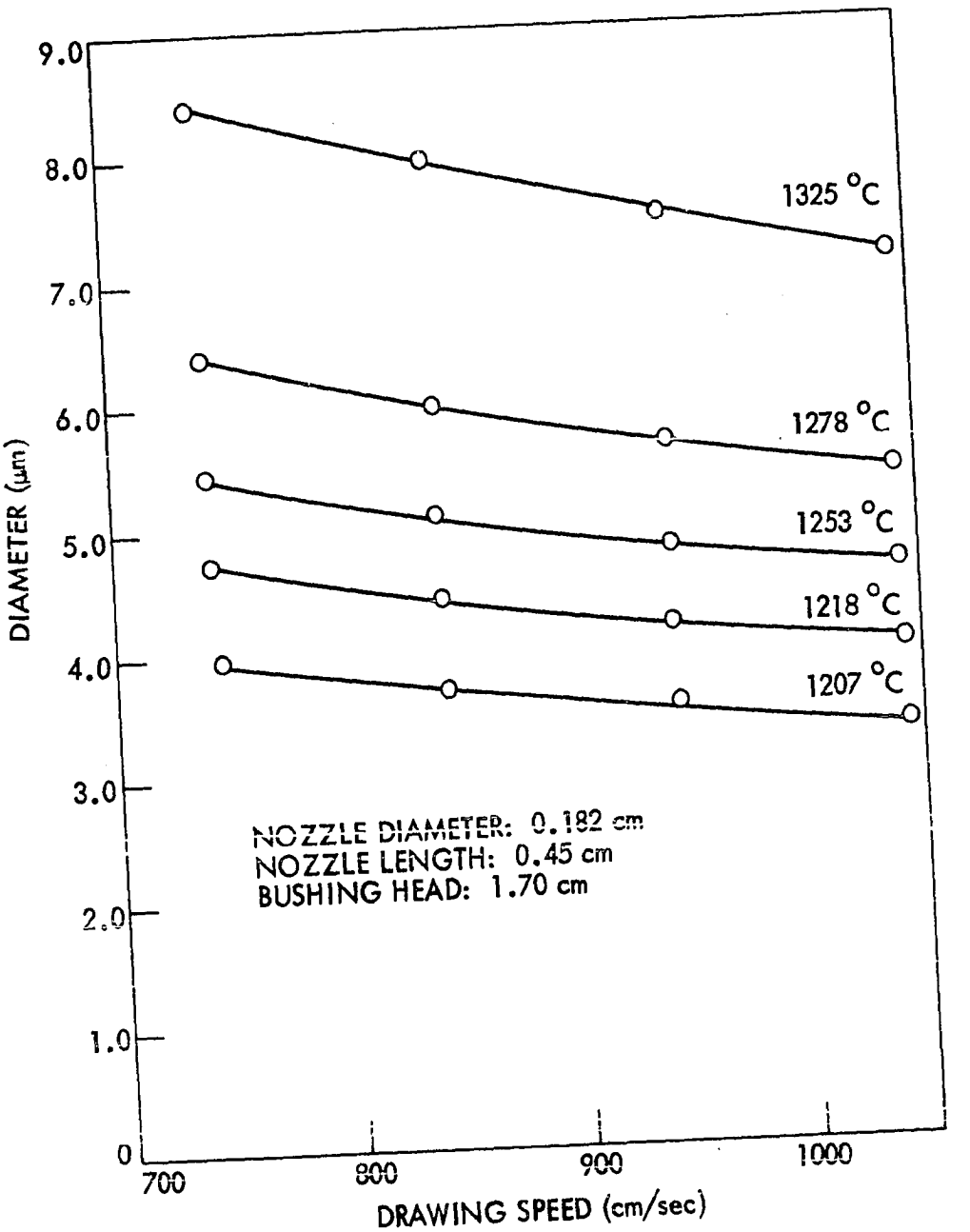

Figure 11. Glass fiber diameter as a function of temperature and drawing speed.

Figure 12. Micrographs for glass fiber diameter measurement

a) Zeiss microscope (x1000)
   (i) Transmitted image
   (ii) Polarized reflecting image

b) SEM (x3000)

(a)

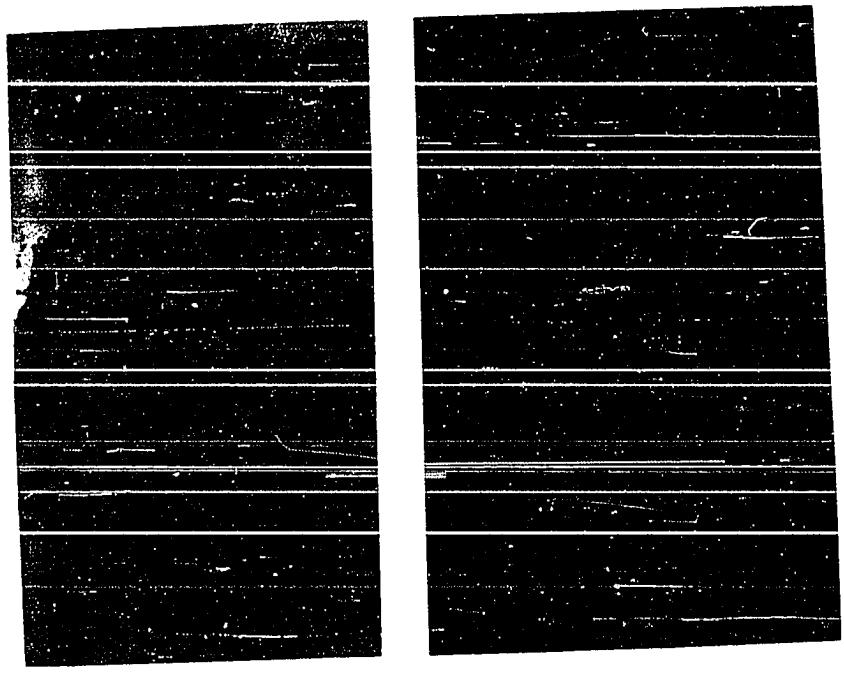

i) ii)

(b)

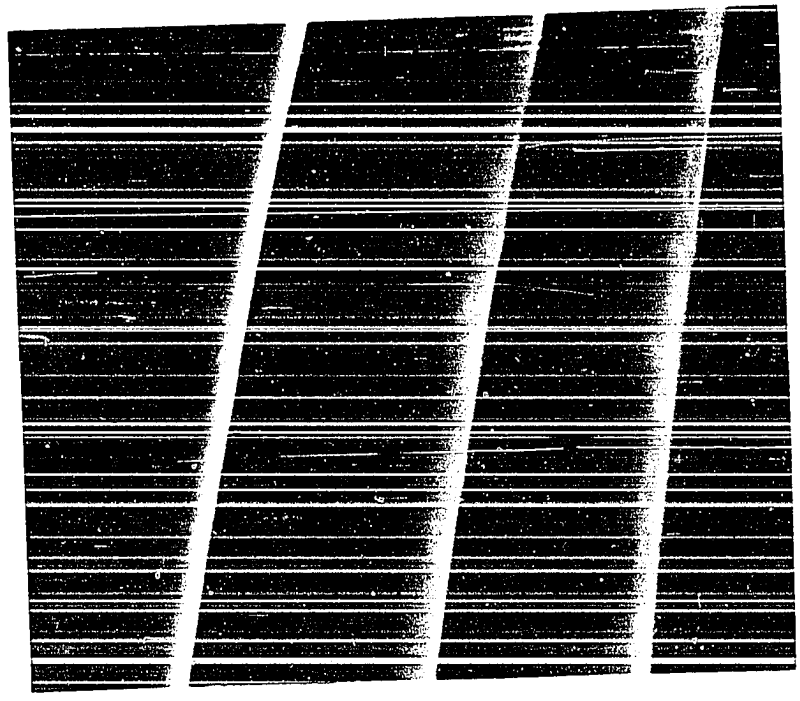

Table 5. Measured average diameters of fiber glass at a drawing speed of 1045 cm/sec

Diameter (μm)	1265°C	1245°C	1210°C	1180°C
Measured	4.91	4.53	3.60	2.90
Predicted	4.85	4.37	3.49	2.85

Table 6. Measured average diameters of fiber glass at T_o = 1240°C

Diameter (μm)	Speed (cm/s) 1045	946	844	742
Measured	4.47	4.63	4.77	4.82
Predicted	4.25	4.46	4.73	5.04

From the measured diameter data, the activation energy for viscous flow was computed by plotting $\ell n\ r_f^2$ versus 1/T°K (as shown in Figure 10). The computed activation energy was 58,400 cal/mole which is approximately the same value as computed from the viscosity data which was provided from the maker (Figure 9).

Flow rate The mass flow rate of the glass was measured by weighing the glass fiber produced per unit time. Table 7 shows the measured weight of fiber drawn in one minute at constant drawing temperature (1225 °C) as a function of drawing speed. From the average weight of glass fiber per minute, the average mass flow rates at different drawing speeds were calculated and are shown in Figure 13, the results were independent of the drawing speed.

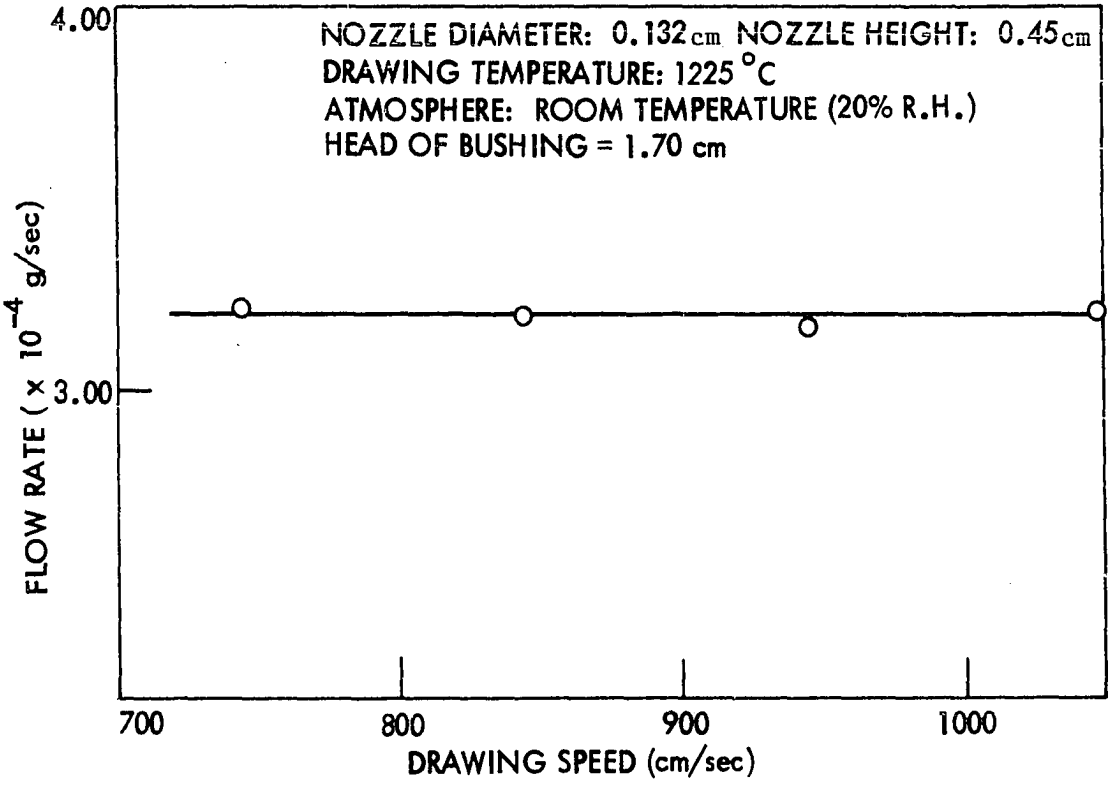

Figure 13. Mass flow rate as a function of drawing speed.

Table 7. Weight of drawn fiber per minute and average mass flow rate

Diameter (μm)	Weight (10^{-2} gm)						Flow rate (10^{-4} g/s)
	1	2	3	4	5	Avg.	
1045	1.95	2.05	1.92	1.87	2.02	1.96	3.26
946	1.91	1.91	1.88	1.90	2.00	1.92	3.20
844	1.91	1.96	1.92	1.91	1.92	1.92	3.20
742	1.91	1.92	1.95	1.98	1.93	1.94	3.23

Jet shape The upper jet shapes observed in this experiment were concave as shown in Figure 14 and 15 and were independent of drawing temperature and drawing speed even though the sizes varied with drawing temperature at constant drawing speed. As shown schematically in Figure 16, the sizes of the jets decreased remarkably with drawing temperature at constant drawing speed, while at different drawing speed at constant drawing temperature the jet shapes remained constant.

The radii of the observed upper jet shapes as functions of axial distance from the nozzle are tabulated in Table 8. The actual locations of the jet origins were determined by plotting $\ell n\ \ell n\ r/r_f$ versus z as shown in Figure 17 and Table 9. The drawing ratios at different drawing temperatures were replotted as a function of actual axial distance as shown in Figure 18.

The drawing ratios of the observed upper jet shape as a function of the drawing temperature were compared with that of theoretical jet shapes predicted from Equation 9c as shown in Figure 19. The Nusselt numbers (Nu) used in these calculations were determined from the slopes of the

Figure 14. Jet shapes for different drawing temperatures at constant drawing speed (v = 1045 cm/s)

a) T_o = 1265 °C

b) T_o = 1245°C

c) T_o = 1210°C

d) T_o = 1180°C

(a)

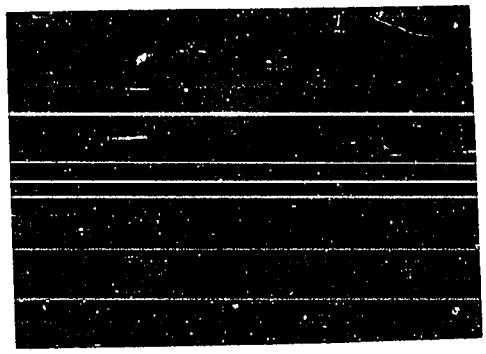

(b)

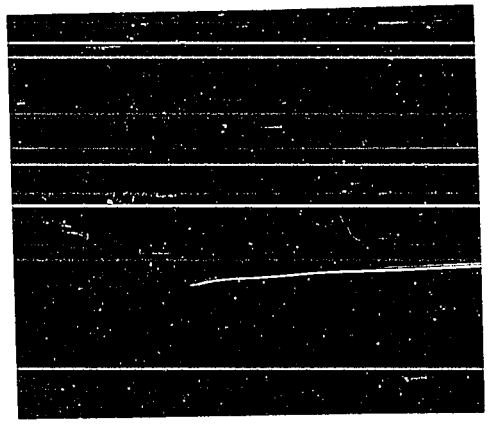

(c)

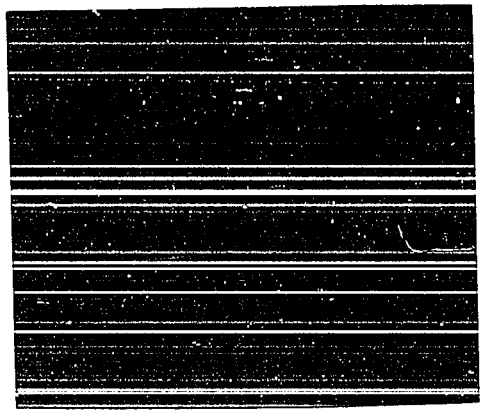

(d)

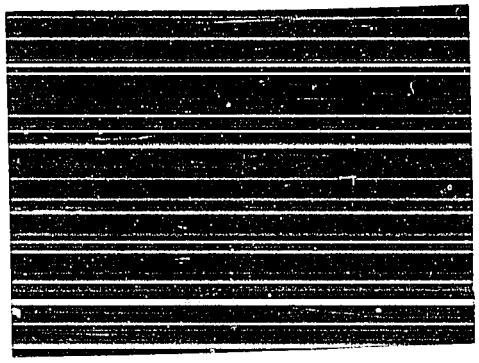

Figure 15. Jet shapes for different drawing speeds at constant drawing temperature (T_o = 1265°C)

a) v = 1045 cm/s

b) v = 946 cm/s

c) v = 844 cm/s

d) v = 742 cm/s

(a)

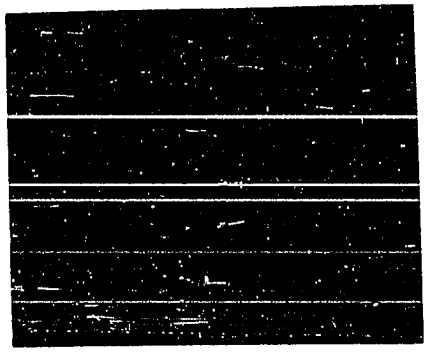

(b)

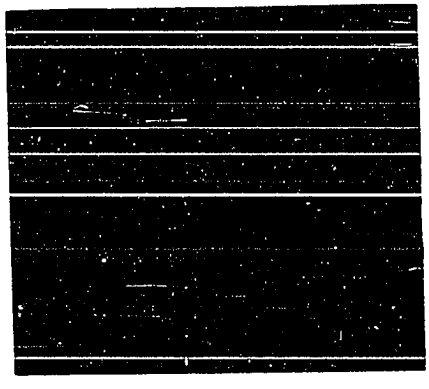

(c)

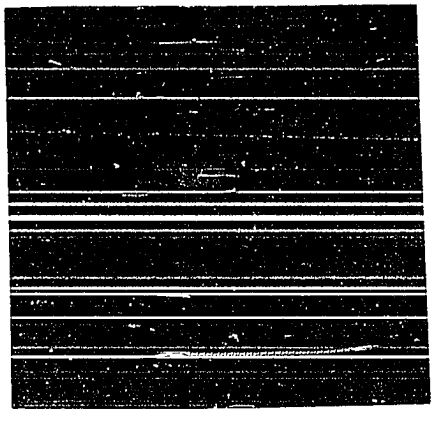

(d)

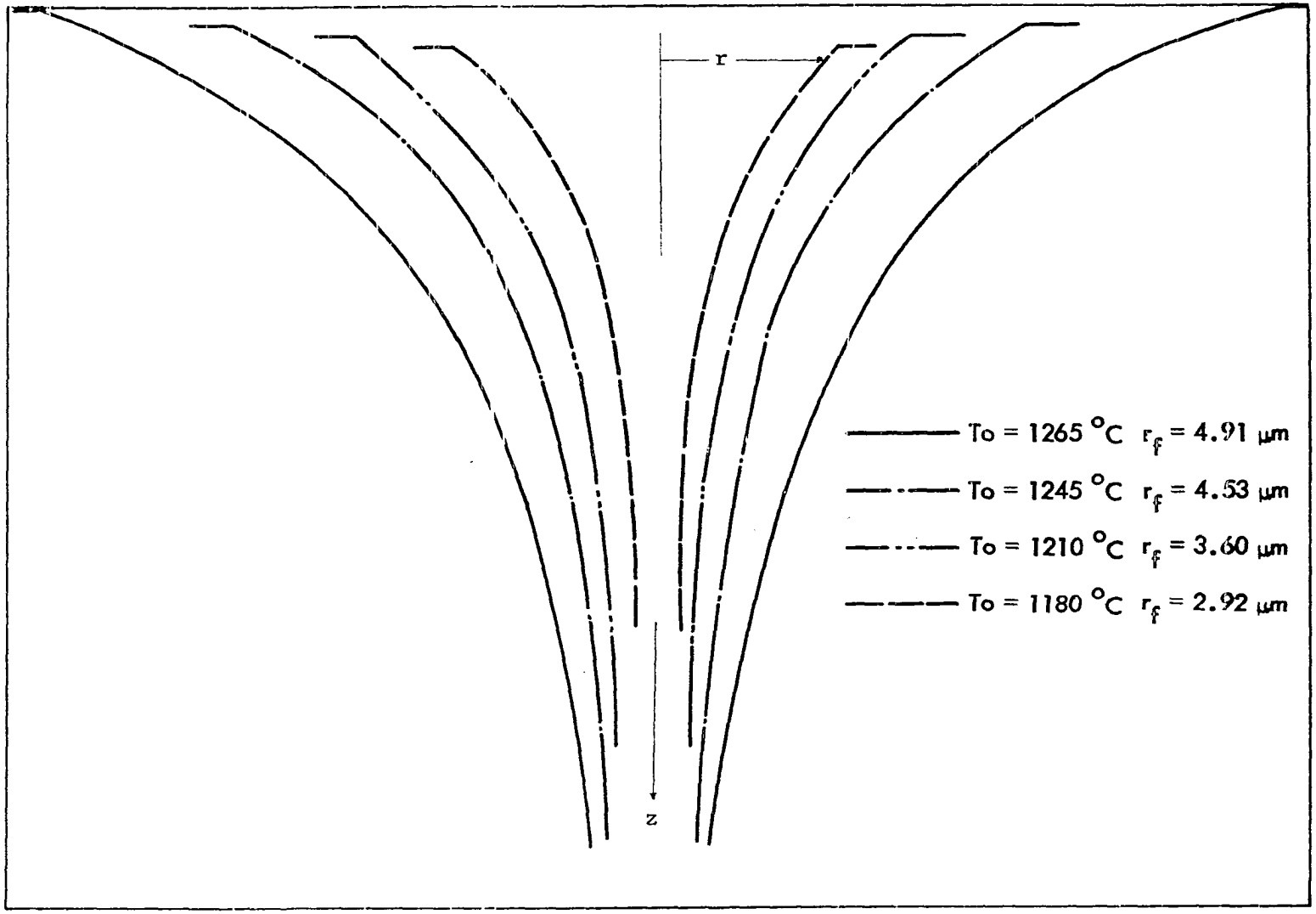

Figure 16. Jet shapes at different drawing temperatures.

Table 8. Jet shapes with drawing temperatures (v = 1045 cm/sec)

1			2		
T_o=1180°C	r_f=1.46 x 10^{-4}cm		T_o=1210°C	r_f=1.80 x 10^{-4}cm	
z(x10^{-3}cm)	r(x10^{-3}cm)	$\ell n \ell n\ r/r_f$	z(x10^{-3}cm)	r(x10^{-3}cm)	$\ell n \ell n\ r/r_f$
0.0	10.71	1.45	0	15.17	1.48
3.57	7.41	1.36	3.92	11.07	1.41
7.14	5.17	1.27	7.84	8.35	1.34
10.71	3.83	1.18	11.76	6.19	1.26
14.28	2.80	1.08	15.68	4.73	1.18
17.85	2.14	0.98	19.60	3.83	1.11
21.42	1.66	0.88	23.52	3.21	1.05
25.00	1.42	0.82	27.44	2.67	0.99
28.57	1.25	0.76	31.36	2.41	0.95
32.14	1.19	0.74	35.28	2.12	0.90

3			4		
T_o=1245°C	r_f=2.265 x 10^{-4}cm		T_o=1265°C	r_f=2.455 x 10^{-4}cm	
z(x10^{-3}cm)	r(x10^{-3}cm)	$\ell n \ell n\ r/r_f$	z(x10^{-3}cm)	r(x10^{-3}cm)	$\ell n \ell n\ r/r_f$
0	21.60	1.51	0	44.60	1.59
5.0	14.82	1.43	5.35	23.21	1.51
10.0	10.67	1.34	10.71	16.87	1.44
15.0	7.89	1.26	16.07	14.46	1.40
20.0	6.25	1.19	21.42	9.87	1.30
25.0	5.01	1.13	26.78	7.85	1.24
30.0	4.12	1.06	32.14	6.25	1.17
35.0	3.46	1.00	37.49	5.03	1.10
40.0	2.94	0.94	42.85	4.16	1.04
45.0	2.55	0.88	48.21	3.41	0.96

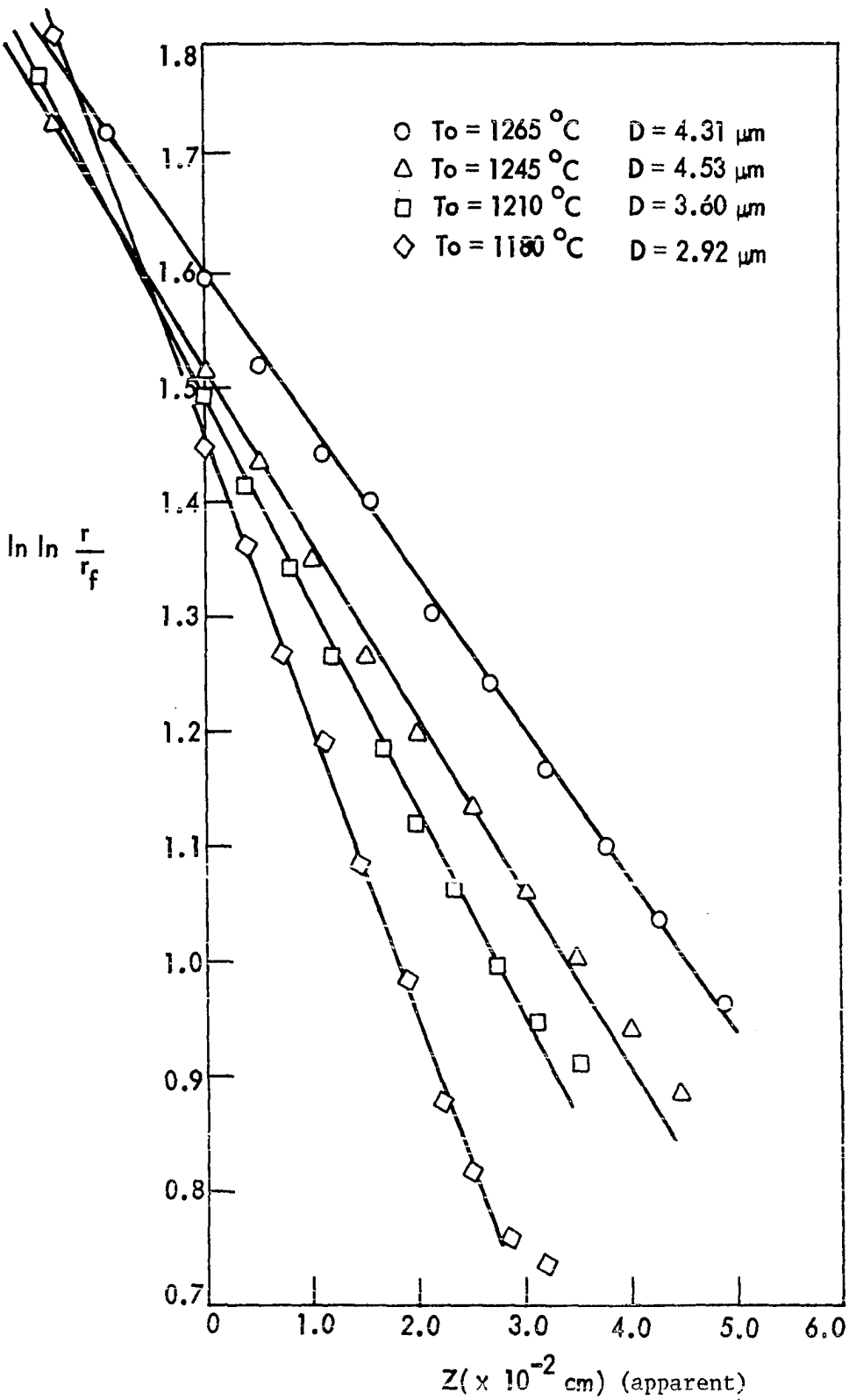

Figure 17. Drawing ratio as a function of axial distance and determination of jet origin.

Table 9. Drawing ratios as a function of actual axial distance

1			2		
T_o=1180°C	r_f=1.46 μm	K=24.998	T_o=1210°C	r_f=1.80 μm	K=17.855
$\ell n \ell n\ r/r_f$	$z(10^{-2}cm)$	$Kz(10^{-2}cm)$	$\ell n \ell n\ r/r_f$	$z(10^{-2}cm)$	$Kz(10^{-2}cm)$
1.81	0	0	1.77	0	0
1.45	1.40	3.49	1.48	1.55	2.76
1.36	1.75	4.39	1.41	1.94	3.46
1.27	2.11	5.28	1.34	2.33	4.16
1.18	2.47	6.17	1.26	2.72	4.86
1.08	2.82	7.06	1.18	3.11	5.67
0.98	3.18	7.96	1.11	3.51	6.26
0.88	3.54	8.85	1.05	3.90	6.96
0.82	3.90	9.74	0.99	4.29	7.66
0.76	4.25	10.64	0.55	4.68	8.36
0.74	4.61	11.53	0.90	5.07	9.06

3			4		
T_o=1245°C	r_f=2.265 μm	K=15.487	T_o=1265°C	r_f=2.455μm	K=13.332
$\ell n \ell n\ r/r_f$	$z(10^{-2}cm)$	$Kz(10^{-2}cm)$	$\ell n \ell n\ r/r_f$	$z(10^{-2}cm)$	$Kz(10^{-2}cm)$
1.73	0	0	1.72	0	0
1.51	1.40	2.16	1.59	0.85	1.13
1.43	1.90	2.94	1.51	1.38	1.84
1.34	2.40	3.71	1.44	1.92	2.56
1.26	2.90	4.49	1.40	2.45	3.27
1.19	3.40	5.26	1.30	2.99	3.98
1.13	3.90	6.03	1.24	3.52	4.70
1.06	4.40	6.81	1.17	4.06	5.41
1.00	4.90	7.58	1.10	4.59	6.13
0.94	5.40	8.36	1.04	5.13	6.84
0.88	5.90	9.13	0.96	5.67	7.56

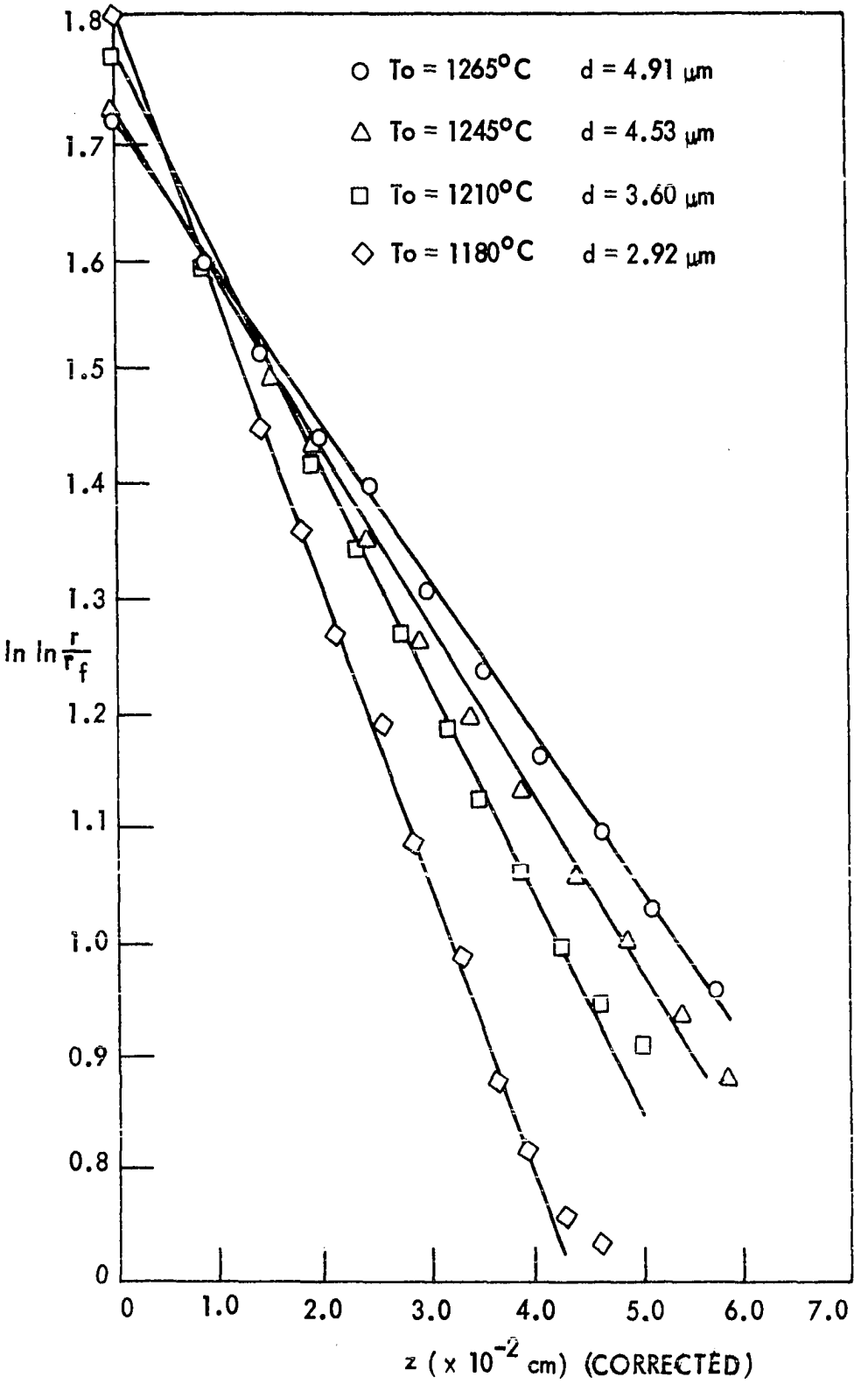

Figure 18. Drawing ratio as a function of actual axial distance.

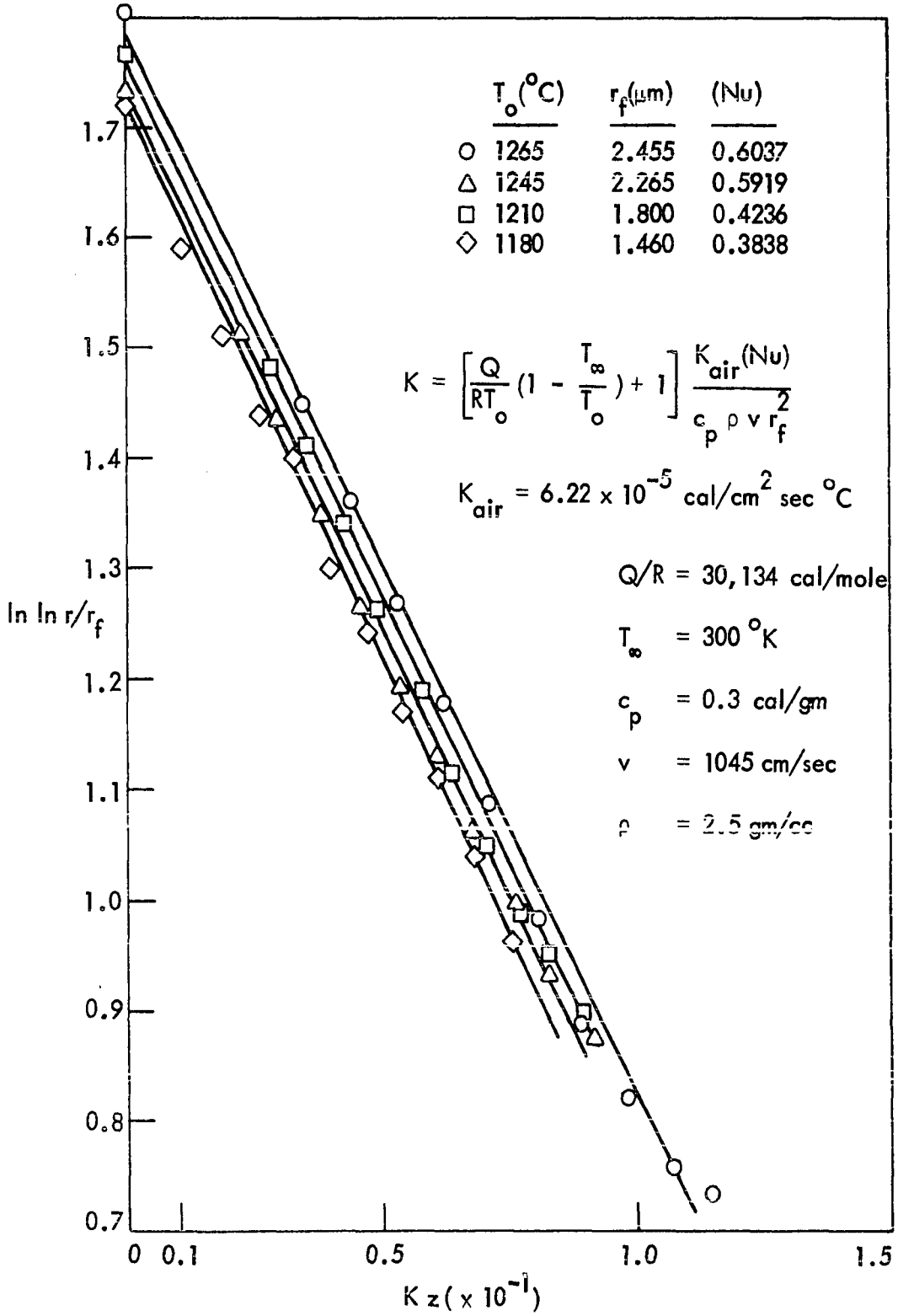

Figure 19. Comparison of theoretical and experimental jet shapes.

lines in Figure 17 under the assumption of constant heat transfer properties such as specific heat and thermal conductivity of environmental atmosphere (air).

Gas effects on E-glass fiber

Adsorption isotherm analysis Adsorption isotherm analysis is useful to evaluate the effects of gas drawing atmosphere on the adsorption of water in a controlled aging atmosphere. The adsorption isotherm analyses for this work, including the determination of weight of adsorbate and BET surface area, were done by Mr. Mufit Akinc, Engineering Research Institute, Iowa State University. By employing basic gravimetric systems such as Cahn type R. G. Electrobalances the weight of adsorbate was determined as a function of the pressure of the adsorbate. Figure 20 shows the experimental adsorption kinetics of water on fibers drawn in different gas atmospheres, i.e. the weight gained plotted as a function of aging period at constant vapor pressure.

Table 10 summarizes the results of calculated BET area and heat of adsorption for E-glass fibers drawn in the different atmospheres. The geometrical surface areas were calculated from the known fiber diameters.

Table 10. The results of adsorption isotherm analysis

Drawing atmosphere	No. exposure to $p/p_o = 1$	Geometrical Area	BET Area	ΔH(cal/mole) for monolayer
Room atmosphere	1	0.347 m^2/g	0.65 m^2/g	2400
(p/p_o =	2	"	0.76 m^2/g	2600
0.35 H_2O)	3	"	0.80 m^2/g	2850
CF_4 atmosphere (p/p_o=0.02 H_2O)		0.432 m^2/g	3.42 m^2/g	3550

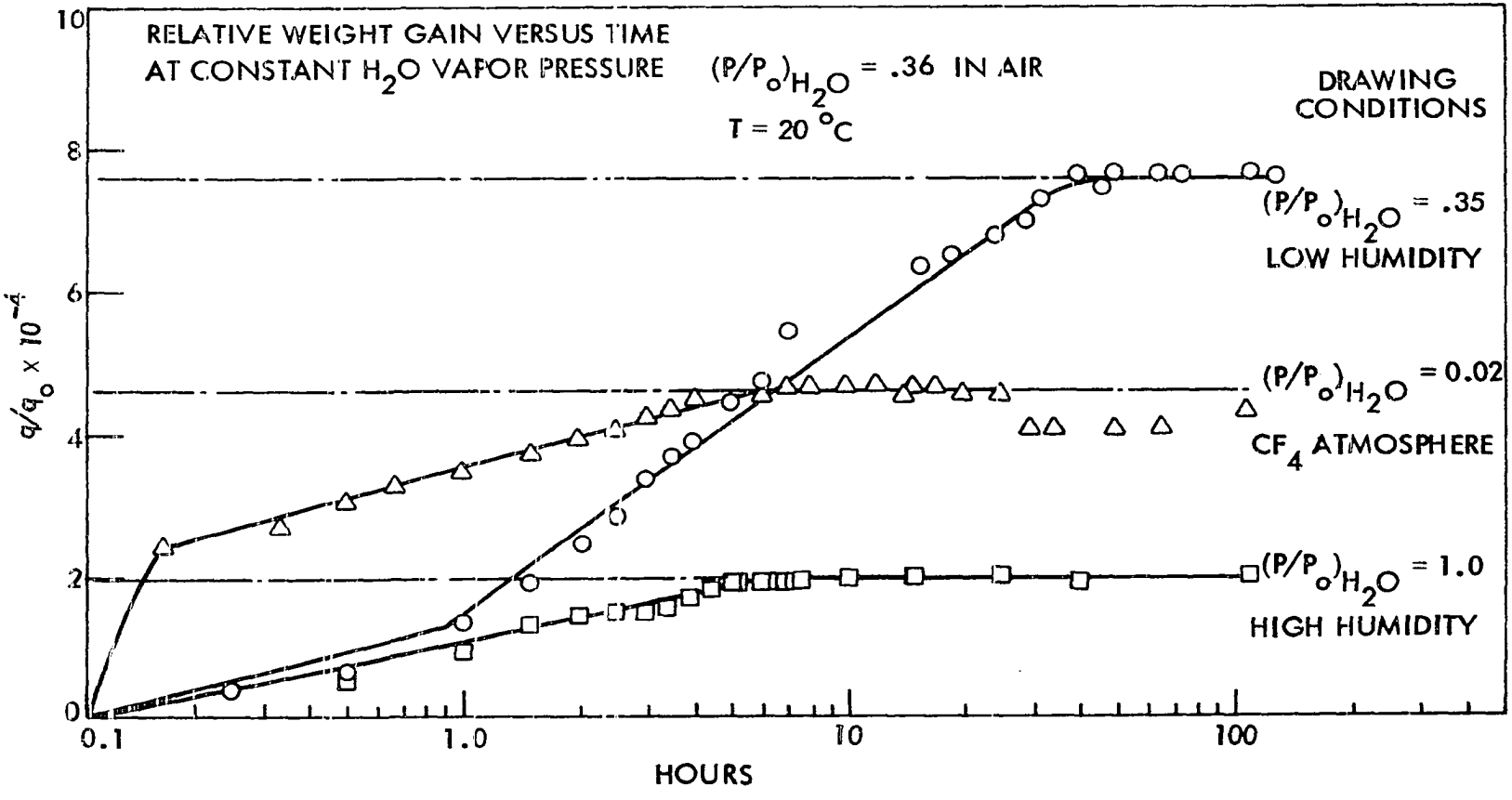

Figure 20. Weight gains due to adsorbed water as a function of aging time.

Tensile strength Filaments of E-glass fibers were individually mounted on a paper strip which provided 10 individual testing samples for the Instron Testing Machine. It took about 30 minutes to prepare sample specimens and the minimum setting time of "Super Strength" glue used for zero-day aged samples was 1.5 hr so that total time of preparation of specimens for zero-day aged groups was about 2 hours. Other groups of sample specimens were stored in the humidity control chamber (36% R.H.) for the desired aging period from one-half day to 30 days.

Tensile strengths of the glass filaments for each group were calculated from the maximum breaking load measured in the Instron Testing Machine at a strain rate of 0.2 cm/cm/min. Most individual sample specimens were broken completely throughout the gauge length of specimen at maximum breaking load in a manner similar to tempered glasses. However, one or two of 10 individual specimens did not show the complete break and had the lowest breaking load among the group of specimens. This fact indicates that those specimens could have been accidentally damaged during the preparation of specimen, such data were not used in this work.

The most significant variable of this experiment is the measurement of fiber diameter since any error in diameter measurement will seriously influence the calculated strength (load divided by the cross-section area of the fiber, e.g. a 0.5 micron error for a 5 micron fiber changes the strength by 20%). The measured diameters of fibers drawn in different atmospheres and aged for different periods vary from 3.5 to 5.8 microns (SEM, 3000X) even though the main diameter controlling parameters such as drawing speed and drawing temperature were kept constant throughout the experiment. Diameter is not uniform along a single filament.

The smallest diameter measured from the micrographs of the broken fiber filament was used in calculating the stress.

The slopes of stress and strain curves in the measurement of the tensile strengths were not uniform as shown in Figure 21. The elastic modulii of E-glass fibers in different groups were calculated from the curves and some groups showed high variation in calculated elastic modulii. This may be due to nonuniform gauge length of the specimens or different fiber diameters.

The summaries of data for all experiments are presented in the Appendix. The data are also presented, where possible, in a graphical form in Figures 22 through 24, including comparisons between the present writer's work and that of other authors.

Jet shape To determine the effect of selected gas atmosphere on glass forming conditions, the upper jets at the bushing nozzle tip were observed. Constant drawing conditions were employed during the observation (i.e. T_o = 1265 °C and v = 1045 cm/s).

Figure 25 shows the upper jets observed through the telemicroscope in the different drawing atmospheres (i.e. high humidity, low humidity and CF_4 gas atmospheres) during glass fiber drawing. No noticeable changes in upper jets with the different atmospheres were observed in this experiment.

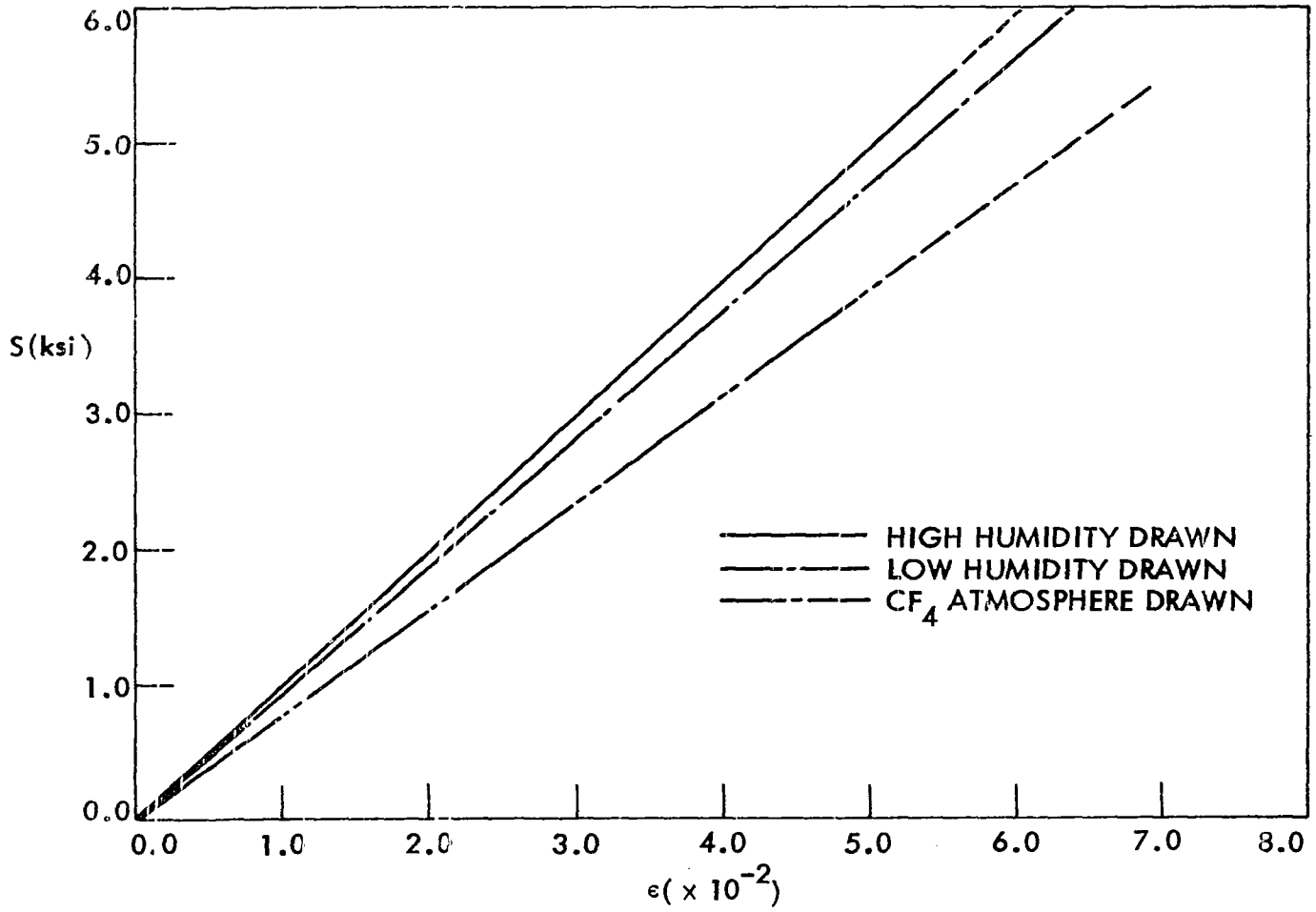

Figure 21. Typical stress and strain curves.

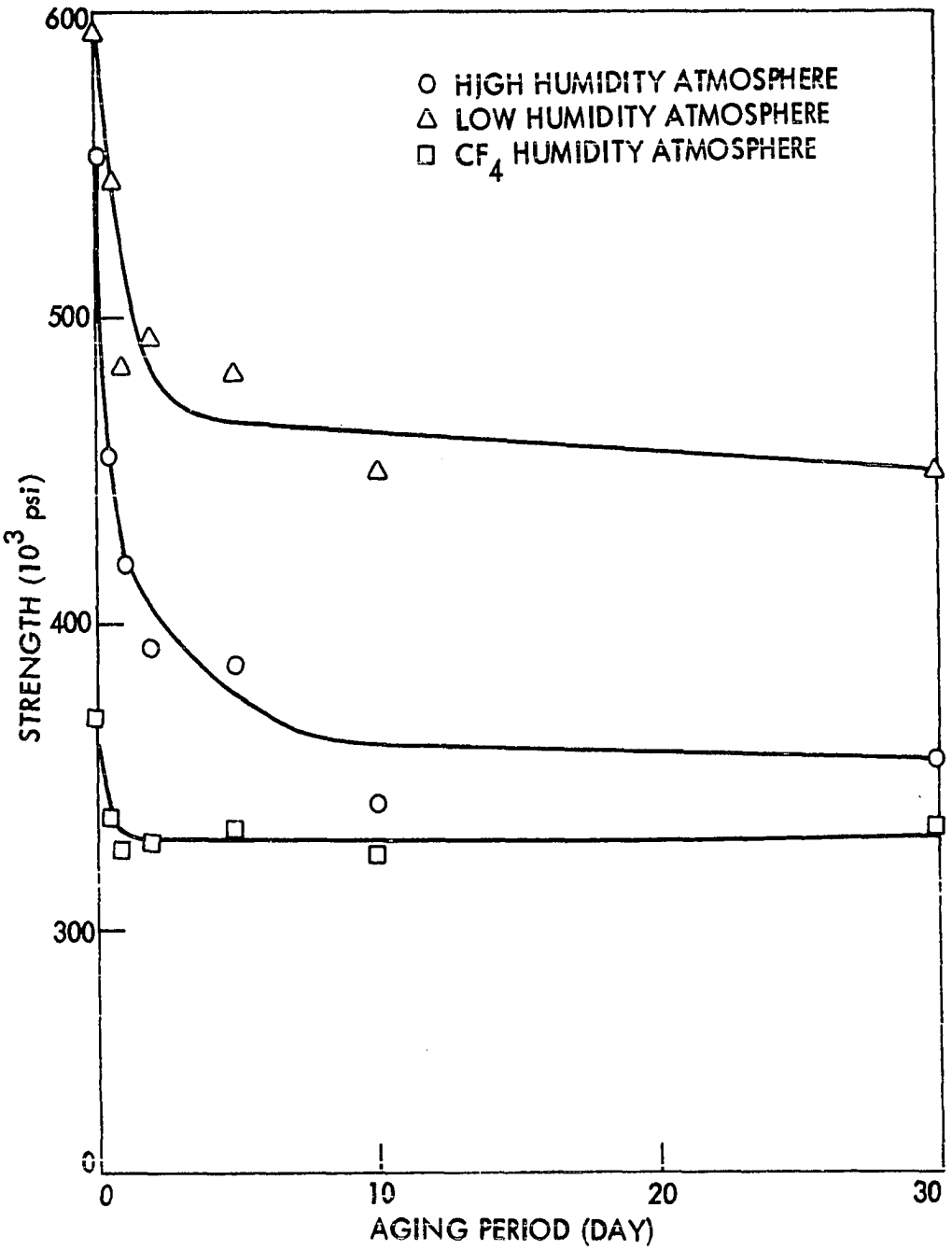

Figure 22. Tensile strength as a function of aging time.

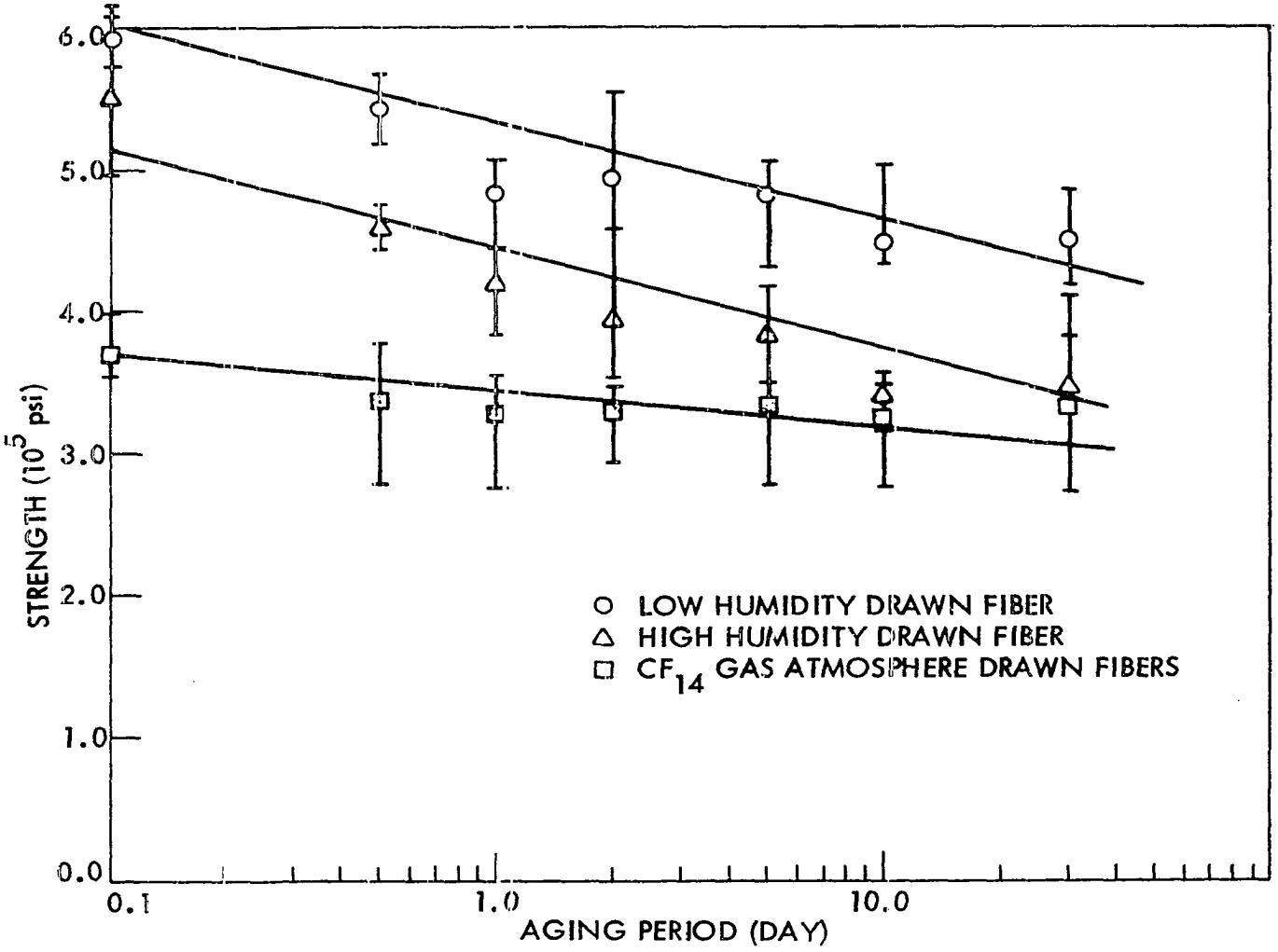

Figure 23. Tensile strength versus the log aging time.

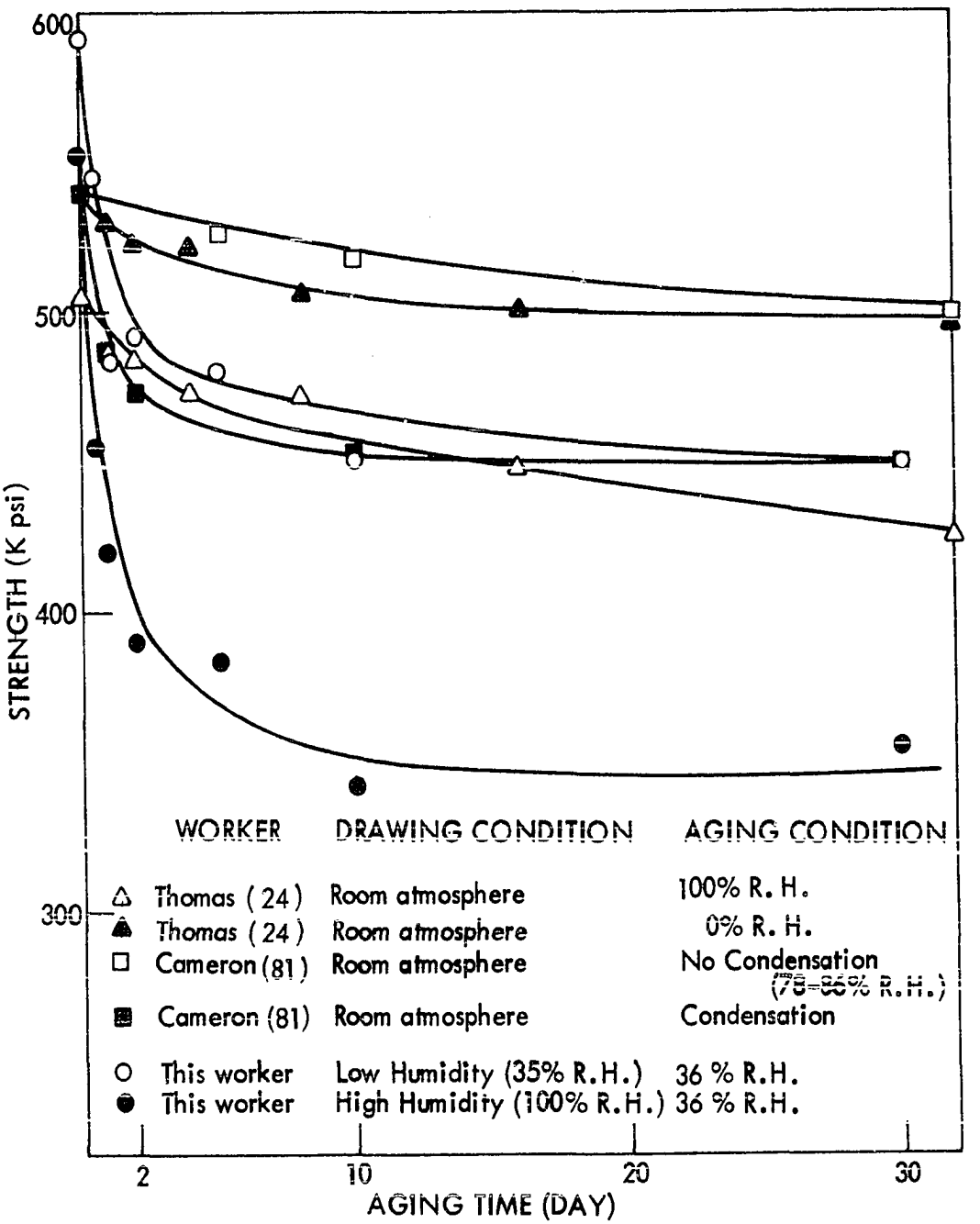

Figure 24. Comparisons of this work and other work.

Figure 25. Jet shapes in the different drawing atmospheres

a) Low humidity

b) High humidity

c) CF_4 gas

(a)

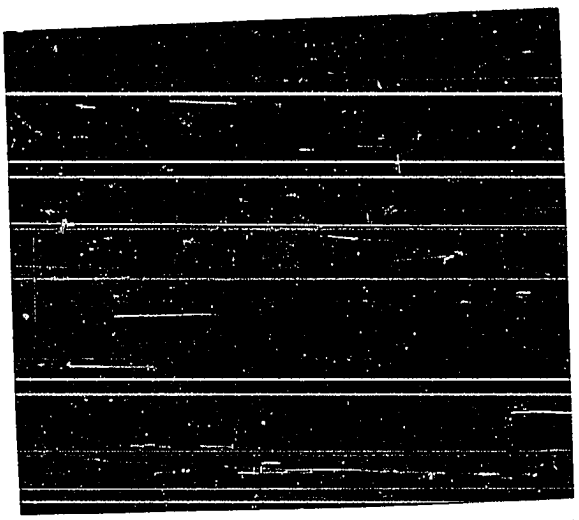

(b)

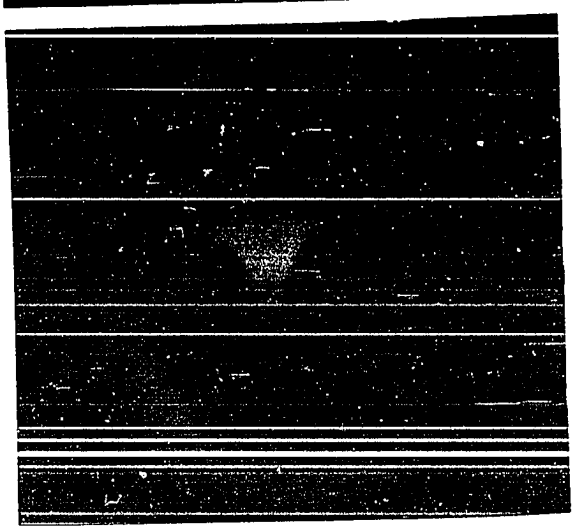

(c)

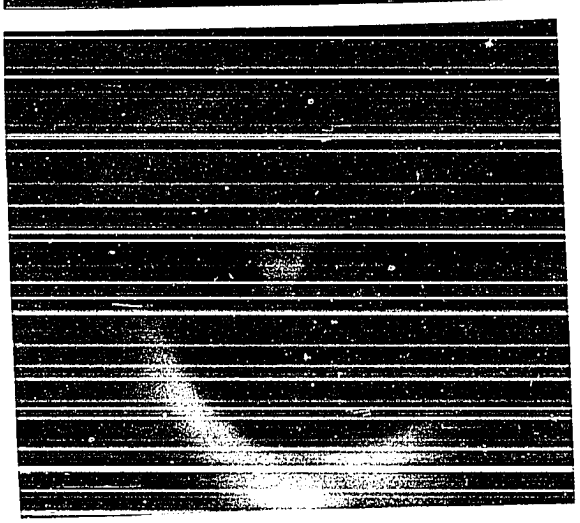

DISCUSSION OF RESULTS

Properties of E-glass

Thermal analyses

E-glass, characterized by an alkali oxide content of less than 1% by weight, contains two volatile constituents, B_2O_3 and F_2 as shown in Tables 1 and 2. The losses of these volatile constituents during glass melting are likely to be considerable, so that batch calculation of E-glass should be carried out by considering these losses (2). In general, during melting of E-glass the losses are 15-25% of B_2O_3 from the batch mixture and on the order of one-half the F_2, which is evolved as SiF_4. The exact amount of losses of these volatile constituents during remelting process is unknown since this will depend on the melting conditions. However, a number of investigators pointed out that the volatilization weight loss for E-glass or aluminoborosilicate glass heated up to 2500°F (1371°C) is small, less than 1% (83, 97).

To eliminate inhomogeneity in molten glass used for drawing fibers, E-glass is first premelted and formed into marbles. During melting, water may be introduced into the E-glass marble from the combustion reaction of fuel such as a natural gas. The other source of water introduced into E-glass marbles is moisture in the raw materials, even though there are maximum manufacturing limitations of allowable water contents in raw materials for E-glass.

The alkali components such as Na_2O, CaO and MgO are also volatile constituents. By using Auger electron analysis Rynd and Rastogi (69) found that the E-glass fiber surfaces are low in magnesium, boron and

calcium which may be evolved from the surface. Thus, it may be concluded that the weight loss of 1.56% in this experiment is primarily due to the weight loss of the volatile constituents, and water. A slower heating rate in a continuously dry vacuum system may provide appreciable weight loss of water (26).

An abrupt change in the slope of the DTA curve during heating represents the rearrangement of intermolecular bonds in the open structure of glass which gives rise to changes in the properties of glass such as specific volume, heat capacity and elastic modulus. Transformation due to rearrangement in the glass structure depends on the glass composition and heating and cooling rate. The DTA has become established as a technique for finding glass transformation temperature. It is designed to measure relatively high enthalpy processes with chemical reaction or first order transition and thus is marginally useful for observing the low energy transition phenomena. Recently, the transformation temperature of glass and polymers has been determined using a more sensitive simple heat flow apparatus (98).

The first slope change in the endothermic DTA curve occurs at 350°C and it may be caused by the rearrangement of glass structure due to either the dehydration of chemically bonded water or volatilization of B_2O_3, or to the transformation of a high B_2O_3 phase since B_2O_3 has a glass transition at about 350°C. The most remarkable change in the slope of the DTA curve during heating occurs at 730°C, which represents the transformation temperature of E-glass at a heating rate of 40°C/min.

Density

The density of E-glass reported in the literature ranges from 2.50 to 2.60 gm/cc (99, 100, 101). The massive annealed form of E-glass has a higher density than that of fiber from E-glass. The annealed bulk density of E-glass marbles used for fiber drawing in this work was reported to be 2.60 gm/cc by the manufacturer (91).

The reason for the difference in density between bulk form and fiber form is evident from the following considerations. The glass density depends on the glass composition and thermal history (e.g. transformation temperature). A number of formulae for the calculation of density from the glass composition have been proposed (102). The composition of E-glass fiber surfaces is different from that of E-glass bulk as shown by Rynd and Rastogi (69). The different cooling rate gives a different transformation temperature, i.e. the massive annealed form of E-glass has a structural configuration representing thermal equilibrium at some lower temperature than that for the fiber form E-glass. Thus, the value of density of E-glass fiber is lower than that of bulk E-glass.

The density of fiber glass is subject to change by heat treatment due to densification as reported by Otto (99). He found that the density of fiber increases with the temperature of the heat treatment. However, as a parameter in the drawing equation and cooling rate equation, the density of E-glass fiber used throughout this work was taken to be constant value of 2.50 gm/cc. This value is based on the measured value from the pycnometric method, even though the bulk density of E-glass marbles was found to be 2.558 gm/cc.

Viscosity and activation energy

The viscosity of a glass varies greatly with temperature and composition. The activation energy for viscous flow is almost independent of temperature over certain ranges of temperatures, but is dependent on the glass composition. For example, the activation energy for vitreous silica is about 170 Kcal/mole (1100°C ~ 1400°C), and the activation energy for vitreous B_2O_3 is much lower than for vitreous silica, but a wide range is reported, i.e. 12-83 Kcal/mol between 300-1200°C (27). The viscosity of a pure oxide glass is found to be decreased by the presence of small amounts of non-glass former impurities.

The lowering of B_2O_3 content in E-glass by lengthening the dwell time yields higher viscosity of the E-glass melt because of reduction the amount of the low activation energy component B_2O_3 as discussed before. Thus, it is very important to control the volatile B_2O_3 content in continuous drawing process of E-glass fiber. In this experiment B_2O_3 content was assumed to be kept constant by additions of powdered E-glass to the crucible during fiber drawing in order to maintain a constant gravity head which probably offset B_2O_3 and F_2 loss during the experiment.

The calculated activation energy for viscous flow from the flow rate method in the drawing temperature range (1180°C-1265°C) agreed approximately with the value computed by least squares method from the manufacturer's data (91) in a wide range of temperature (1149°C-1483°C). However, a large discrepancy between the measured and the computed value was found when only the manufacturer's data in the drawing temperature range was considered; the activation energy calculated from the manufacturer's data was higher than that obtained experimentally. This

discrepancy is believed to be due to either some error in the measurement of drawing temperature or final diameter; it could also be due to temperature drop in the nozzle as pointed out by Tiede (23), or to errors in the manufacturer's data.

Drawing Conditions

Diameter of glass fiber and flow rate

The final fiber diameter is a very important factor affecting dynamic processes such as cooling rate, cooling time and stress on the fiber. The most significant effect of diameter is on the stress (σ) and cooling rate ($\dot{T}$) which are dependent on the square of the diameter as shown by Oh and Martin (20), i.e.

$$\sigma = \frac{K \ln r_o/r_f}{r_f^2(T_o - T_\infty)} \exp[-\bar{\Phi}(Q,T) \ln \frac{r_o}{r_f}] \tag{36}$$

and

$$\dot{T} = \frac{K(T - T_\infty)}{r_f^2} \exp[-\bar{\Phi}(Q,T) \ln \frac{r_o}{r_f}] \tag{37}$$

where K is cooling constant and $\bar{\Phi}$ (Q,T) is a function of temperature and activation energy for viscous flow.

The control of final fiber diameter in a drawing process can be accomplished by using Equation 15, which was derived from the Poisulle' equation and continuity equation, by controlling drawing temperature and drawing speed as reported by Thomas (24). The drawing constant K' calculated from the measured flow rate for a given nozzle geometry in this work is acceptable only when the bushing head is kept at a constant level since the flow rate is proportional to the whole of the gravity head at any given temperature. The other factor to be con-

sidered in determining final diameter from the flow rate in Poisuille's equation is the viscosity of glass in the nozzle. The viscosity of the molten glass undoubtedly increases during its passage down through the nozzle due to nonuniform temperature distribution throughout the nozzle. As pointed out by Tiede (23), it is thus not possible to predict the exact final diameter from the flow rate as a function of drawing temperature and drawing speed. Only the approximate value of the final diameter can be predicted.

The viscosity of glass is also dependent on its composition as discussed in the previous section. Any change in the glass composition during drawing will result in a viscosity change. For example, the volatilization of B_2O_3 from the melt will cause a viscosity increase. This change in viscosity will affect the final diameter.

The measurement of fiber diameter by using microscopes also involves problems. The diameters of fibers were found to be nonuniform. One single filament as observed by SEM at high magnification (3000X) showed a variation of 5 ~ 10%, but such variation was not ordinarily observed.

Glass head in bushing

As reported by other workers (17, 24) and discussed earlier, the flow rate of the molten glass at a given temperature is independent of drawing speed. Thus the flow rate at a given temperature is constant if the nozzle geometry and gravity head of the molten glass is constant. However, the geometry of a given nozzle is always constant and the temperature can be easily controlled by using a calibrated temperature controller. The gravity head usually changes with drawing time so that a constant gravity head can be maintained by adding the amount of glass

consumed by drawing. When the flow rate is low compared to the total volume of molten glass the gravity head change is in general negligible for short drawing periods.

Jet shapes

The jet shapes observed in the drawing conditions of this experiment are concave since the slope of jet surface continuously decreases until the final diameter is reached. The apparent base diameters of glass jets are smaller than the nozzle exit diameter depending on drawing conditions such as drawing temperature. However, it is difficult to determine the actual base diameter of the glass jet from the photographs of jet shapes. The initial jet radius of the jet shapes is not the nozzle radius as observed by Burgman (102). However, at higher temperatures the initial jet radius seemed to be close to the nozzle diameter as shown in Figure 14. A discontinuity in slope of jet radius at apparent basal line was observed at lower temperatures, which is not physically reasonable. There are two possible reasons for this phenomena. One is that the initial jet radius is equal to the inside nozzle radius, but it starts at $z \neq 0$, i.e. inside orifice as shown by the dotted line in the following figure. The other is that the initial jet radius starts at $z = 0$, but the roughness of the nozzle edge hides the initial jet radius. Thus the location of initial jet radius (i.e. origin) was determined by using the drawing ratio equation which was derived under condition that the critical jet radius is assumed to be equal to the nozzle radius. The results of the photographic jet shape analysis indicated that the jet origin was higher in the nozzle for low temperature drawing than for high temperature drawing.

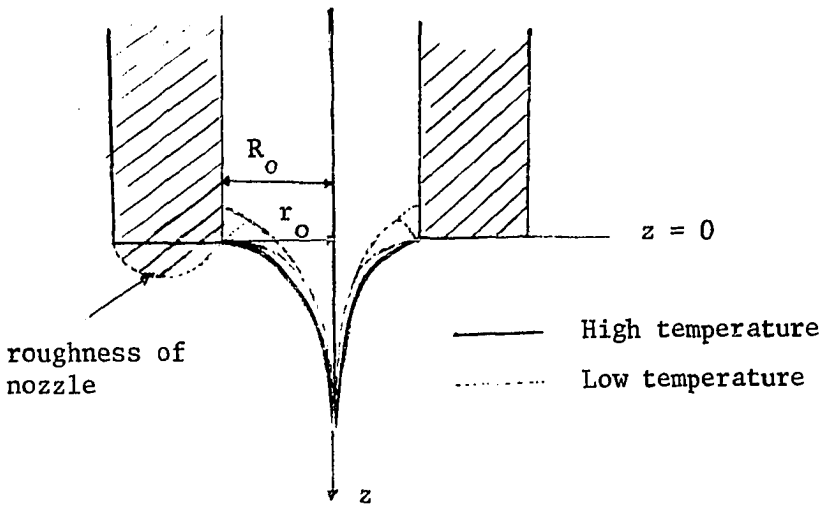

Figure 26. The possible jet origins

The upper jet shapes as described by Glicksman (15), i.e. $dr/dz > 0.1$, were observed in detail by telemicroscope. The concave type upper jet shapes observed belong to either Burgman's category I or II (17). The Reynolds numbers were usually within the category I range. The calculated Reynolds numbers for the different drawing conditions are tabulated in Table 11.

Table 11. Reynolds numbers for the various drawing conditions

T_o (°C)	η (poise)	v(cm/s)	$r_f(10^{-4}$cm)	$U_\infty(10^{-2}$cm/s)	$Re(10^{-6})$	Burgman's jet shape category
1265	580	1045	2.455	1.44	8.19	I or II
1245	751	1045	2.265	1.23	5.40	I
1210	1200	1045	1.800	0.77	2.13	I
1180	1826	1045	1.460	0.55	0.92	I
1240	802	946	2.315	1.16	4.77	I
1240	802	844	2.385	1.10	4.52	I
1240	802	742	2.410	0.99	4.06	I

As reported by Burgman (17) and predicted by the drawing ratio Equation 9c, the shape of the upper glass jet is dependent on the flow rate. Thus the effect of drawing temperature at constant drawing speed on the size of the upper jet is large as shown in Figures 14 and 16. The control of drawing temperature is very important in dealing with jet shape analysis because of the strong dependence of flow rate on temperature.

The upper jet shape is independent of the drawing speed since the flow rate is also independent of the drawing speed as discussed in the previous section. No noticeable changes in the shape of the upper glass jet with different drawing speeds were observed in this work. The upper jet shapes observed were the same for drawing speeds between 742 and 1045 cm/sec at constant drawing temperature as shown in Figure 15. Burgman (17) found that upper jet shape changes for drawing speeds greater than 4060 cm/sec and he regarded this change as an error in measurement. He concluded that the basic character of the upper jet shape is independent of the drawing speed for a given glass flow rate, glass viscosity and nozzle geometry. This can be shown by the drawing equation, Equation 11c, which can be rewritten as follows:

$$\ell n \ell n\, r = \ell n \ell n r_o - \frac{K^*}{w} z \,. \tag{38}$$

The radius of upper glass jet as a function of axial distance is dependent on the mass flow rate. Thus, constant flow rate which is independent of drawing speed at given temperature cannot affect the jet shape.

Neither oscillation nor instability of jet shape which were reported by a number of investigators (8, 21) were observed. It was often

observed that the glass jet tended to move to the center of the nozzle even though it started off center. A stable off center jet as shown in Category I of Burgman's analysis was not observed. This phenomenon may result from a winding drum which is not in the same axial position as the orifice or to pertubations from starting the glass fiber with a quartz rod.

Gas Effects on E-glass Fibers

General considerations for measured strength

Before the results of gas effect on the fiber strength are analyzed it would be well to discuss certain factors which could possibly influence the results of the measured strength. The results of the experiments, tabulated in the Appendix, show high dispersion of strength data with coefficients of variation ranging from 2.4 to 13.6 %. The reasons for the high data scatter in measured strength can be explained by considering the following factors which may affect the measured strength either internally or externally.

External factors Since fine glass fibers are particularly susceptible to surface damage, accidental damage to the fiber during specimen preparation may seriously influence the results of strength investigations. If the freshly formed fine fibers were touched accidentally during catching, mounting, aging and cutting operation, undesirable stresses or flaws introduced could lead to low strength with high data scatter. Stress introduced before mounting of filament on the paper strip (i.e. during catching and handling of single filament on the collecting wood frame) is unfavorable for the strength since stress

would be distributed throughout the whole fiber filament. This may result in low breaking strength with low standard deviation for a single group of fibers (e.g. the tensile strength of 10-day aged group of high-humidity drawn fibers). However, after mounting of the filament on the paper strip the stress introduced during aging and mounting on the testing machine would be limited to an individual specimen and result in high data scatter.

Another significant factor is nonuniform fiber diameter. The diameter used in the measurement of tensile strength of each group was assumed to be constant. Figure 27 shows the different values in diameter along the single filament, i.e. 0.3 μm variation in diameter. This example is extreme and such variation was not often found in this experiment. Generally, the variation of diameter was less than 0.3 μm which would lead to a variation of 12% in strength for a 5μm diameter fiber.

As discussed in the literature survey, the effect of gauge length on the strength should be considered for the data scatter. From the statistical point of view, the distribution of pre-existing microcracks on the freshly formed fiber is dependent on its length. For low dispersion in measured strength data a uniform gauge length which gives the same probability of a major flaw should be used. The specimen mounting paper strip was designed to form one-half inch gauge length specimens as shown in Figure 7. The positions of the glue on the paper strip varied within 0.2 cm which could have changed the gauge length by 15%. Little work has been carried out on the effect of gauge length on the strength of single filament glass fibers. Metcalfe and Schmitz (103) did, however, study the effect of gauge length of E- and S-glass fiber (about 10 micron

Figure 27. SEM micrograph of glass fiber having nonuniform diameter

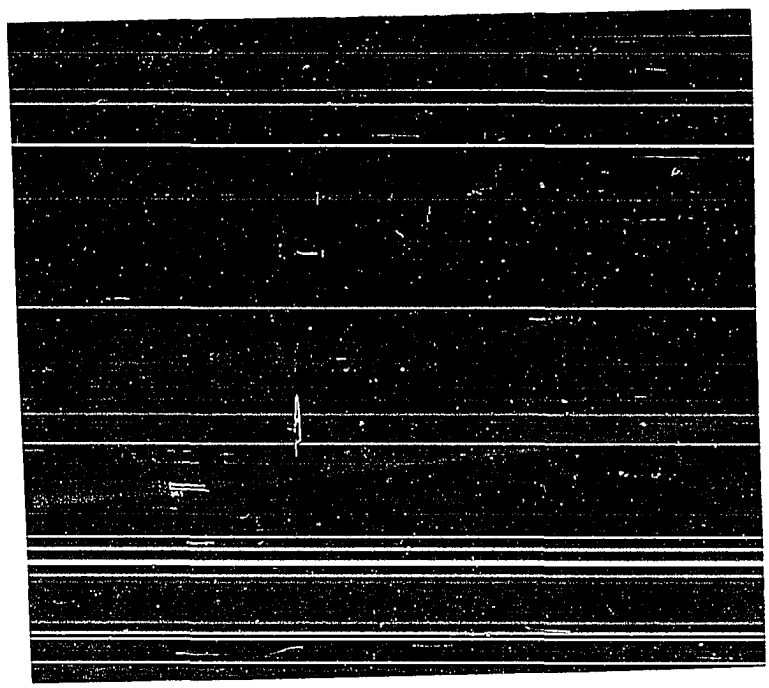

diameter) on the strength. They found that the logarithmic strength-length plots were not linear over the entire length range from 0.025 to 30 cm, i.e. a slope change occurred at a critical gauge length (about 1.1 cm for E-glass fiber), which implies varying contributions of mixed flaw populations to failure strength. In other words, there are two types of flaws. One is the severe flaw which involves the second control mechanism of failure such as an accidental damage at long gauge length. The other is less severe flaws at short gauge length (1.0 cm). The former type is more probable as the diameter decreases. They also found that Weibull type analysis (104) is not adequate to describe failure in glass fiber since it excludes such a second type flaw. Thus, the effect of gauge length on strength in this work may be important because of the small diameter (5 μm) and gauge length (i.e. bigger than 1.0 cm).

Accurate measurement of the maximum breaking load also affects data scatter. In the present testing machine the maximum breaking load can be read to ± 0.1 gm. A variation of ± 0.1 gm in breaking load may seriously influence the calculation of strength for weak glass fibers (e.g. 0.1 gm error for zero-day aged fibers drawn in high humidity changes strength by 1.6%, but for 2-day aged fiber drawn in CF_4 atmosphere by 4.5%). Thus, data scatter is also caused by the inaccurate measurement of the maximum breaking load.

The selection of glue for attaching the fiber filament to the paper strip is also an important factor which may affect the data scatter. The physical and chemical reactions of a glue with a glass fiber depends on its composition and properties. If glue contains water, it certainly

may influence the strength by stress corrosion. Chemicals corrosive to glass should not be contained in the glue. "Super Strength" glue used for zero-day aged specimens in this experiment contains allyl isothiocyanate (CH_2=CH CH_2NCS) and may have reacted with the glass surface due to its high vapor pressure. It was difficult to find a good glue. Wax used for this purpose by other investigators must be heated, which results in heat treatment of the fiber. Epoxy glue used for the aged specimens was satisfactory even though it had a long setting time. The other consideration in the selection of glue is the physical properties. For instance, tension may be produced on the fiber filament by shrinkage of glue with setting time. This tension produced before testing may also affect the measured strength.

If a fiber specimen was not mounted on the stress axis, i.e. some deviation from the loading axis, the actual strength of fiber would depend on the tilt angle due to shear stress involved. For example, the deviation of 10° from the normal axis changes the actual strength by 1.5% for 5 micron diameter fiber. In addition, complex stress states would be generated due to bending moments.

The final factor to be discussed is the technique of catching the fiber from the drawing apparatus. It was difficult to obtain undamaged virgin fibers from the present drawing apparatus. By using a collecting frame, the fiber filament which has a tension balanced by the drawing force and whose temperature is still not at room temperature is caught. The most serious stresses may be introduced by one finger of the collecting frame striking the glass fiber before the other finger does even though it occurs in a very short time period.

Discussions have been presented concerning the external factors affecting the high data scatter in the measured strength, which may be caused by experimental error. The probable error (P.E.) can be estimated from the consideration of above critical factors and it was estimated be 12.9%, i.e.

$$P.\ E. = [\Sigma(E_i)^2]^{\frac{1}{2}} \tag{39}$$

Internal factors A number of investigators have pointed out that a higher drawing temperature reduces the data scatter in measured strength. Thomas (24) obtained low variation in strength data by using high bushing temperature and he found that below a bushing temperature of 1220°C it was very difficult to form a suitable fiber and large variations in diameter were possible in a short length of fiber. According to Cameron's work (77) scatter in the strength of E-glass fibers can be reduced from about 18% to 1% by simply increasing the temperature by 300°F (170°C), and then decreasing to the drawing temperature. He could not logically justify the reason for the high "cookout" temperature since it was just recommended by industry for thermal equilibrium of glass.

Considering the stress equation developed by Oh and Martin (20), the stress along the fiber during the drawing process can be expressed as a strong function of drawing temperature as shown in Equation 36. According to Equation 36 the stress at high temperature is low while the opposite is true for low drawing temperature. But increasing drawing temperature may be accompanied by two unfavorable phenomena as pointed out by Cameron (77). One of these is the possibility of the occurrence of reboil from

the dissolved gases and from the decomposition of glass components. The second phenomena is the change of glass properties by changing the composition due to volatile components of E-glass composition. Thus, this operation requires some caution.

As discussed before, different final diameters give different cooling rates which may influence the room temperature properties. It has been shown that the glass transformation temperature depends upon the cooling rate of glass. The rapid cooling rate in the glass fiber forming process may be related closely to the strength of fibers. Burgman and Hunia (12) studied the effect of cooling time on the filament breaking strength of E-glass fibers. They found no effect of the total cooling time on breaking strength with fiber diameters in the range of 7-17 microns. Both cooling rate and cooling time are governed by many parameters such as drawing temperature, environmental temperature, diameter and jet shape as shown in Equations 1, 2, and 37. The cooling rate in the region of glass transition increases with drawing temperature and decreases with fiber diameter.

There is an unusual strength behavior observed experimentally by Cameron (77), i.e. labeled the "second fiber anomaly," which leads to high data scatter due to poor quality of glass fiber. This anomaly is associated with the condition of the glass in the nozzle. After several drawings of fiber, defect formation occurs in the glass in the bushing nozzle. These defects are the result of devitrification due to different temperature distribution between the nozzle and bushing body. This anomaly can be eliminated by completely wiping the stagnated molten glass from the nozzle.

Water vapor atmosphere

A number of investigators (24, 81) studied the effect of moisture on the strength of glass fibers and found that water vapor has a significant effect on the strength of the fibers. However, few investigators have examined the effect of water vapor in the drawing atmosphere. Recently, Burgman and Hunia (12) found a decrease in the strength of fibers with an increase in specific humidity of drawing and testing atmosphere, i.e. a reduction of about 15% in strength by increasing specific humidity, defined as the ratio of mass of water vapor to mass of dry air, from 4×10^{-3} to 11×10^{-3}. According to their data the strength of unaged fibers drawn in high humidity should be low (less than 450 Kpsi) even though they did not test the high humidity atmosphere as much as this work.

The main differences between their work and this work are the experimental conditions including different fiber thermal history. Fibers having diameters in the range 11-13 μm (compared to 4.5-5.8 μm in this work) were drawn in a humidity controlled room and the strengths were tested in exactly the same atmosphere as the drawing atmosphere 45 minutes after forming (105). However, it is difficult to compare their work with this work because of lack of sufficient experimental information. For example, they determined the specific humidity from wet-dry bulb temperatures, but the exact location of the psychrometer in the drawing room was not known. The temperature distribution of the laboratory room might not have been uniform, e.g. the temperature close to the drawing apparatus might have been higher than room temperature. Thus, the relative humidity would vary with location in the laboratory.

Since there is a lack of sufficient data from the literature concerning the effect of water vapor in the drawing atmosphere on strength, the possible reactions of water with E-glass at both high and low temperatures should be considered. The following reactions might occur during glass fiber drawing. The first one is the reaction of water with silica glass to form hydroxyl groups in the following way:

$$-\overset{|}{\underset{|}{Si}}-O-\overset{|}{\underset{|}{Si}}- + H_2O \longrightarrow -\overset{|}{\underset{|}{Si}}-OH\ HO-\overset{|}{\underset{|}{Si}}- \qquad (26d)$$

Water reacts with the strong silicon-oxygen network of silicate glasses, breaking it up and consequently modifying the glass properties such as strength. The dangling bonds of freshly formed silica glass surface react rapidly with atmospheric moisture to form silanol groups. Such a reaction can also occur when water vapor is adsorbed on the freshly formed surface or water molecules diffuse into the glass.

The hydroxyl groups provide adsorption sites for water molecules and are partially responsible for the hydrophilic character of glass surfaces. Hydrogen bonds can be formed by the reaction of water with these hydroxyl groups i.e.

$$-\overset{|}{\underset{|}{Si}}-\ OH + H_2O \longrightarrow -\overset{|}{\underset{|}{Si}}-\ OH\ ---\ O\begin{matrix}\diagup H\\ \diagdown H\end{matrix} \qquad (40)$$

These hydrogen bonded groups are relatively stable but the reverse reaction of this can be made easily by just heating to around 200°C. Physically adsorbed water molecules are also apparently bonded to the hydrogen-bonded molecules on SiOH groups as shown in Equation 40 but the bonding energy is considerably smaller so that it can be easily removed from the surface by pumping or just heating to 100 °C. These water molecules can also

diffuse into glass.

The most important reaction of water with a complex glass is the ion exchange which results in stress corrosion of most glasses, i.e.,

$$-\overset{|}{\underset{|}{Si}}- OR^{+} + H_2O \longrightarrow -\overset{|}{\underset{|}{Si}}- OH + R^{+} + OH^{-} \quad . \qquad (41)$$

The rate of water attack by ion exchange involves ionic diffusion such as self diffusion or interdiffusion of alkali, protons, and OH^{-} ions in the glass, and is dependent on diffusion coefficients for such ions, time and temperature. Thus, the rate of ion exchange reaction depends on the glass composition.

The temperature is an important parameter in the interaction of water vapor with glass when considering the possible reaction mechanisms such as adsorption, diffusion and ion exchange.

High temperature At high temperature the interaction of water vapor with glass is complex since the structure of glass is sensitive to the temperature. Young (45) and Bernett and Zisman (106) noted that at temperatures greater than 400°C the dehydration of silica surfaces is irreversible and water vapor can not be chemisorbed following dehydration so that such a high temperature should be avoided if subsequent water vapor adsorption is desired. Young (45) thus suggested that the surface formed by dehydration of silanol sites at high temperature ($-\overset{|}{\underset{|}{Si}}-O-\overset{|}{\underset{|}{Si}}-$) differs from the surface formed at lower temperature ($-\overset{|}{\underset{|}{Si}}-\overset{*}{O}-\overset{|}{\underset{|}{Si}}-$),

$$-\overset{|}{\underset{|}{Si}}- OH\ HO\ -\overset{|}{\underset{|}{Si}}- \xrightarrow[\text{low temp.}]{-H_2O} -\overset{|}{\underset{|}{Si}}- O^{*}-\overset{|}{\underset{|}{Si}}- \xrightarrow[\text{high temp.}]{-H_2O} -\overset{|}{\underset{|}{Si}}-O-\overset{|}{\underset{|}{Si}}- \qquad (42)$$

The structure of glass at high temperature could be changed by rearrangement. Salmang and Becker (107) also found that water could not be intro-

duced into small batches of glass melted on a laboratory scale under humid conditions. In the fiber industry water (deionized water or steam) is sprayed onto the fiber filament on their way from the bushing to the applicator in order to provide lubrication and protection of the filaments during conversion into strands from the interfilament abrasion and also to avoid electrostatic charge build up. The quantity of water which is deposited on the fiber is very small (2). There is more evidence for removal of water from the glass during heating (26). The conclusion has been reached that at high temperatures adsorption (e.g. Equation 40) can not occur at low water pressures due to loss of water molecules from the surface.

Surface attack by reaction (Equation 41) is entirely responsible for the extraction of soluble components such as modifying alkali ions. At high temperature the rate of ionic diffusion is so high that stress corrosion is accelerated. However, at temperatures greater than 250°C silica is also soluble in water (26) and reaction (Equation 26d) can then occur by diffusion or chemisorption of water, and will be governed by the diffusion coefficient and solubility of water in the glass.

The diffusion coefficient of water is certainly strongly temperature dependent while solubility has a small temperature dependence at high temperature. However, both the diffusion coefficient and solubility of water in silica glass were found to be a dependence of thermal history of glass below the transformation temperature (108). Also, the diffusion of water molecules is proportional to the concentration of SiOH groups (27).

The solubility of water is generally proportional to the square root

of water vapor pressure and follows Henry's law. Thus, the dissolved water is present in the glasses in the form of OH groups and not as H_2O molecules (due to reaction as shown in Equation 26d). The solubility of H_2O is very strongly dependent on the glass composition as shown by Franz (109).

Low temperature At low temperature rapid, strong chemisorption followed or accompanied by physical adsorption occurs as the glass is cooled, as described by Deitz (47). Adsorption, a reaction depending on the surface hydroxyl groups, is a preliminary step for the reaction as shown in Equations 26d and 41. The rate of adsorption is governed by the water vapor pressure and time. The effect of gas adsorption from the environmental atmosphere on the cohesive strength of solid material was described by Metcalfe and Schmitz (85) as follows. The gas adsorption causes a decrease in the surface energy required for fracture and hence a reduction in strength according to the Griffith-Orowan equation. Parikh (71) demonstrated that the surface tension of soda-lime glass was reduced by about 22% by water vapor at 400°C-700°C.

At lower temperature (<250°C) a continuous ion exchange reaction (Equation 41) by adsorption and diffusion of water results in surface attack even though rate of ionic diffusion is slow. Reaction (Equation 41) is dependent on the glass composition because acid substances such as boric oxide which are present in the glass tend to be extracted and neutralize the alkali ion. Thus, surface attack by ion exchange can be reduced by control of glass composition such as boric oxide in E-glass even though it has a low alkali content. It is generally believed that successive prolonged contacts with water vapor corrodes E-glass surface

by removing Ca^{++} and Na^{+}, and increases the number of surface silanol groups which provide additional OH^{-} sites for water vapor adsorption (47, 48, 49). Surface corrosion by such ion exchange is governed by wide range of conditions including pH, alkali-to-hydrogen ion ratio, strain rate, temperature, availability of water, and glass composition.

As reported by Metcalfe et al. (110), spontaneous cracking of glass filaments can occur in the absence of externally applied stress. Water reaction at a crack tip can accelerate crack propagation (26), which may result from the adsorption and diffusion of water vapor. The surface attack by stress corrosion is certainly a diffusion-related process since water molecules can diffuse into glass. If a diffusion coefficient is independent of the concentration, the thickness of the corroded layer (δ) is a parabolic function of diffusion time, i.e.

$$\delta = (4Dt)^{\frac{1}{2}} \tag{43}$$

At lower temperature the time is a very important parameter governing the surface corrosion by water since the diffusion coefficient of water is very low (e.g. 10^{-17} cm^2/sec for E-glass at room temperature) (62).

Consequently, the interaction of water vapor with glass in the drawing atmosphere is an extremely complex phenomena involving adsorption, diffusion and ion exchange and depends on the thermal history. Thus, it is difficult to predict the predominating one of the reactions discussed above and to define the exact boundary temperature at which it can occur due to lack of high temperature thermodynamic data for the reactions.

In order to justify the degradation of measured strengths by

increasing the humidity in the drawing atmosphere, all possible reactions of mechanisms discussed should be considered. The degradation of strength is regarded as a result of water attack which depends mainly on the diffusion coefficient and solubility of water in glass (i.e. permeability of water). If the penetration depth of water molecules as a corrosion layer is proportional to the permeability of water, the ratio of the permeability in a high humidity atmosphere (P_{high}) to that in a low humidity atmosphere (P_{low}) is equivalent to the ratio of crack depth of high humidity drawn fiber (c_{high}) to that of low humidity drawn fiber (c_{low}), i.e.

$$\frac{P_{low}}{P_{high}} = \frac{D_{H_2O}\, S_{low}}{D_{H_2O}\, S_{high}} = \left\{\frac{p_{H_2O}\ (low)}{p_{H_2O}\ (high)}\right\}^{\frac{1}{2}} = \frac{c_{low}}{c_{high}} \qquad (44)$$

The water vapor pressure in high humidity atmosphere p_{H_2O}(high), (i.e. 85% R.H. 35°C) was 35.84 mm Hg with 11.1 mm Hg in low humidity atmosphere, $p_{H_2O(low)}$, (i.e. 35% R.H., 30°C). However, the calculated ratio of crack depth from Equation 44 did not agree with the ratio of crack depth in the Griffith equation from the measured strengths. This result implies that the other factors should be considered in surface attack by water relating to the measured strength. One possible factor is that the diffusion coefficient of water is not independent of water concentration since the effective diffusion coefficient is directly proportional to the concentration of SiOH groups which depends on thermal history, humidity and surface treatment (27).

The other factor is the contribution of adsorption at low temperature. A number of investigators (26, 47) found that the rate of

surface corrosion by ion exchange accelerates with increasing humidity. From the gas kinetic point of view, the number of water molecules striking the unit area of glass surface per unit time is also proportional to the water vapor pressure as shown in Equation 23.

As an alternative justification for the strength degradation in high humidity drawing atmospheres, adsorption isotherm analysis such as BET surface area is helpful in analyzing the results of strength data of unaged E-glass fibers. The BET surface area which is covered by monomolecular layer depends on the shape and numbers of cracks. Under the assumption that the BET surface area is proportional to the square of crack depth for three dimensional cracks, the following relationship between BET surface area and crack depth would be

$$\left\{\frac{A_{high}}{A_{low}}\right\}^{\frac{1}{2}} \approx \frac{c_{high}}{c_{low}} \tag{45}$$

where A_{high} and A_{low} are the BET surface areas of high humidity drawn fiber and of low humidity drawn fiber respectively. c_{high} and c_{low} are the crack depths. If this is true, the square root of crack ratio is equal to the reciprocal ratio of the measured strength (S) only if the surface energy is constant in the Griffith equation, i.e.

$$\left(\frac{c_{high}}{c_{low}}\right)^{\frac{1}{2}} = \frac{S_{low}}{S_{high}} \ . \tag{46}$$

The BET surface area of high humidity drawn fiber could not be obtained due to experimental problems but fortunately the data of BET surface area for No. 3 in Table 10 can be used since the sample specimens were

saturated with water after drawing in the adsorption isotherm apparatus (i.e. 100% R.H.) even though it was not drawing atmosphere (111). The ratio of square root of BET surface area was to be 1.10 and is almost equal to the ratio of the reciprocal square of measured strength data ($(\frac{S_{high}}{S_{low}})^2 = 1.07$). This result satisfies the above hypothesis and also implies that the interaction of water vapor at low temperature in the drawing atmosphere contributed to corrosion of E-glass fibers.

The thickness of corroded layer during the half day aging at 36% R.H. reaches about 150 Å (calculated from Equation 43). This indicates a complete break of so-called strong surface layer (100 Å) of Bartenev's model (88). Thus, the mean strength of half day aged fibers dropped rapidly from 550 to 450 Ksi for high humidity drawn fiber and from 590 to 540 Ksi for low humidity drawn fibers. The high reduction in the strengths of fibers drawn in high humidity by one-half day aging indicates more corrosion due to complete saturation with water vapor obtained by 5 hour aging as shown in the kinetic adsorption analysis in Figure 20. But low humidity drawn fibers reached complete saturation with water vapor 10 hours later than high humidity drawn fibers.

After one day passed the rate of corrosion by water is slow so that the reduction in the strength is small as shown by other investigators (24, 81) (see Figure 24). It is noted that the initial surface attack for several hours including the drawing time, is severe and depends on the water vapor pressure. Thus, the initial surface attack determines the strength level of the glass fiber in this work, and the pre-existing microcracks act as stress raisers (112) and the water reaction at the crack tip accelerates the crack propagation (26).

However, a significant effect of aging on the strength was found in this work. The relationship between the measured strengths and the logarithmic aging time is almost linear within the individual data scatter of each group as shown in Figure 23. This linear relationship of the mean tensile strength for each group was confirmed by the least squares method and showed at least a 93% correlation coefficient. Both the fibers drawn in the high and low humidity atmospheres have the same slope which means the same rate even though they have different strength levels due to initial water attack, i.e.

$$\ell n\, t = A - KS \qquad (47)$$

where t is aging time and K is the corrosion rate. This kind of behavior is often observed in the study of static fatigue of glasses (36, 113).

Freon-14 gas atmosphere

E-glass surfaces flourinated by Freon-14 gas (CF_4; tetrafluoromethane) during fiber drawing results in degradation of fiber strengths compared to that of water-vapor atmosphere drawn fibers. However, fluorinated E-glass fiber surfaces showed a reduction of sensitivity to atmospheric moisture as shown in strength data for aged fibers. This was expected from the literature survey, i.e. the surface character of E-glass fiber shifted from hydrophilic to hydrophobic due to fluorine adsorption.

The initial lowering of fiber strengths of fluorinated E-glass is contrary to the expected increase in strength associated with the complete removal of surface hydroxyl groups by replacement by fluorine ions

(52, 53). However, the unexpected results in this work are reasonable if the following possibilities of CF_4 reaction with the glass are considered.

Similar phenomena can often be observed as a result of chemical etching. For example, etching in hydrofluoric acid reduced the strength of flaw-free alumina bolosilicate glass fibers (i.e. about 30% strength reduction) (98).

It is evidently true that the surface layer of glass can be removed by hydrofluoric acid reaction, i.e.

$$SiO_2 + 4HF_{gas} \longrightarrow SiF_4\uparrow + 2H_2O\uparrow \qquad (48a)$$

or

$$SiO_2 + 6HF_{liquid} \longrightarrow (H_2SiF_6) + 2H_2O. \qquad (48b)$$

The strong Si-O bond can be easily broken by fluorine and form a gas of tetrafluorosilane which is very stable even at very high temperatures. (of the order of 2000°C) (114). It has been observed that the complete removal of the microcracked surface layer by HF etching increases the strength of bulk glasses (26, 27). But for the glass fibers it shows contrary results, i.e. a derease in strength. The reason for the decrease in strength by removal of the surface layer can be explained by Bartenev's model (88).

According to his model, the strength of glass fibers depends primarily on a strong surface layer of about 100 Å, which has a different structure than the core of the glass fiber. This strong surface layer could be destroyed by HF acid etching so that the strength of fiber glass would be decreased.

It was found that the reaction of CF_4 gas with the glass surface could be similar to that of HF as shown in reaction Equation 48a. The freshly formed glass fiber surface reacts spontaneously with CF_4 gas giving SiF_4 gas and CO_2 gas, i.e.

$$SiO_2 + CF_4 \longrightarrow SiF_4\uparrow + CO_2\uparrow . \qquad (32)$$

This reaction occurs more more spontaneously by increasing the temperature due to the negative free energy of formation of the SiF_4. The carbon dioxide gas produced can also react with the alkali in the glass even at room temperature (ion exchange) and this is an initial stage of the stress corrosion if water is present as described by Tichane (115).

If the glass surface has some hydroxyl groups, the possible reaction might be

$$-\overset{|}{\underset{|}{Si}}-OH + CF_4 \longrightarrow -\overset{|}{\underset{|}{Si}}-F + CO\uparrow + HF + F_2\uparrow . \qquad (49)$$

The by-products such as a HF react again with glass to form SiF_4 gas by the reaction Equation 32. Evidence for existence of HF was observed visually in this work, i.e. the surface of glass containers in the drawing chamber became opaque.

Since the replacement of hydroxyl groups in the glass by fluoride ions requires elevated temperature and low water vapor pressure system, complete removal of hydroxyl groups can not be expected in this work. The humidity was so low (about 2% R.H.) that the number of water molecules striking the fluorinated glass surface was one order of magnitude lower than the water atmosphere drawn fibers. The time for complete removal of hydroxyl groups was short because the fiber was exposed for

less than 10^{-3} sec at temperatures greater than 800°C. Thus, reaction by Equation 48a is regarded as a predominating reaction in CF_4 drawing atmosphere.

The dissolution of glass surface layer in CF_4 atmosphere depends on the concentration of CF_4 gas. The rate (R) of dissolution of amorphous silica film in acid fluoride solution was studied by Judge (116) who expressed the rate as follows,

$$R = A[HF] + B[HF_2^-] + C \qquad (50a)$$

or

$$R = A'[H^+][F^-] + B'[H^+][F^-]^2 + C. \qquad (50b)$$

The dissolution rate thus depends on the pH in addition to the fluoride concentration. The concentration of CF_4 used in this work was two orders higher than the value calculated from the Equation 24 based on the number of surface hydroxyl groups. This may result in degradation of the measured strength but it is doubtful that such a high dissolution leads to the reduction of final diameter to 3.5 ~ 3.8 μm as measured. Probably other drawing parameters, viscosity (drawing temperature or composition change) or drawing speed may have changed during the operation.

BET surface area of fluorinated E-glass fiber is very large (i.e. about 5 times that of water vapor atmophere drawn fibers) even though it has a slightly larger geometrical surface area. The large BET surface area represents the more corroded surface produced by CF_4 attack. If the BET surface area (A) is proportional to the square of crack depth (c), the strength degradation by CF_4 treatment was justified on the basis of

Griffith's theory, i.e.

$$\left(\frac{A_{H_2O}}{A_{CF_4}}\right)^{\frac{1}{2}} = \frac{c_{H_2O}}{c_{CF_4}} = \left(\frac{S_{CF_4}}{S_{H_2O}}\right)^{2} \qquad (51)$$

where S_{CF_4} and S_{H_2O} are the measured strengths of CF_4 treated and water vapor treated fibers respectively. The crack ratio calculated is almost equal to that calculated from the measured strength data. This agreement satisfies the hypothesis $\left(\frac{A_{H_2O}}{A_{CF_4}} = 0.403, \frac{S_{CF_4}}{S_{H_2O}} = 0.393\right)$.

The other reason for the high degradation in strength by CF_4 treatment can be explained as follows. As reported by Chapman and Hair (117) the hydroxyl groups on the fluorinated surface play a role as cracking catalyst, i.e. the electronegativity of the fluorine atom replaced for hydroxyl ion is such that it could cause an electron shift in the neighboring atoms which would culminate in the weakening of the hydroxyl bond in the silanol groups and a consequent increase in surface acidity and a high surface area. It is generally accepted that the efficiency of the cracking catalyst is dependent upon the acidity of the surface (118).

The initial degradation (about 10%) of CF_4 treated fibers strength by half-day aging is believed to be due to water attack in the aging atmosphere as shown in the adsorption kinetic analysis (in Figure 20), i.e. the quantity of water adsorbed increased rapidly in half an hour with high adsorption rate and it continued to gain weight up to 5 hours. Then it no longer gained water from the aging atmosphere. The strength also remained constant throughout the aging period up to 30 days in this work.

This is a significant result in this work, which implies that CF_4 treatment in drawing atmosphere results in degradation of strength due to complete destruction of the strong surface layer of Bartnev's model, but it evidently reduced the sensitivity to atmospheric water vapor by replacement of hydroxyl groups which could provide adsorption sites for water vapor. Consequently, the initial attack by CF_4 is exactly same mechanism as water attack even though the reactivity of fluorine is quite different from that water.

Elastic modulus

The elastic (Young's) modulus of glass depends greatly on the glass composition and it varies from 7.2×10^6 psi for borosilicate glass to 12.5×10^6 psi for aluminosilicate glass (119). As with many properties of glass fibers which differ from those of massive bulk glass, based on the thermal history, the elastic modulus of glass fiber is lower than that of bulk glass, i.e. 15% lower than that of the annealed bulk glass (105). The typical value of E-glass fibers is 10.5×10^6 psi (2).

The elastic modulus data of this work, which was determined by measuring the deflection in tension, varied from 6.8×10^6 psi to 9.8×10^6 psi. There are several factors affecting the elastic modulus of glass. A number of methods can be used to measure the elastic modulus of glass, which correspond to different orders of frequency and determine whether the modulus represents adiabatic or isothermal conditions (102). The deflection in tension is normally measured under static load but in this work under a slow dynamic load.

A number of investigators (4, 120) reported the dependence of

elastic modulus on fiber diameter. Murgatroyd (120) observed that the modulus decreased rapidly below about 30 μm diameter. But Norman and Oakley (121) could not find the modulus dependence for fiber diameters which varied from 10 μm to 200 μm, but observed that the modulus decreased rapidly below about 10 μm diameter. They pointed out that the dependence on the diameter depends on the method of measurement in a certain range of diameter. No data in the literature were available for diameters less than 5 μm.

For most glasses except silica glass the modulus decreases with increasing temperature. However, the modulus of glass fiber increases with increase of heat treatment temperature since the modulus tends to return to the value of bulk glass (101). Thus, thermal history such as fictive temperature influences the modulus of glass. Fiber glass drawn in fixed conditions has uniform modulus. The measured value of modulus of the groups in this work showed low variation but large, apparently random variation between groups.

No correlation between modulus and any other parameter such as diameter, strength or strain was found in this work. But the testing group which had high variation in the measured strength usually showed a high variation in the modulus data. This implies that damage to the fiber surface by accidental touching during specimen preparation may affect the modulus. It was found by investigators that unannealed glass which has thermal stress showed a smaller elastic modulus than annealed glass (101), i.e. fibers strained by stress introduced before testing should have a low value of elastic modulus. The other possible reasons for

this variation are nonuniform diameter and/or the gauge length as discussed in the external affecting factors. It was also noted that the fibers of groups which were drawn on the same day showed approximately the same elastic modulus. Therefore, the elastic modulus of glass fiber may depend strongly on the details of the drawing conditions.

Jet shape

The concave-type jet shapes observed in this experiment, which belong to Burgman's category I or II, showed a good agreement with the jet shapes predicted from the drawing equation, Equation 11c, as discussed earlier. This fact implies that the assumptions made for the drawing equation are acceptable for the upper jet analysis.

One important assumption used in the derivation of the drawing equation is that the surface tension component in the drawing force is negligible compared to the viscosity component. A gas such as a water vapor reacting with glass can affect the surface tension of glass surface as reported by Parikh (71). However, as long as the surface tension force is much smaller than the viscous force no change in jet shape will be observed in the upper jet. According to the drawing equation, the upper jet shape depends on the temperature, activation energy for viscous flow and the heat transfer properties such as thermal conductivity and heat capacity. The environmental temperature in the closed chamber was usually little higher than that in the open chamber during the observation, the activation energy for viscous flow may also be influenced by the different gas atmosphere. All these parameters will have a small effect on the drawing equation.

However, it cannot be concluded that the drawing atmosphere had no effect at all on the jet shape in this work because it was difficult to observe the lower jet region in detail.

CONCLUSIONS

The following conclusions have been reached on the basis of the results obtained.

1. DTA curve indicates the possibility of existence of inhomogeniety in E-glass in the form of a high B_2O_3 phase which has a glass transition at about 350°C. More work on the microstructure of E-glass (such as phase separation) should be conducted by using a TEM.
2. The basic character of observed jet shape at low Reynolds number ($10^{-7} \sim 10^{-6}$) is concave and is independent of the drawing conditions, but the dimensions of jet depend strongly on the temperature. This implies that the viscosity component is the predominating force in the drawing force.
3. The upper jet shapes in this work appeared to be Burgman's category II based on the observation but category I based on the calculation of Reynolds numbers. Therefore, Burgman's analysis is not exact.
4. The effect of water vapor in the drawing atmosphere on the strength of glass fibers is significant. Initial water attack by stress corrosion in the drawing atmosphere reduces the strength of a glass fiber. The strength level of a glass fiber depends on the water concentration in the drawing atmosphere.
5. Under the hypothesis that the specific surface area of the glass fiber is proportional to the square of crack or flaw depth of the glass surface, good correlation exists between the BET surface

area from the adsorption isothermal analysis and the measured strength. The strength reduction by water attack can be justified from the Griffith's microcrack theory. However, a more extensive study should be conducted to confirm this hypothesis.

6. The strength of fine glass fibers (4.5 ~ 5.8μm) drawn in the water vapor atmosphere tended to decrease exponentially with increasing aging time in certain aging conditions, i.e., a linear relationship between the measured strength and log aging time as is observed in the static fatigue behavior of glass. Both high and low humidity drawn fibers have almost the same corrosion rate in the same aging atmosphere, even though they have different strength levels due to initial water attack in the drawing atmospheres.
7. The high loss of strength of glass fibers drawn in a CF_4 gas atmosphere is believed to be due to the initial attack of glass surface by fluorine. This surface attack is similar to the mechanism of stress corrosion by water vapor, even though the severity of attack is different due to the high reactivity of fluorine. The initial attack by CF_4 results in microfissuring which is shown by the relatively large BET surface area.
8. The E-glass fiber surface fluorinated by CF_4 in the drawing atmosphere is characterized as having a low sensitivity to atmospheric moisture during aging due to replacement of fluoride ions for the surface hydroxyl ions which provide the adsorption sites for water vapor. To confirm this conclusion surface analyses such as infrared absorption analysis or Auger electron analysis

are necessary.

9. The mean elastic modulus of fine E-glass fibers ($d < 6\mu m$) drawn in different drawing atmospheres and aged at 36% R.H. varied widely from $6.63 \times 10^6 \sim 9.68 \times 10^6$ psi. No correlation existed between the elastic moduli and parameters such as diameter, stress and aging time. However, there seemed to be some relationship between the modulus and the drawing day. This implies that the elastic modulus of glass fiber as well as other glass properties is dependent on the details of the drawing conditions.

10. No observation of noticeable changes in the upper jets during glass fiber drawing in the selected gas atmospheres indicates that gas reaction with glass surface during glass fiber forming has small effect on the upper jet shape and that the concave jet shape analysis is valid for the temperatures and flow rates used in this study.

BIBLIOGRAPHY

1. Terence Maloney, F. J. 1967. Glass in the Modern World. Doubleday & Co., New York.

2. Loewenstein, K. L. 1973. The manufacturing technology of continuous glass fibers. Elsevier Scientfic Publishing Co., New York.

3. de Dani, A., and Jellyman, P. E. 1957. A study of glass-fiber forming process by means of high speed cine and flash photography. J. Soc. Glass Technol. 41(203):276-282.

4. Bateson, S. 1958. Critical study of the optical and mechanical properties of glass fibers. J. Appl. Phys. 29(1):13-21.

5. Geiger, G. H., and Poirier, D. R. 1973. Transport phenomena in Metallurgy. Addison-Wesley Publishing Co., Reading, Mass.

6. Deeg, V. A., and Dietzel, A. 1955. Cause of the anomalous mechanical properties of glass fibers. Glastech. Ber. 28:221-232 (in German).

7. Anderson, O. L. 1958. Cooling time of strong glass fibers. J. Appl. Phys. 29(1):9-12.

8. Kutukov, S. S., and Khodakovskii, M. D. 1964. Investigating the movement of glass in the forming of continuous glass fiber by high speed filming. Steklo Keram. 21(27):3 (in Russian, English translation) Glass and Ceramics 21 (1964).

9. Arridge, R. G. C., and Prior, K. 1964. Cooling time of silica fibers. Nature London. 20:386-387.

10. Manfre, G. 1967. Survey of cooling rate of glass fibers. Paper presented at the Fall Meeting of Amer. Ceram. Soc., Bedford Springs, Pa., Oct.

11. Glicksman, L. R. 1968. The cooling of glass fibers. Glass Technol. 9(5):131-138.

12. Burgman, J. A., and Hunia, E. M. 1970. The effect of fiber diameter, environmental moisture and cooling time during fiber formation on the strength of E-glass fibers. Glass Technol. 11(6):147-152.

13. Severs, E. T. 1962. Rheology of Polymers. Reinhold Publ. Co., New York.

14. Middleman, S. 1968. The Flow of High Polymers. Interscience Publishers, New York.

15. Glicksman, L. R. 1968. The dynamics of heated free jet of variable viscosity liquid at low Reynolds numbers. J. Basic Engr. Trans of ASME, D(90):343-354.

16. Manfre, G. 1969. Forces acting in the continuous drawing of glass fibers. Glass Technol. 10(4):99-106.

17. Burgman, J. A. 1970. Liquid glass jets in the forming of continuous glass fibers. Glass Technol. 11(4):110-116.

18. Krishman, S., and Glicksman, L. R. 1971. A two-dimensional analysis of a heated free jet at low Reynolds numbers. J. Basic Engr. Trans. ASME 93 (D):355-364.

19. Glicksman, L. R. 1974. Prediction of the upper temperature limit for glass fiber spinning. Glass Technol. 15(1):16-20.

20. Oh, S. M., and Martin, D. M. 1975. The dynamics of glass fiber drawing. Paper presented at the Annual Meeting of Amer. Ceram. Soc., Washington, D. C. May.

21. Manfre, G. 1967. Temperature profile of gob in spinning continuous glass fibers. Paper presented at the Fall Meeting of Amer. Ceram. Soc., Bedford Springs, Pa. Oct.

22. Manfre, G. 1965. Some aspects of rheology during spinning of glass fibers. International Congress on Glass, 7th Brussels, Paper No. 78.

23. Tiede, R. L. 1955. Viscometer for measuring glass viscosity by means of flow through an orifice. J. Amer. Ceram. Soc. 38(5):183-186.

24. Thomas, W. F. 1960. An investigation of factors likely to affect the strength of glass fibers. Phys. & Chem. Glasses 1(1):4-18.

25. Otto, W. H. 1955. Relationship of tensile strength of glass fibers to diameter. J. Amer. Ceram. Soc. 38(3):122-124.

26. Holland, L. 1964. The Properties of Glass Surface. John Wiley and Sons, Inc., New York.

27. Doremus, R. H. 1973. Glass Science. John Wiley and Sons, Inc., New York.

28. Stanworth, J. E. 1950. Physical Properties of Glass. Oxford Press, London.

29. Dacay, J. R. 1965. Surface diffusion of adsorbed molecules. Ind. & Engr. Chem. 57(6):26-33.

30. Deitz, V. R. 1965. Gas adsorption. Ind. & Engr. Chem. 57(5):49-66.

31. Gibbs, J. W. 1957. The Collected J. W. Gibbs. Vol. 1. Yale University Press, New Haven, Conn.

32. Polanyi, M. 1914. Uber Die Adsorption Von Standpunkt Des Dritten Warmesatzes. Verhandlung Deusche Physkalische Gesellschaft 16: 1012-1016.

33. Demirel, T., and Enüstün, B. V. 1957. Free energies of wetting of minerals. I. Communications de la Faculte des Sciences de L' Universite, D' Ankara, Series B, 6:1-19.

34. Brunauer, S., Deming, L. S., and Teller, E. 1940. On a theory of the van der Waals adsorption of gases. J. Amer. Chem. Soc. 62: 1723-1732.

35. McBain, J. W. 1909. Der Mechanismus der Adsorption von Wassertoff durch Kohlenstoff. Zeitschriff für Physikalische Chemie 68: 471-497.

36. Barrer, R. M. 1941. Diffusion in and through Solids. Cambridge University Press, London.

37. Langmuir, J. 1918. The adsorption of gases on plane surfaces of glass mica and platinum. J. Amer. Chem. Soc. 40:1361-1403.

38. Panetier, G., and Soucmay, P. 1967. Chemical Kinetics. Elsevier Publishing Co., New York.

39. de Boer, J. H. 1953. The Dynamical Character of Adsorption. Oxford University Press, London.

40. McDonald, R. S. 1958. Surface functionality of amorphous silica by infrared spectroscopy. J. Phys. Chem. 62(10):1168-1177.

41. Basila, M. R. 1961. Hydrogen bonding interaction between adsorbate molecules and surface hyohoxyl groups on silica. J. Chem. Phys. 35(4):1151-1158.

42. Kiselev, A. V. 1965. Calorimetric vs. infrared measures of adsorption bond strengths on silica. Surface Science 3:290-291.

43. Mikhail, R. S., and Shebl, F. A. 1970. Adsorption in relation to pore and microporous silica gel. J. Colloid Interface Sci. 34(1): 65-75.

44. Kawasaki, K., Senzaki, K., and Tsuchiya, I. 1964. Adsorption of studies of water vapor on porous glass. J. Colloid Sci. 19(1): 144-151.

45. Young, G. J. 1958. Interaction of water vapor with silica surfaces. J. Colloid Sci. 13(1):67-85.

46. Folman, M., and Yates, D. J. C. 1958. Infrared and length-change studies in adsorption of H_2O and CH_3OH on porous silica glass. Trans. Faraday Soc. 54(431):1684-1691.

47. Deitz, V. R. 1968. Interaction of water vapor with pristine E-glass fiber. Naval Research Laboratory Report No. 6812, Washington, D.C.

48. Johnson, R. D. 1971. The effect of water vapor adsorption on the specific surface of Fiberglass E. Unpublished M.S. thesis. Library, Iowa-State University of Science and Technology, Ames, Iowa.

49. Huang, R. J., Demirel, T., and McGee, T. D. 1972. Adsorption of water vapor on E-glass. J. Amer. Ceram. Soc. 55(8):399-405.

50. Eitel, W. 1954. The Physical Chemistry of the Silicate. The University of Chicago Press, Chicago, Ill. 1123 pp.

51. Sprecht, R. S. 1956. Interaction of fluoride ions and ground glass. Anal. Chem. 28(6):1015-1017.

52. Sonders, L. R., Enright, D. P., and Weyl, W. A. 1950. Wetability, a function of the polarizability of the surface ions. J. Appl. Phys. 21(4):338-344.

53. Elmer, T. H., Chapman, I. D., and Nordberg, M. E. 1963. Changes in infrared transmittance of fluorine-containing porous glass on heating. J. Phys. Chem. 67(10):2219-2222.

54. Jorgensen, S. S., and Jensen, A. T. 1967. Acid-base properties of quartz suspensions. J. Phys. Chem. 71(3):745-750.

55. Charles, R. J. 1958. Dynamic fatigue of glass. J. Appl. Phys. 29(12):1657-1662.

56. Nordberg, M. E., Mochel, E. L., Garfinkel, H. M., and Olcott, J. S. 1964. Strengthening by ion exchange. J. Amer. Ceram. Soc. 47(5): 215-219.

57. Scholze, H. 1969. Gases in glasses. Eighth International Congress on Glass. Soc. Glass Technol., Sheffield, England. pp. 69-83.

58. Shelby, J. E., and Keeton, S. C. 1974. Temperature dependence of gas diffusion in glass. J. Appl. Phys. 45(3):1458-1460.

59. Moulson, A. J., and Roberts, J. P. 1961. Water in silica glass. Trans. Faraday Soc. 57(7):1208-1216.

60. Stephenson, G. W., and Jack, K. H. 1960. Water in silica glass. Trans. Brit. Ceram. Soc. 59(9):388-394.

61. Hetherington, G., and Jack, K. H. 1962. Water in vitreous silica. Part I. Influence of water content on the properties of vitreous silica. Phys. & Chem. Glasses 3(4):129-133.

62. Doremus, R. H. 1962. Diffusion in non-crystalline silicates. Pages 1-71 in J. D. Mackenzie, ed. Modern Aspects of the Vitreous State, Vol. 2. Butterworths, Washington, D.C.

63. Huang, R. J. 1971. Mechanism of vapor sorption on Fiberglass-E. Unpublished Ph.D. thesis. Library, Iowa State University of Science and Technology, Ames, Iowa.

64. Babcock, G. L. 1940. Surface tension measurements on molten glass by modified dipping cylinder method. J. Amer. Ceram. Soc. 23(1): 12-17.

65. Dietzel, A. 1942. Practical importance and calculation of surface tension in glasses, glaze and enamels. Sprechsaal 75. 82 (in German, English summary) Chem. Abst. 37(1):2422 (1943).

66. Lyon, K. C. 1944. Calculation of surface tensions of glasses. J. Amer. Ceram. Soc. 27(6):186-189.

67. Pavlish, A. E., and Mockrin, I. 1947. Development of hard glasses. J. Amer. Ceram. Soc. 30(2):54-61.

68. Rubenstein, C. 1964. Factors for the calculation of the surface tension of glasses at 1200 C. Glass Technol. 5(1):36-40.

69. Rynd, J. P., and Rastogi, A. K. 1974. Auger electron spectroscopy--New tool in the characterization of glass fiber surfaces. Amer. Ceram. Soc. Bull. 53(9):631-634.

70. Griffith, A. A. 1920. The phenomena of rupture and flow in solids. Phil. Trans. Roy. Soc. Ser. A, 221(A):196-198.

71. Parikh, N. M. 1958. Effect of atmosphere on surface tension of glass. J. Amer. Ceram. Soc. 41(1):18-22.

72. Kingery, W. D. 1963. Introduction to Ceramics. John Wiley and Sons, Inc., New York.

73. Kingery, W. D. 1959. Property Measurement at High Temperature. John Wiley and Sons, Inc., New York.

74. Aisanova, M. S., and Khazanov, V. Z. 1968. Effect of cooling rate on strength of quartz and glass fiber. Steklo Keram. 25(9):1 (in Russian, English translation). Glass and Ceramics 25 (1968).

75. Thomas, W. F. 1971. An investigation of the factors affecting the strength of glass fiber strands. Glass Technol. 12(3):60-64.

76. McKinnis, C. L., and Sutton, J. W. 1959. Glass melting process. II. The effect of melting history on glass structure and glass properties. J. Amer. Ceram. Soc. 42(5):250-253.

77. Cameron, N. M. 1966. Relation between melt treatment and glass fiber strength. J. Amer. Ceram. Soc. 49(3):144-148.

78. Jurkov, S. A. 1935. The effect of the increased strength of thin filaments. J. Tech. Phys. U.S.S.R. 1: 386-399 (Translated in English).

79. Bartenev, G. M. 1970. The Structure and Properties of Inorganic Glasses. Wolters-Noodhoff Publishing Co., The Netherlands.

80. Cameron, N. M. 1968. The effect of environment and temperature on the strength of E-glass fibers. Part I. High vacuum and low temperature. Glass Technol. 9(1):14-21.

81. Cameron, N. M. 1968. The effect of environment and temperature on the strength of E-glass fibers. Part II. Heating and aging. Glass Technol. 9(5):121-130.

82. Otto, W. H. 1959. Properties of glass fibers at elevated temperatures. Final report on U.S. Navy Contract, No. 58-841-C. Owens-Corning Fiberglas Corp., Granville, Ohio.

83. Cameron, N. M. 1965. An investigation into the effect of environmental treatments. Ph.D. Thesis, Library, University of Illinois.

84. Orowan, E. 1948-49. Fracture and strength of solids. Rept. Prog. Phys. (12):185-232.

85. Metcalfe, A. G., and Schmitz, G. K. 1972. Mechanism of stress corrosion on E-glass filament. Glass Technol. 13(1):5-16.

86. Ritter, J. E., and Sherburne, C. L. Dynamic and static fatigue of silicate glasses. J. Amer. Ceram. Soc. 54(2):602-604.

87. Baker, T. C., and Preston, F. W. 1946. The effect of water on the strength of glass. J. Appl. Phys. 17(3):179-182.

88. Bartenev, G. M. 1969. The structure and strength of glass fibers if different chemical composition. Mater. Science & Engr. 4:22-28.

89. Stockdale, G. F., Tooley, F. V., and Ying, C. W. 1951. Change in tensile strength of glass caused by water immersion. J. Amer. Ceram. Soc. 34(4):116-121.

90. Proctor, B. A., Whitney, I., and Johnson, J. W. 1967. Strength of fused silica. Proc. Roy. Soc. (London) 297(1451):534-557.

91. Tiede, R. L. 1974. Private communication. Owens-Corning Fiberglas, Granville, Ohio. August.

92. Braker, W., and Mossman, A. L. 1971. Matheson Gas Data Book. Matheson Gas Products Co., New Jersey.

93. Wicks, C. E., and Block, F. G. 1963. Thermodynamics of 65 elements. USBM Bull. 605.

94. Washburn, E. W., ed. 1928. International Critical Tables of Numerical Data of Physics and Chemistry, Technology. Vol. 3. McGraw-Hill Book Co., New York. 370 pp.

95. Jones, J. T., and Berard, M. F. 1972. Ceramics--Industrial Processing and Testing. Iowa State University Press, Ames, Iowa. 213 pp.

96. Kolthoff, I. M., and Elving, P. J. 1967. Treatise on Analytical Chemistry. Part I. Theory and Practice. Interscience Publishers, New York.

97. Oldfield, L. F., and Wright, R. D. 1963. The volatilization of constituents from borosilicate glass at elevated temperatures. Pages 114-115 in F. R. Matson and G. E. Rindone, eds. Advances in Glass Technology, Plenum Press, New York.

98. Manley, T. R. 1970. The use of heat flow apparatus to find polymer transition points. Thermal analysis 2(4):411-417.

99. Otto, W. H. 1961. Compaction effects in glass fibers. J. Amer. Ceram. Soc. 44(2):68-72.

100. Hauk, J. E. 1966. New inorganic filaments are stiffer and lighter than metals. Materials in Design Engr. 63(2):82-85.

101. Morey, G. W. 1954. The Properties of Glass. Reinhold Publishing Company, New York.

102. Burgman, J. A. 1975. Private communication. PPG Industries, Pittsburgh, Pa. June.

103. Metcalfe, A. G., and Schmitz, G. K. 1964. Effect of length on the strength of glass fibers. ASTM Proc. 64:1075-1093.

104. Weibull, W. 1939. A statistical theory of the strength of materials. Ing. Votenkaps Akard. Handl., No.151, Stockholm.

105. Burgman, J. A. 1975. Private communication. PPG Industries, Pittsburgh, Pa. May.

106. Bernett, M. K., and Zisman, W. A. 1969. Effect of adsorbed water on wetting property of borosilicate glass, quartz, and sapphire. J. Colloid and Interface Sci. 29(3):413-423.

107. Salmang H., and Becker, A. 1929. Gases in glass. Part II. The gas and moisture content of glasses. Glastech. Ber. 7:241 (in German) Trans. J. Soc. of Glass Technol. 13:98-111. (1929)

108. Roberts, G. R., and Roberts, J. P. 1964. Influence of thermal history on the solubility and diffusion of water in silica glass. Phys. & Chem. Glasses 5(1):26-32.

109. Franz, H. 1966. Solubility of water vapor in alkali borate melts. J. Amer. Ceram. Soc. 49(9):473-477.

110. Metcalfe, A. G., Gulden, M. E., and Schmitz, G. K. 1971. Spontaneous cracking of glass filaments. Glass Technol. 12(1): 15-23.

111. Mufit, A. 1975. Private communication. Engineering Research Institute, Iowa State University, Ames, Iowa. June.

112. Wiederhorn, S. M. 1967. Influence of water vapor on crack propagation in soda-lime glass. J. Amer. Ceram. Soc. 50(8):407-414.

113. Mould, R. E., and Southwick, R. D. 1963. Strength and static fatigue of abraded glass under controlled ambient conditions. J. Amer. Ceram. Soc. 42(12):582-592.

114. Ebsworth, E. A. 1963. Volatile Silicon Compounds. A pergamon Press Book. The Macmillan Co., New York.

115. Tichane, R. M. 1966. Initial stages of the weathering process on soda-lime glass surface. Glass Technol. 7(1):26-29.

116. Judge, J. S. 1971. A study of the dissolution of SiO_2 in acidic fluoride solutions. J. Electrochem. Soc. 118(11):1772-1775.

117. Chapman, I. D., and Hair, M. L. 1963. The role of the surface hydroxyl groups in catalystic cracking. J. Catalysts 2(2):145-148.

118. Plank, C. J., Sibbett, D. J., and Smith, R. B. 1957. Composition of catalysts in cracking pure methylcylohexane and n-decane. Ind. Engr. Chem. 49(4):742-749.

119. Corning Glass Works. 1965. Properties of selected commercial glasses. Corning Glass Works, Corning, New York.

120. Murgatroyd, J. B. 1944. The strength of glass fibers. Part I. Elastic Properties. J. Soc. Glass Technol. 28:368-387.

121. Norman, B. J., and Oakley, D. R. 1971. The diameter dependence of the Young's modulus of glass fibers. Glass Technol. 12(2):45-46.

122. Weast, R., ed. 1972-1973. Handbook of Chemistry and Physics. The Chemical Rubber Co., Cleveland, Ohio.

123. Livingston, H. K. 1949. The cross-sectional area of molecules adsorbed on solid surface. J. Colloid Sci. 4(5):447-458.

124. Penman, H. L. 1958. Humidity. Chapman and Hall Ltd., London.

ACKNOWLEDGMENT

The financial support of this work by the Engineering Research Institute, Iowa State University and the National Science Foundation under Grant No. GK39206 is sincerely appreciated.

The author would like to acknowledge the guidance and support he received from his committee comprised of Dr. D. R. Wilder, Dr. T. D. McGee, Dr. P. Chiotti, Dr. T. Demirel and Dr. D. M. Martin. The author expresses sincere gratitude to Dr. Martin for his encouragement, guidance, and helpful discussions during the course of this investigation. The author is indebted to Dr. Wilder and Dr. M. F. Berard for their consultation and advice on many matters pertinent to this dissertation. The technical assistance of Mr. Mufit Akinc for adsorption isotherm analysis was invaluable. The author sincerely wishes to thank Mrs. Mary Brown not only for her patience and organizational suggestions during the typing of this dissertation, but also for personal help and friendship she has offered throughout the years.

Finally, the author would sincerely like to acknowledge the faithful patience and understanding of his wife, Dorothy and his three sons, Choo Hawn, John and Andy through that long and arduous trial known as graduate education.

APPENDIX

Determination of Drawing Temperature

The measurement of exact actual temperature of the molten glass at high temperature under dynamic conditions is difficult by current techniques. The measurements of temperature with common methods such as thermocouples and optical pyrometer do not exclude errors which are difficult to take into account because of complex phenomena of combined conduction and radiation in a molten, nonisothermal, semitransparent glass.

Especially, in the glass fiber drawing process, it is extremely difficult to determine the actual drawing temperature at the nozzle exit because of rapid temperature drop due to the high flow rate and exposure to environmental air. It has been reported that the temperature of the bushing tip, determined by optical pyrometer, is generally about 200°F (110°C) lower than the body temperature during fiber drawing (83). The temperature of the bushing tip is generally regarded as the drawing temperature in this work.

Since thermocouples cannot be inserted into the glass flow in the nozzle of the resistance-heated platinum crucible due to the small dimensions and blocking of the glass flow, thermocouples were welded close to nozzle as shown in the following figure.

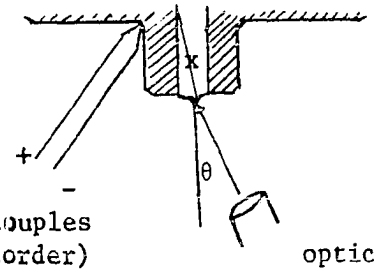

Figure A1. Drawing temperature measurement.

According to Wien's law, the actual temperature (T_a) can be estimated by the brightness temperature (T_B, optical brightness temperature) (73),

$$\frac{1}{T_a} - \frac{1}{T_B} = \frac{\lambda \ell n E_\lambda}{c_2} \qquad \text{(A1)}$$

Here λ is wave length (0.65×10^{-4}cm), c_2 is a constant (1.44cm°K) and E_λ is emissivity. For a long, narrow platinum tube, E_λ is equal to unity and $T_a = T_B$, but a correction must be made for reflection loss at the glass surface and transmission loss through the glass.

For nonblackbody case, the effective emissivity (E_{eff}) which is the product of black body emissivity and transmission factor (T) should be used instead of E_λ in equation (A1), i.e.,

$$E_{eff} = E_\lambda T \qquad \text{(A2)}$$

and

$$T = (1-R)^2 e^{-ax} \qquad \text{(A3)}$$

where R is reflection factor and is given by the refractive index ($n_D = 1.47$) (122),

$$R = \left\{\frac{(n_D - 1)}{(n_D + 1)}\right\}^2 \qquad \text{(A4)}$$

a is the absorption coefficient (a = 0.3/cm) and x is the thickness of the nonblackbody, which can be calculated from the nozzle geometry and the refracting angle of incident beam.

The actual temperature in the nozzle tip during fiber drawing was calculated by correcting optical pyrometer measurements and the results are plotted as a function of the recorder temperature as shown in Figure A2.

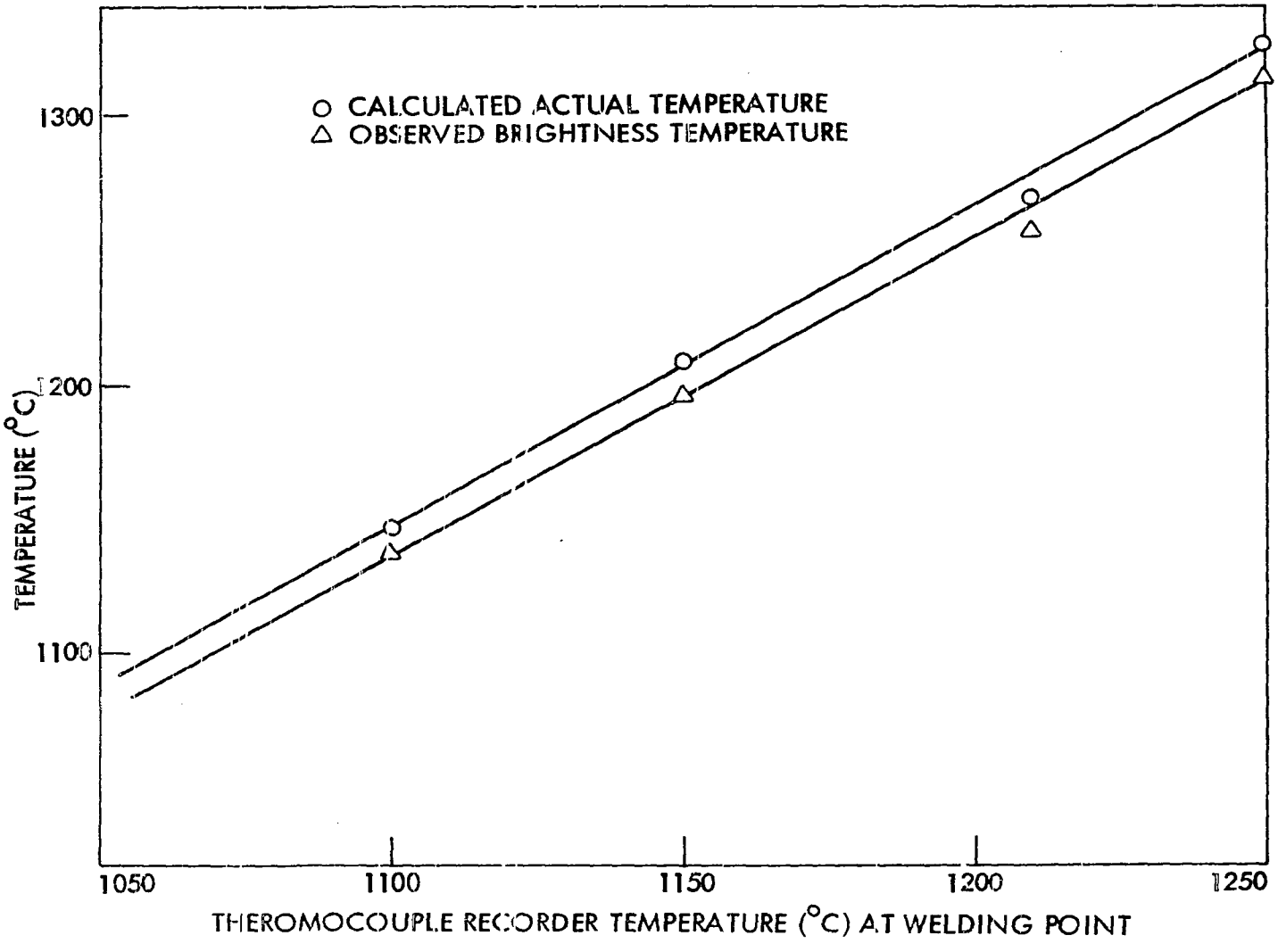

Figure A2. Drawing temperature as a function of recorder temperature.

Calculation of Freon-14 Gas Concentration

First of all, in order to compute the volume of a selected gas such as Freon-14 gas in the drawing chamber, the actual volume of the drawing chamber should be known accurately. The approximate geometrical chamber volume can be easily calculated simply by measuring its dimmensions but the chamber contains a lot of items such as the drawing drum with motor, the platinum crucible with refractory covers and several kinds of containers. The actual volume occupied by gas is therefore smaller than the geometrical volume of chamber.

Actual volume of drawing chamber

By using a simple method, i.e., by measuring the pressures of chamber after changing the volume, the actual volume of the drawing chamber can be calculated, i.e.,

$$p_1 V_1 = p_2 V_2 \tag{A5a}$$

where p_1 and p_2 are the pressures of volume V_1 and V_2 respectively. Let V_1 be the actual volume of the drawing chamber and V_2 a total volume which is the chamber actual volume (V_1) plus the known extra volume (V_{ex}). Rewrite the Equation A5a as follows:

$$p_1 V_1 = p_2 (V_1 + V_{ex}) \tag{A5b}$$

or

$$V_1 = \frac{p_2 V_{ex}}{p_1 - p_2} \tag{A5c}$$

Here p_1 and p_2 were measured by manometer and computed by the following equations, i.e.,

$$p_1 + \rho g h_1 = p_2 + \rho g h_2 \tag{A6a}$$

$$p_2 = p_1 - \rho g (h_2 - h_1) \tag{A6b}$$

where h_1 and h_2 are measured heads of manometer at p_1 and p_2 respectively. p_1 was about 1 atmosphere and P_2 was found to be 0.9932 atmosphere. The actual volume (V_1) was calculated to be 12.428 ft^3 when V_{ex} was 2.4ℓ (= 0.08474 ft^3) by connecting an evacuated bottle (about 10^{-1} torr) to the chamber.

This computed actual volume of drawing chamber is smaller than the geometrical volume calculated from its dimmensions, which was 12.912 ft^3. However, this computed actual volume is still an approximate value with a variation of 8% because of variation in reading the head ($\pm$ 0.1 cm due to the flexibility of dry box gloves attached to the drawing chamber).

Concentration of Freon-14 gas

The minimum concentration of Freon-14 gas required in the drawing chamber was based on gas kinetics. In other words, at least one CF_4 molecule should strike the glass fiber surface while the surface was hot. The number of molecules on the glass surface was calculated based on the adsorption results. The number of surface hydroxyl groups per cm^2 was computed from the literature; i.e., one hydroxyl group occupies 10.8 $Å^2$ (123). Thus, the number of hydroxyl groups per cm^2 was found to be 9.25×10^{14} OH molecules/cm^2.

The number of CF_4 molecules should be larger than the number of hydroxyl groups for complete glass-CF_4 reaction. Thus, the concentration of CF_4, which corresponds to the partial pressure of CF_4 gas in Equation (23), can be calculated for one impact molecule per surface OH ion in 10^{-3} sec. The required partial pressure of CF_4 gas turned out to be 7.795×10^{-2} mm Hg, which corresponds to a concentration of CF_4 gas

less than 1%. In order to achieve complete reaction of CF_4 gas with the glass surface, a sufficient amount of CF_4 (2%) was introduced to the drawing chamber.

Humidity Control

Calibration of psychrometer

Since the wet-dry bulb hygrometer is the best available tool for general humidity measurement, it is often the standard for calibration of psychrometers in the laboratory.

By using the following equation the relative humidity (R.H.) of the testing room was measured (124), i.e.,

$$R.H.(\%) = \frac{p_w - a(T_D - T_w)}{p_D} \times 100 \qquad (A7)$$

where p_w = the saturation vapor pressure at T_w

p_D = the saturation vapor pressure at T_D

T_w = wet bulb temperature

T_D = dry bulb temperature

a = psychrometer constant depending on the ventilation rate. (e.g., for laboratory air with air conditioner $a = 4.382 \times 10^{-4}$ atm/°F and for aging chamber $a = 6.583 \times 10^{-4}$ atm/°F).

The results of measurement R.H. as a function of wet-dry bulb temperature were shown in Figure A3.

Aging chamber

The most reasonable method of humidity control for an aging chamber is control by means of salt solutions. A number of salts suitable for this

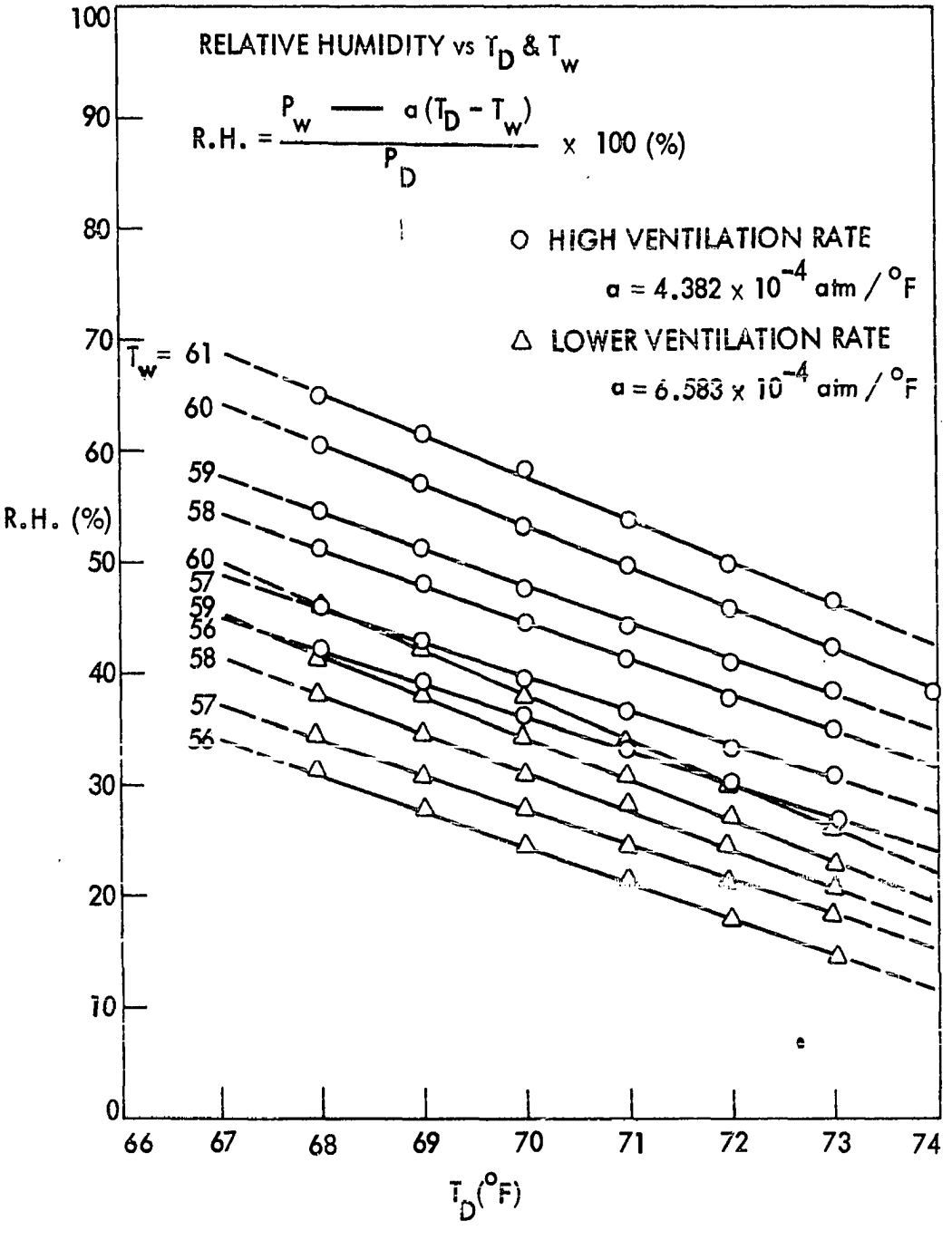

Figure A3. The measurement of relative humidity by using wet-dry bulb temperatures.

purpose are available but sparingly soluble and volatile salts can not be used, nor can those be used that cannot be obtained in a sufficiently pure state to warrant such humidity control.

Relative humidity is the ratio of the vapor pressure of water vapor present to the pressure of saturated water vapor at the same temperature. The vapor pressure data of certain salt solutions as a function of concentration and temperature are available in the literature. For this purpose NaOH was used and the vapor pressure data were obtained from the International Critical Table, (Vol. 3, p. 370) (94), i.e.,

Table A1. Vapor pressures of NaOH aqueous solution at 20°C

Conc. $\frac{NaOH(g)}{100\ g\ H_2O}$:	0	5	10	20	30	40	50
p (mm Hg) :	17.539	16.90	16.0	13.90	11.30	8.70	6.30

A typical calculation of relative humidity at 20°C with 50 g NaOH/100gmH_2O is shown as follows

$$R.H. = \frac{p}{p_o} \times 100 = \frac{6.30}{17.539} \times 100 = 35.9\% \ (36\%) \qquad (A8)$$

Testing room

The humidity of the testing room (Instron Testing Machine) was controlled by using a cold vaporizer and two dehumidifiers. An automatic control device was developed as shown in Figure A4. The relative humidity set point control of the testing room was kept at 35% but the actual relative humidity varied from 33% to 42% with the outside temperature of the building because of adsorption and desorption from the building walls.

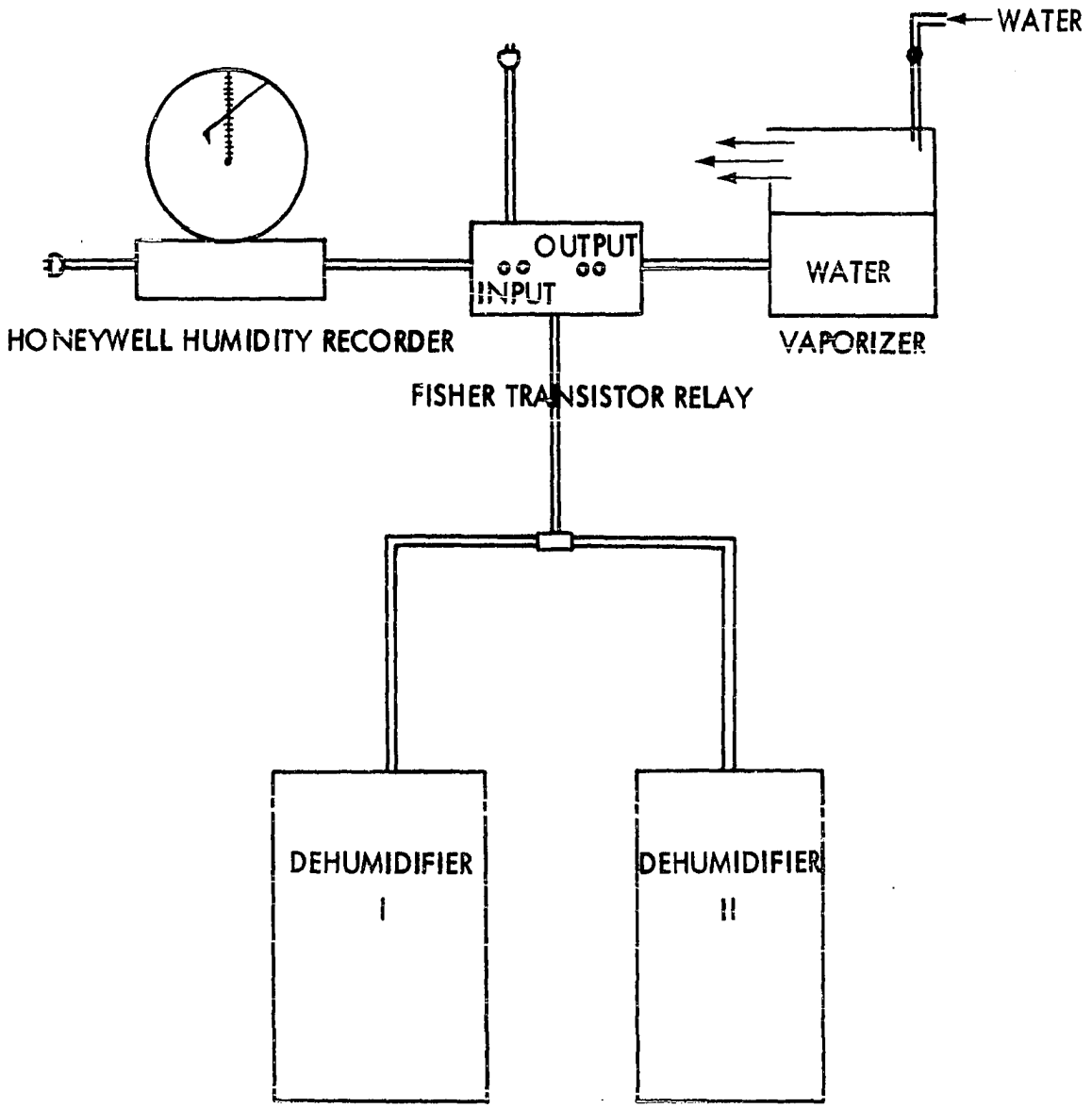

Figure A4. Schematic diagram of humidity control.

Data of Tensile Strength

Table A2. High humidity-atmosphere drawn fibers

Aging day	No.	L (gm)	S (10^5psi)	ε (10^{-2})	E (10^6psi)
0	1	8.50	5.80	5.63	10.27
	2	8.70	5.94	5.63	10.50
(d =5.15μm,	3	8.30	5.66	5.96	9.44
R.H.=87%,	4	7.80	5.33	5.63	9.44
T_∞=32°C)	5	7.30	4.98	5.46	9.09
	6	8.90	6.08	5.63	10.74
	7	8.90	6.08	5.63	10.74
	8	7.30	4.98	5.63	8.81
	9	7.40	5.05	5.02	10.03
	M	8.15	5.54	5.58	9.89
	σ	0.67	0.46	0.24	0.72
	α	8.37	8.37	4.30	7.28
0.5	1	6.20	4.73	5.27	8.89
	2	6.00	4.58	5.56	8.11
(d=4.87μm,	3	6.00	4.58	5.41	8.46
R.H.=80%,	4	5.80	4.42	5.41	8.14
T_∞=34°C)	5	6.00	4.58	5.27	8.70
	6	5.90	4.50	5.71	7.87
	7	6.00	4.73	5.56	8.46
	8	6.00	4.73	6.04	7.79
	M	5.99	4.60	5.52	8.30
	σ	0.14	0.11	0.25	0.39
	α	2.39	2.39	4.52	4.69
1	1	5.60	4.16	5.27	7.91
	2	5.60	4.16	5.25	7.91
(d=4.94μm,	3	5.90	4.38	5.08	8.62
R.H.=80%,	4	5.20	3.85	5.71	6.73
T_∞=35°C)	5	5.90	4.38	5.56	7.87
	6	5.50	4.08	4.92	8.26
	7	5.70	4.23	5.71	7.40
	8.	6.00	4.45	5.08	8.74
	M	5.66	4.21	5.32	7.93
	σ	0.26	0.19	0.30	0.65
	α	4.63	4.63	5.63	8.19

Table A2 (Continued)

Aging day	No	L (gm)	S (10^5 psi)	ϵ (10^{-2})	E (10^6 psi)
2	1	4.30	3.52	5.08	6.92
(d=4.70μm,	2	5.00	4.09	4.77	8.54
R.H.=85%,	3	5.30	4.34	5.71	7.55
T_∞=33°C)	4	5.60	4.59	5.08	9.02
	5	4.40	3.60	4.59	7.80
	6	4.40	3.60	4.59	7.80
	7	4.30	3.52	4.44	7.91
	8	4.80	3.93	5.08	7.71
	9	4.90	4.01	4.44	9.02
	M	4.77	3.91	4.86	8.03
	σ	0.46	0.38	0.41	0.69
	α	9.84	9.84	8.43	8.59
5	1	5.80	3.91	5.23	7.44
(d=5.18μm,	2	5.80	3.91	4.77	8.15
R.H.=86%,	3	5.80	3.91	4.45	8.78
T_∞=33°C)	4	5.30	3.57	4.45	8.03
	5	6.20	4.18	4.75	8.77
	6	5.20	3.50	4.32	8.07
	7	6.00	4.04	5.41	7.44
	8	6.20	4.18	5.41	7.72
	9	5.20	3.50	4.42	7.91
	M	5.72	3.85	4.80	8.03
	σ	0.40	0.27	0.44	0.49
	α	7.03	7.03	9.16	6.10
10	1	6.20	3.39	4.78	7.08
(d=5.75μm,	2	6.50	3.55	4.78	7.40
R.H.=85%,	3	6.20	3.39	5.41	6.25
T_∞=34°C)	4	6.10	3.34	5.33	6.25
	5	5.90	3.23	5.21	6.18
	6	6.20	3.39	5.46	6.18
	7	5.80	3.17	4.83	6.53
	8	6.50	3.55	6.04	5.86
	9	6.50	3.55	5.84	6.06
	M	6.21	3.40	5.29	6.41
	σ	0.24	0.13	0.45	0.50
	α	3.95	3.95	8.50	7.78

Table A2 (Continued)

Aging day	No	L (gm)	S (10^5psi)	ε (10^{-2})	E (10^6psi)
30	1	7.00	4.10	4.06	10.08
	2	5.50	3.22	3.37	9.52
(d=5.56μm,	3	5.60	3.28	3.37	9.68
R.H.=80%,	4.	7.00	4.10	4.14	9.88
T_∞=32°C)	5	5.20	3.04	3.17	9.56
	6	6.50	3.80	4.14	9.17
	7	6.00	3.51	3.81	9.21
	8	5.90	3.45	3.66	9.41
	M	6.08	3.56	3.71	9.56
	σ	0.68	0.39	0.38	0.31
	α	11.20	11.20	10.24	3.24

Table A3. Low humidity-drawn fibers

Aging day	No	L (gm)	S (10^5psi)	ε (10^{-2})	E (10^6psi)
0	1	6.40	5.82	6.37	9.09
	2	6.80	6.19	6.37	9.68
(d=4.46μm,	3	6.90	6.28	7.16	8.74
R.H.=27%,	4	6.80	6.19	6.98	8.85
T_∞=29°C)	5	6.40	5.82	7.95	7.28
	6	6.40	5.82	6.37	9.09
	7	6.30	5.73	6.37	8.97
	8	6.30	5.73	6.05	9.45
	M	6.53	5.94	6.70	8.89
	σ	0.25	0.23	0.62	0.72
	α	3.87	3.87	9.25	8.09
0.5	1	6.40	5.68	7.16	7.93
	2	6.10	5.38	7.16	7.51
(d=4.53 m,	3	6.40	5.68	8.28	6.85
R.H.=25%,	4	6.30	5.56	6.99	7.95
T_∞=29°C)	5	6.20	5.47	7.16	7.60
	6	6.10	5.38	7.49	7.18
	7	5.90	5.20	7.49	6.94
	8	5.90	5.20	8.28	6.28
	M	6.16	5.43	7.50	7.28
	σ	0.21	0.19	0.51	0.57
	α	3.49	3.49	6.80	7.82

Table A3. (Continued)

Aging day	No	L (gm)	S (10^5psi)	ε (10^{-2})	E (10^6psi)
1 (d=4.63 m, R.H.=30%, T_∞ =28°C)	1	6.00	5.06	5.99	8.45
	2	5.60	4.73	5.89	8.03
	3	6.00	5.06	6.68	7.57
	4	5.90	4.98	6.04	8.24
	5	5.90	4.98	6.04	8.24
	6	5.60	4.73	5.89	8.03
	7	5.40	4.56	5.89	7.74
	8	5.30	4.47	5.61	7.96
	M	5.71	4.82	6.00	8.03
	σ	0.27	0.23	0.30	0.28
	α	4.77	4.77	5.00	3.48
2 (d=4.53 m, R.H.=26%, T_∞ =29°C)	1	5.70	5.02	6.35	7.91
	2	5.40	4.76	5.21	9.13
	3	6.10	5.38	6.05	8.89
	4	6.30	5.56	6.98	7.97
	5	5.30	4.67	6.53	7.15
	6	5.20	4.58	6.35	7.21
	7	5.20	4.58	6.04	7.58
	8	5.60	4.94	5.33	9.26
	9	5.60	4.94	5.28	9.35
	M	5.60	4.94	6.01	8.27
	σ	0.38	0.34	0.62	0.89
	α	6.96	6.96	10.31	10.76
5 (d=4.63 m, R.H.=30%, T_∞=28°C)	1	5.70	4.81	6.04	7.97
	2	5.90	4.98	6.35	7.84
	3	5.90	4.98	6.98	7.13
	4	6.00	5.07	6.68	7.58
	5	5.30	4.48	6.42	6.98
	6	5.80	4.90	7.31	6.70
	7	5.90	4.98	6.83	7.29
	8	5.10	4.30	6.35	6.77
	M	5.70	4.81	6.62	7.28
	σ	0.32	0.27	0.40	0.47
	α	5.71	5.71	6.04	6.45

Table A3 (Continued)

Aging day	No	L (gm)	S (10^5psi)	ε (10^{-2})	E (10^6psi)
10 (d=4.60 m, R.H.=28%, T_∞=31°C)	1	5.10	4.36	5.56	7.84
	2	5.10	4.36	6.05	7.21
	3	5.10	4.36	6.05	7.21
	4	5.90	5.04	6.32	7.97
	5	5.10	4.36	5.41	8.05
	6	5.50	4.71	5.56	8.47
	7	5.10	4.36	6.35	6.87
	8	5.10	4.36	6.35	6.87
	M	5.25	4.49	5.95	7.56
	σ	0.29	0.25	0.39	0.59
	α	5.65	5.65	6.57	7.80
30 (d=4.60 m, R.H.=25%, T_∞=29°C)	1	5.10	4.36	4.88	8.77
	2	5.10	4.36	4.73	9.05
	3	5.70	4.87	5.02	9.52
	4	5.10	4.36	4.87	8.77
	5	4.90	4.19	4.63	9.01
	6	5.40	4.62	4.76	9.56
	7	5.70	4.87	5.48	8.74
	8	5.20	4.44	5.18	8.46
	M	5.27	4.50	4.94	8.98
	σ	0.29	0.25	0.27	0.38
	α	5.60	5.60	5.46	4.23

Table A4. Freon-14 atmosphere drawn fibers

Aging day	No	L (gm)	S (10^5psi)	ε (10^{-2})	E (10^6psi)
1 (d=3.57 m, R.H.=2%, T_∞=37°C)	1	2.50	3.55	4.77	7.44
	2	2.60	3.69	4.59	8.03
	3	2.60	3.69	4.77	7.73
	4	2.80	3.97	4.92	8.06
	5	2.60	3.69	4.77	7.73
	6	2.50	3.55	4.44	7.99
	7	2.50	3.55	4.14	8.57
	8	2.50	3.55	4.59	7.73
	9	2.80	3.97	5.08	7.81
	M	2.60	3.69	4.67	7.89
	σ	0.12	0.17	0.27	0.31
	α	4.71	4.71	5.78	3.92

Table A4 (Continued)

Aging day	No	L (gm)	S (10^5psi)	ϵ (10^{-2})	E (10^6psi)
0.5	1	2.50	3.49	5.41	6.45
	2	2.40	3.35	4.77	7.02
(d=3.60μm,	3	2.30	3.21	4.44	7.23
R.H.=2%,	4	2.70	3.77	5.56	6.78
T_∞=37°C)	5	2.50	3.49	5.56	6.27
	6	2.50	3.49	5.08	6.87
	7	2.00	2.79	4.77	5.84
	M	2.41	3.37	5.08	6.63
	σ	0.21	0.30	0.44	0.47
	α	9.10	9.10	8.66	7.08
1	1	2.20	2.89	3.65	7.92
	2	2.50	3.28	3.81	8.60
(d=3.71μm,	3	2.70	3.55	3.96	8.96
R.H.=2%,	4	2.60	3.42	3.90	8.76
T_∞=35°C)	5	2.60	3.42	4.01	8.52
	6	2.60	3.42	3.81	8.97
	7	2.10	2.76	3.81	7.24
	8	2.60	3.42	4.14	8.26
	M	2.48	3.27	3.89	8.40
	σ	0.21	0.28	0.15	0.58
	α	8.74	8.74	3.85	6.90
2	1	2.40	3.48	4.14	8.40
	2	2.30	3.34	3.81	8.76
(d=3.53μm,	3	2.30	3.34	4.29	7.78
R.H.=2%,	4	2.30	3.34	3.81	8.76
T_∞=31°C)	5	2.40	3.48	4.14	8.41
	6	2.30	3.34	3.81	8.76
	7	2.30	3.34	4.29	7.78
	8	2.00	2.91	3.66	7.95
	9	2.20	3.19	3.78	8.43
	M	2.27	3.30	3.97	8.33
	σ	0.11	0.17	0.24	0.40
	α	5.18	5.18	6.04	4.80

Table A4 (Continued)

Aging day	No	L (gm)	S (10^5psi)	e (10^{-2})	E (10^6psi)
5	1	2.80	3.36	4.54	7.40
(d=3.88μm,	2	2.80	3.36	4.44	7.56
R.H.=1%,	3	2.50	3.00	4.34	6.90
T_∞=35°C)	4	3.00	3.60	4.57	7.87
	5	3.00	3.60	4.64	7.75
	6	2.60	3.12	3.47	8.99
	7	3.20	3.84	5.40	7.11
	8	2.30	2.76	4.03	6.84
	M	2.77	3.33	4.42	7.55
	σ	0.29	0.35	0.54	0.69
	α	10.66	10.66	12.21	9.13
10	1	2.30	2.77	3.02	9.19
(d=3.88μm,	2	2.70	3.24	3.47	9.34
R.H.=2%,	3	2.90	3.48	3.81	9.13
T_∞=37°C)	4	2.70	3.24	3.53	9.17
	5	2.70	3.24	3.96	8.18
	6	2.80	3.37	3.81	8.84
	7	2.70	3.24	3.32	9.75
	8	2.80	3.37	4.14	8.14
	9	2.80	3.37	4.06	8.30
	M	2.71	3.25	3.68	8.89
	σ	0.18	0.20	0.37	0.56
	α	6.18	6.18	10.05	6.29
30	1	2.00	2.73	3.57	7.64
(d=3.64μm,	2	2.80	3.82	4.31	8.86
R.H.=2%,	3	2.70	3.69	4.06	9.08
T_∞=35°C)	4	2.00	2.73	3.62	7.54
	5	2.80	3.82	4.38	8.72
	6	2.50	3.41	4.14	8.23
	7	2.70	3.69	4.28	8.62
	8	2.30	3.14	4.82	8.21
	M	2.47	3.37	4.14	8.36
	σ	0.33	0.46	0.40	0.56
	α	13.60	13.60	9.66	6.69

Table A5. Summary of strength data

Drawing atmosphere	Aging day	N	d (μm)	$\bar{S}$ (10^5psi)	σ (10^5psi)	α (%)
Low humidity	0	8	4.46	5.94	0.23	3.87
	0.5	8	4.53	5.43	0.19	3.49
	1	8	4.63	4.82	0.23	4.77
	2	9	4.53	4.94	0.34	6.96
	5	8	4.63	4.81	0.27	5.71
	10	8	4.60	4.49	0.25	5.65
	30	8	4.60	4.50	0.25	5.60
High humidity	0	9	5.15	5.54	0.46	8.39
	0.5	8	4.87	4.60	0.11	2.39
	1	8	4.94	4.21	0.19	4.63
	2	9	4.70	3.91	0.38	9.84
	5	9	5.18	3.85	0.27	7.03
	10	9	5.75	3.40	0.13	3.95
	30	8	5.56	3.56	0.39	11.20
CF_4 gas	0	9	3.57	3.69	0.17	4.63
	0.5	7	3.60	3.37	0.30	9.10
	1	8	3.71	3.27	0.28	8.74
	2	9	3.53	3.30	0.17	5.18
	5	8	3.88	3.33	0.35	10.66
	10	9	3.88	3.25	0.20	6.18
	30	8	3.64	3.37	0.46	13.60